UNIVERSIDADE DE LISBOA
INSTITUTO SUPERIOR TÉCNICO

Development of an integrated microfluidic platform for biomolecule production and purification

Ricardo Gil Fradique

Supervisor : Doctor Maria Raquel Múrias dos Santos Aires Barros
Co-Supervisor : Doctor João Pedro Estrela Rodrigues Conde

Thesis approved in public session to obtain the PhD Degree in
Biosciences and Biotechnology

Jury final classification: Pass with Distinction

2020

TÉCNICO LISBOA

UNIVERSIDADE DE LISBOA
INSTITUTO SUPERIOR TÉCNICO

Development of an integrated microfluidic platform for biomolecule production and purification

Ricardo Gil Fradique

Supervisor : Doctor Maria Raquel Múrias dos Santos Aires Barros
Co-Supervisor : Doctor João Pedro Estrela Rodrigues Conde

Thesis approved in public session to obtain the PhD Degree in Biosciences and Biotechnology

Jury final classification: Pass with Distinction

Jury

Chairperson : Doctor Duarte Miguel de França Teixeira dos Prazeres, Instituto Superior Técnico, Universidade de Lisboa;
Members of the Committee :
Doctor José António Couto Teixeira, Escola de Engenharia, Universidade do Minho;
Doctor Maria Raquel Múrias dos Santos Aires Barros, Instituto Superior Técnico, Universidade de Lisboa;
Doctor Duarte Miguel de França Teixeira dos Prazeres, Instituto Superior Técnico, Universidade de Lisboa;
Doctor Ana Cecília Afonso Roque, Faculdade de Ciências e Tecnologia, Universidade Nova de Lisboa;
Doctor Ana Margarida Nunes da Mata Pires de Azevedo, Instituto Superior Técnico, Universidade de Lisboa.

Funding Institutions - Fundação para a Ciência e a Tecnologia

2020

Abstract

Ever since the development of the first recombinant human therapeutic protein, the increasing use of microorganisms to produce important therapeutic molecules has led to the need for new, practical and economical manufacturing and processing methods. With the recent focus on holistic approaches, that consider the effects of each process in the overall performance, microfluidics have emerged as a cost-effective method to test a large set of conditions in a short time and with very low reagent consumption.

The objective of this work was the development of a microfluidic platform for biomolecule production and purification, that is, a device that integrates multiple unit operations, accounting for the cascading effects on the overall process performance.

This work describes the development and characterization of three microfluidic modules: a microbioreactor, a cell lysis chip, and a combined cell lysis/protein concentration device.

The microbioreactor integrated a resistive heater for temperature regulation, optical density measurements using an optical sensor, and fluid control by integrated microfluidic valves and persistaltic pump. The device operated at about $55\,\mu l\,min^{-1}$, maintaining a stable temperature in the $37\,^{\circ}C$ to $40\,^{\circ}C$ range, and an *E.coli* cell culture was able to maintain a specific growth rate close to the one found in flask scale cultures.

In addition, a diffusion-based microfluidic device for the rapid screening of continuous chemical lysis conditions was also developed, using the release of a recombinant GFP expressed in *E. coli* as model system. This was used to test the lytic effect of both enzymatic and chemical lysis solutions, with lysis efficiencies of about 60% and 100%, respectively. Also of note is the detection of potential process issues, such as the increased viscosity that can arise for specific lysis conditions and hinder the performance of a bioprocess.

This work was then integrated with an aqueous two phase extraction method in a different device, using a PEG/Phosphate system. This was screened for the separation stage, presenting partition coefficients of about 4, and then used for the continuous screening of multiple condition combinations, highlighting conditions where improvements on the lysis efficiency subsequently impaired the separation, decreasing the partition of the target product, and demonstrating the need for the evaluation of

a process in its entirety.

Keywords

Biomanufacturing, bioprocess integration, microfluidics, bioreactor, cell lysis, aqueous two-phase extraction

Resumo

Desde que a primeira proteína humana recombinante foi produzida, o crescente uso de micro-organismos para a produção de moléculas terapêuticas tem aumentado a necessidade de novos métodos de produção e purificação, mais práticos e económicos. Com o recente foco em abordagens holisticas, capazes de considerar os efeitos de cada passo do processo na sua performance geral, a microfluidica tem surgido como um método eficaz no teste de uma ampla gama de condições, num espaço de tempo curto, e com baixo consumo de reagentes.

O objetivo deste trabalho foi o desenvolvimento de uma plataforma microfluidica para a produção e purificação de biomoléculas, isto é, dispositivos que integrem múltiplas operações unitárias, que avaliem os efeitos em cascata na performance final.

Este trabalho descreve o desenvolvimento e caracterização de três módulos microfluidicos: um microbioreactor, um dispositivo para lise celular, e um dispositivo combinado de lise celular e concentração de proteínas.

O microbioreactor integra um aquecedor resistivo para manutenção da temperatura, avaliação continua de densidade optica usando um sensor optico, e controlo de fluidos usando válvulas e bombas microfluidicas. O dispositivo atingiu fluxos de cerca de $55\,\mu l\,min^{-1}$, mantendo uma temperatura entre $37\,^{\circ}C$ to $40\,^{\circ}C$, e nele uma cultura de *E.coli* susteve uma taxa de crescimento especifico próxima da encontrada em culturas de balão.

Um dispositivo baseado em difusão foi também desenvolvido para a triagem rápida de condições de lise química, utilizando a libertação de GFP recombinante produzida em *E.coli* como sistema modelo. Este foi utilizado para testar a eficiência de várias soluções de lise química e enzimática, com eficiências de cerca de 60% e 100%, respetivamente. De notar a deteção de possíveis problemas durante esta fase, tal como o aumento de viscosidade em determinadas condições, que pode afetar a performance do sistema.

Este sistema foi então combinado, num novo dispositivo, com um método de extração por duas fases aquosas, utilizando um sistema de PEG/Fosfato. Este sistema foi primeiro testado para separação, com coeficientes de partição próximos de 4, e então utilizado para a triagem continua de múltiplas combinações de condições, demonstrando condições em que melhorias na eficiência de lise podem prejudicar a separação, demarcando a necessidade de avaliação dos processos no seu

todo.

Palavras Chave

Bioprodução, Integração de bioprocessos, microfluidica, bioreactor, lise celular, extracção de duas fases aquosas

Acknowledgments

First and foremost, I must express my deepest gratitude to my supervisors, Professor Raquel Aires Barros and Professor João Pedro Conde. Thank you for giving me the opportunity join and work at your groups, and for all your guidance, support and patience during this time. I am very grateful for your encouragement and all the knowledge you have given me, as well as the liberty to make mistakes and learn from them.

To Doctor Virginia Chu, not only for the less visible management work that maintains the laboratory fully operational, but for all the support, guidance, and work suggestions that we could always rely on.

It would be impossible not to acknowledge all the work that the technicians and senior researchers do on a daily basis to keep all the machines and services operational. While your work is often times invisible when everything goes well, your absence is usually followed by chaos, so a big thank you to Fernando Silva, José Bernardo, Rita Macedo, Ana Silva, Diana Leitão, and Virginia Soares.

While all research work is filled with disappointment and failure before the appearance of any good results, it is important not to forget that no man is an island, and this would not be complete without acknowledging all my colleagues that in one way or another have helped me reach this point.

To Rui Pinto and Eduardo Brás. The countless shenanigans, bizarre days, weird conversations, holy coffee and the occasional beer run have been key to keep my sanity through these years. I know that I will always look fondly at all the time we spent together. May the end of the world arrive by the hands of "The Three Wise Man"!

Because I would certainly forget to name at least one of you, a big thank you to all my colleagues at both INESC-MN and IBB. While sometimes testing one's patience, the truth is that days would be much more boring without all of you.

I also must acknowledge Inês Pinto, Ruben Soares, and Denis Santos. While I didn't share much time with you, your work ethics, commitment, and productivity will always stand to me as the gold standard that every scientific researcher should work towards. Thank you for always being willing to help, regardless of where you were.

And finally, I would like to thank my family for all the support they have given me throughout my entire life. Everything I've achieved is due to all their love and support, and I couldn't have done it without them. Thank you for always being there for me.

I must also acknowledge Fundação para a Ciência e a Tecnologia (FCT) for my PhD grant (PD/BD/113958/2015), and funding my research through the research project OptLoc (PTDC/BBB-

NAN/5927/2014), MiNerv (PTDC/BIM-MED/4041/2014) and POINT4PAC (SAICTPAC/0019/2015) as well as financing through the Institute of Nanoscience and Nanotechnology (UID/NAN/50024).

If we knew what it was we were doing, it would not be called research, would it?

Albert Einstein

Contents

List of Figures

List of Tables

Acronyms

ADC Analog to Digital Converter. 51

ATPE aqueous two-phase extraction. 20, 86, 90, 91

ATPS aqueous two-phase system. xi, xiii, xvi, 21, 22, 43, 75–80, 82–86, 90–92

B-PER® Bacterial Protein Extraction Reagent. xv–xvii, 62, 63, 65, 68–70, 76–78, 80–82, 84

CAD Computer Assisted Design. 48

CNC Computer Numerical Control. 48

COC cyclic olefin copolymer. 29

CVD chemical vapor deposition. 27

DC direct current. 50

DI de-ionized. 48, 49

DWLii direct write photolithography (DWLii, Heidelberg Instruments). 27, 50

E. coli *Escherichia coli*. ix, xv, xvii, 3, 4, 15, 16, 37, 39, 45–47, 52, 53, 57–59, 61, 62, 64–66, 71, 76, 83, 89

EDTA ethylenediaminetetraacetic acid. 16

EOPO Ethylene oxide (EO-propylene oxide (PO). 20

GFP green fluorescent protein. ix, xiii, xv, 3–5, 46, 52, 61, 62, 64–66, 68, 79, 83–85, 90

GFP-LYTAG green fluorescent protein lytag. xvi, 76, 83, 84

HPLC high pressure liquid chromatography. 72

LoC Lab on Chip. 23, 92, 93

LPS lipopolysaccharide. 71, 90

MEMS microeletromechanical systems. 29

OD optical density. xiv, xv, 52, 54–57

PDMS polydimethylsiloxane. xiv, xv, 29, 31, 33, 39, 47–50, 52, 53, 56–58, 62, 76, 89

Pe Péclet number. 25, 26

PEG polyethileneglycol. xvi, 21, 62, 76–80, 82–84

PGMEA propylene glycol methyl ether acetate. 29

PMMA polymethylmethacrylate. 29, 30, 47, 48

PRP polymer rich phase. 83–85

PVD physical vapor deposition. 27

Re Reynolds number. 24

RIPP Recovery, Isolation, Purification and Polishing. 10, 18

SDS sodium dodecyl sulphate. 4, 15

SRP salt rich phase. 83–85

TiW Titanium-Tungsten. 49

TTL tie line lenght. 21

1 Introduction

1.1 Project motivation

Humanity has used the biological processes of various microorganisms for thousands of years in the making of several types of food products, and the scientific and technological advances of the last century has allowed us to better understand these processes, and adapt them to develop new and innovative therapeutics [1]. Since the development and approval of the first human therapeutic protein, insulin, in 1984, several other therapeutic molecules have been developed and produced using microorganisms [1–3]. This has led to an increasing need for new, practical and economical manufacturing and processing methods [3].

Recently, attention has been focused on the development of holistic approaches, that consider the biomanufacturing process as a whole, in contrast with previous atomistic approaches where the performance of each unit operation was optimized separately [4, 5]. However, while promising, this can be a tedious and expensive process to perform at larger scales, so that novel screening methodologies are thus needed.

Microfluidic technologies have emerged as effective tools in the development of new bioprocessing methods, becoming a cost-effective method to test a large set of conditions in a short time and with very low reagent consumption [6–8]. The smaller size of these systems also gives them certain special characteristics that do not exist at larger scales. The greater fluidic control, resulting from the laminar flow regime under which these chips operate, allows for the precise testing of different conditions under continuous operation [6, 8, 9]. A key advantage is that the whole process can be assembled using different microfluidic modules coupled together, making it possible to characterize and model the cascading effects of each operation on the following ones.

The goal of this work was to investigate the use of microfluidic devices as a platform for the

study and optimization of biomanufacturing processes. Considering the modular aspect of this type of devices, the final target was the integration of multiple unit operations in the same application, in order to study and characterize the full process and any cascading effects that could emerge.

1.2 Bioproduct manufacturing

The manufacturing of a biological product can usually be divided in two parts, an upstream manufacturing stage, concerned with the production of a molecule, and the downstream processing stage, that encompasses the concentration and purification of this target product (Figure 1.1) [1–3]. Downstream processing includes all the processes used to recover and purify a biological product from the starting material, removing impurities until the pre-specified purity or biological activity is met. This stage can be the limiting factor for the commercialization of a biological product, and its technical difficulty can lead to high costs that can account for up to 80% of the total cost [10].

Taking into account these two stages, it becomes obvious that an optimization process should always take the whole process into account. However, there still does not exist a method that can bridge both for an integrated optimization, so that each stage is usually developed independently. The main focus of this work is to develop a microfluidic system that can integrate both the production and purification phases into a single process, so that variables can be evaluated regarding the entire system.

This work will thus focus on the interface between upstream manufacturing and downstream processing, including the production of a biological product, its release from the cell and its sequential concentration.

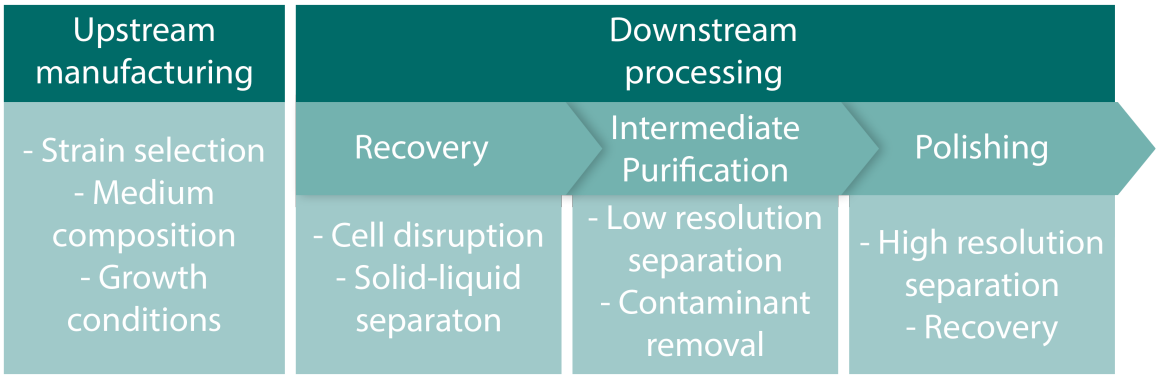

Figure 1.1: Biomanufacturing process overview

1.3 Upstream manufacturing

Several aspects are considered in this stage. First, while any protein can be produced using genetically engineered organisms, the reverse is not true, and so the target product dictates the type of organism that can be used [3], the most common choice being a microbial or mammalian cell, depending on the characteristics of the molecule of interest [2, 3]. Then, there is also the need to

choose between cultivation system, modes of operation, and the ideal composition of the cultivation medium [3]. It is also important to consider the impact that the various products of fermentation can have on further processing [11].

1.3.1 Microbial systems

Humanity has used bacteria for several purposes for millennia, such as in the production of dairy products, and lately in sewage treatment, or in biotechnology, to help produce antibiotics. Bacteria, in particular *E. coli*, represent a significant portion of the systems used for the manufacturing of biological products [2, 12], being the host used to produce about one third of all approved therapeutic proteins [11]. While not capable of producing all products, specially when post-translational modifications are needed, microbial systems present some great advantages when compared with the use of other organisms. They have a fast, robust and reliable growth, that relies on cheap and simple growth mediums, and can create very high product yields. Most of the potential issues with the use of bacteria are well understood, so that companies and laboratories have developed various microbial expression toolboxes that can quickly assemble a functioning and suitable production organism [11].

These can typically be divided into three main sections, the cytoplasm, the periplasm, and the extracellular space. While recombinant proteins can be targeted to each of these spaces, a significant part of microbial products of interest is intracellular, so that effective techniques for their release are required [13–15]. The selected disruption methods can greatly affect the extent of product recovery, the purification process, and the quality of the final product [16], and can have a large economic impact on the final cost of the product, by affecting the amount of impurities that need to be removed downstream.

In addition, bacteria they can further differ on their cell wall composition (Figure 1.2), which must be considered when choosing a cell lysis method.

1.3.1.1 *E. coli* as model organism

This well studied gram-negative microorganism has been extensively used to produce a variety of products of interest, ranging from proteins and plasmids for biopharmaceutical applications [12, 17], to polymers for synthetic plastics [18], and its robustness and ease of handling have made it effectively into a laboratory workhorse [19, 20]. After being the host for the production of the first recombinant product in 1982 [11], the use of this microorganism has been accompanied by advances in biological engineering techniques that have allowed for specific pathway and metabolic optimizations, creating highly efficient *E. coli* strains for specific purposes.

Table 1.1 describes the relative advantages and challenges of using *E. coli* as a production system.

1.3.2 GFP as a model protein

GFP is a protein composed by 238 amino acid residues, with a total molecular weight of 26.9 kDa, that presents green fluorescence when exposed to light in the blue to ultraviolet range [21, 22]. Since

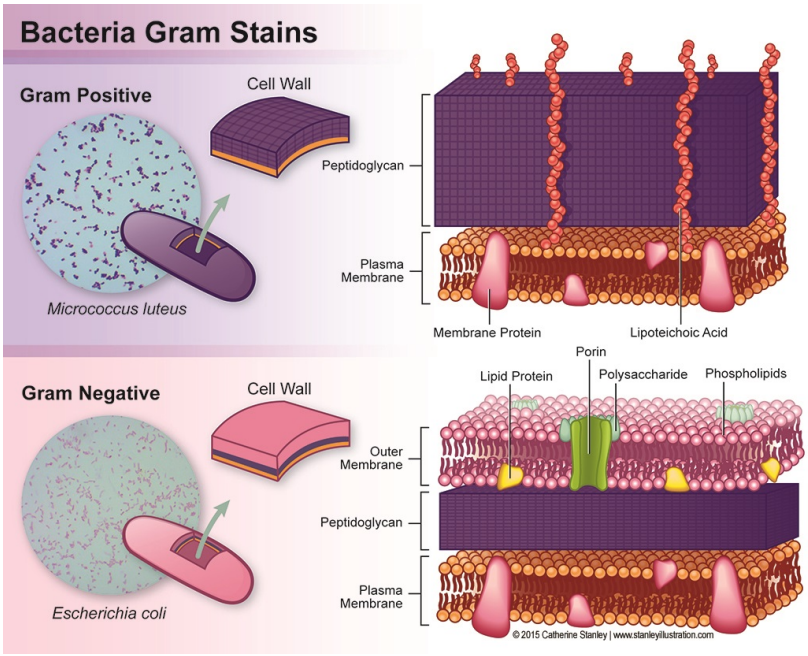

Figure 1.2: Schematic representation of the cell structure of Gram positive and Gram negative bacteria. Gram-positive bacteria have a thick peptidoglycan layer on the bacterial cell wall, which takes up the violet stain in the Gram stain test. Although they present a much thicker peptidoglycan layer, this type of bacteria is more susceptible to antibiotics, due to the absence of an outer membrane. Gram-negative bacteria cannot retain the same stain, and present a much thinner peptidoglycan layer, sandwiched between an inner cell membrane and a bacterial outer membrane. By Stanley Illustration

its first description in 1969 [23], this protein has been adapted for a variety of uses, becoming a common tool in molecular biology, medicine and cell biology as a biological marker and expression reporter [24]. It can be rapidly produced in multiple organisms in high quantities, with several variants already described [25].

It has also found its use in the development of bioprocesses as a model protein for its great stability. In fact, GFP remains stable in a wide range of pH, is not denatured by common protein denaturing solutions, such as urea, sodium dodecyl sulphate (SDS) or guanidine hydrochloride, is mostly unaffected by moderate concentrations of common proteases, detergents and chaotropes, can moderately endure the use of organic solvents, and is not easily photobleached [24, 26]. In addition, fusion tags can easily be added to the protein by standard subcloning techniques without

Table 1.1: Relative comparison of advantages and challenges in the use of *E. coli* expression systems

Advantages	Disadvantages
Safe	Plasmid instability
Simple and well characterized genetics	Inclusion body formation
Simple handling	Improper protein folding
Scalable	No post-translational modifications
High growth rates	Expressing high-molecular weight proteins can be complex
Short processing time	Complex downstream processing
Simple growth medium	Endotoxin contamination
High product yields	Proteolytic digestion
Rapid expression	Limitations in available single-use technology

affecting its characteristics [24], thus allowing for its use to model complex separation processes.

Structurally, GFP is a dimeric protein, with a cylindrical structure composed of 11 β-sheets surrounding a single α-helix containing a covalently bound chromophore. The top and bottom of this structure is closed by short α-helical sections. This conformation contributes to the stability of the protein by protecting the chromophore from the surrounding medium [24]. A representation of the 3D structure of the protein can be observed on figure 1.3. While multiple variants have already been

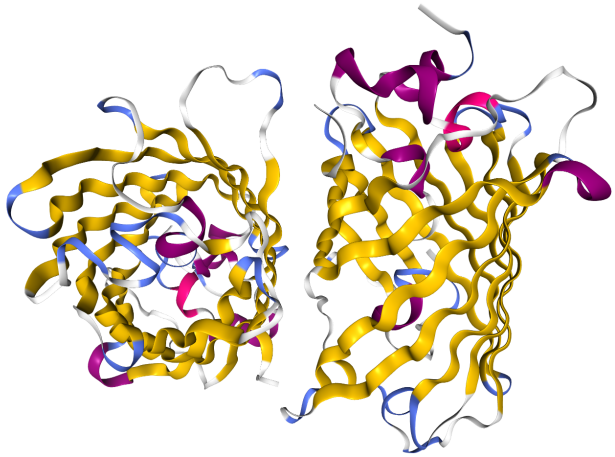

Figure 1.3: 3D structure of GFP, with the chromophore located in the center of the β-sheet cylinder. Image of 1GFL [27] created with NGL [28]

developed, or discovered, with derivative proteins presenting fluorescence across the spectrum, the typical variant was first isolated from the jellyfish *Aequorea victoria*, avGFP, and presents a major excitation peak at 395 nm, with a minor at 475 nm, and an emission peak at 509 nm [26]. The excitation and emission spectra can be observed in figure 1.4.

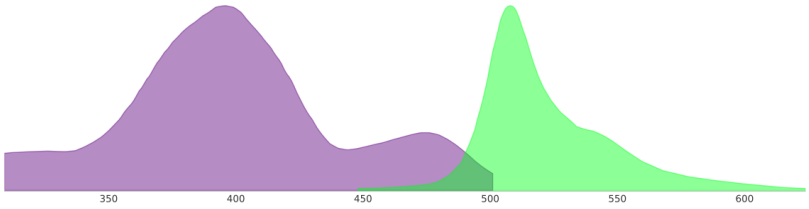

Figure 1.4: Excitation (purple) and emission (green) spectra of GFP. Created using [29]

1.3.3 Bioreactors

A bioreactor is, at its core, simply a vessel where biological reactions occur. However, the accepted definition is a bit more complex, and is described as a designed chamber for growing organisms that can be used for production or conversion of products of interest, such as biomolecular metabolites or biopolymers [30, 31]. This is usually achieved using less energy than a chemical synthesis process would require, while using inexpensive raw materials. Bioreactors are thus the main component in bioprocesses that involve the production of biomass, and biosynthesis or biotransformation of a product [32].

When properly controlled and monitored, a bioreactor can consistently create a desired products faster and at high yield. This is achieved by various sensors that characterize the environment inside the vessel, so that most bioreactors include at least a pH probe, a temperature sensor, and a dissolved oxygen probe [31, 32]. The pH conditions can be controlled by adding an acid or basic solution as needed, or by including pH controlling elements in the fermentation medium [32], oxygen levels are controlled by the agitation and aeration rates [32, 33], and temperature is regulated by flowing cool or hot water in a jacket surrounding the vessel, as needed, or with the use of an electrical heating mantle [33].

Considering the differences in optimal growth conditions and rates between cell types, and even between strains of the same species, it becomes obvious that the best conditions for any particular bioreactor will depend on its objective, so that it is important to properly define it as the basis of the design. There are many different design solutions, each adapted for a particular purpose [30–32].

While the performance of a bioreactor depends on several variables critically related to the transfer rates of mass and energy [30], a proper design must also consider [30, 31, 34]:

- Strain selection - arguably the most important aspect regarding the final product quality, it must be selected with base on the product of interest, and the media and reactor constraints
- Biomass concentration - high enough to maintain the culture with good product yield, and low enough that the nutrient supply is not exhausted
- Sterile conditions - maintaining a pure culture during production, and between cultures in the case of reusable reactors is extremely important, not only because the contaminant organisms can decrease the nutrients available in the medium, but also because their by-products can be extremely hard to remove, and any contamination is unnacceptable from a certification and regulation standpoint
- Effective agitation - while allowing for an uniform distribution of substrate and cells within the bioreactor, it also helps maintaining the dissolved oxygen levels. A balance is required since in some cases excessive agitation can cause localized shear stress which can disrupt the cells, while too low may allow for cell aggregation or accumulation in the reactor walls and stirrer.
- Temperature maintenance - the reactor needs to be kept as close as possible to optimal temperature for the particular application, this can require both a heating mechanism to maintain a higher temperature, or the efficient removal of metabolic heat if needed
- Media composition - cells require specific nutrients and substrates for cell growth. This can also be used to exploit different metabolic pathways that may be beneficial for a particular product
- Product removal - some products can affect the cells when they accumulate in the surrounding medium. Not only can their removal help maintain the culture for longer, but it can also facilitate the downstream processing by including less fermentation by-products.

- Scale-up procedure - since not all conditions are tested at larger scales, it is important that the parameters tested can later be maintained at larger scales

Several types of bioreactor designs have been created, each with their own advantages and disadvantages.

1.3.3.1 Types of bioreactors

Stirred tank bioreactor This is the most common type of bioreactor used in industry, due to its versatility, operability, and manufacturability [30, 31, 35]. Their regular use can be credited to their ability to easily reach a well-mixed state, and thus good substrate contact, pH and temperature control, and uniform cell distribution [35].

Usually built out of glass in small scale experimental applications, or stainless steel for industrial units, these reactors can vary in diameter from $0.1\,\mathrm{m}$ to $10\,\mathrm{m}$ [31, 35], and present a variable aspect ratio (height:diameter ratio) [31, 35] between 2:1 and 6:1 [31]. A schematic representation is presented in Figure 1.5. The largest shortcoming of this type of reactors is its mechanical agitation, so

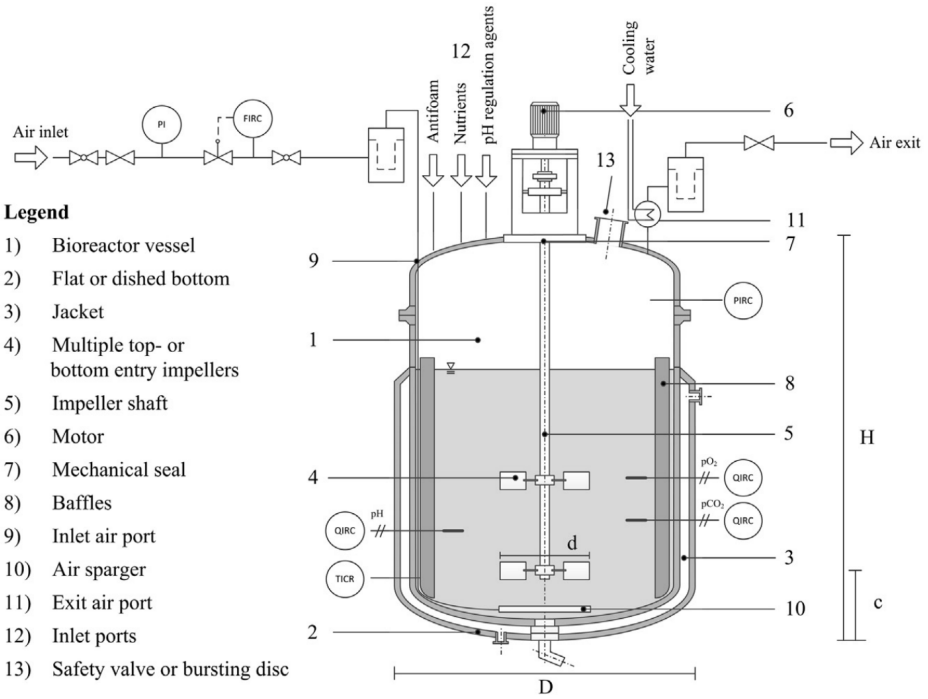

Figure 1.5: Schematic structure of a typical stirred tank bioreactor for aerobic cultivations. Adapted from [36].

that great attention has been dedicated to describe the optimal combination of number, shape and size of rotors, their position, as well as their velocity [31, 35].

Bubble column bioreactor The second most common type of reactor, bubble column reactors address some of the problems associated with the mechanical agitation by replacing it with a column of raising bubbles [30, 35, 37]. These consist of a cylindrical vessel with a gas distributor at the bottom [35, 38], and present an aspect ratio greater than 2 (Figure 1.6) [31, 37]. The change in fluid density caused by the air injection leads to convection motion in the dispersion, and can be used to

achieve a thorough mixing if sufficient high gas flows are used [37]. The lack of mechanical parts is a great advantage when compared with stirred tank reactors, by presenting lower maintenance and operating costs, while maintaining excellent heat and mass transfer characteristics [35, 37, 38]. There are virtually no limitations in terms of size for this type of reactor, so that very large vessels have been almost exclusively airlift reactors [37]. However, since the behaviour of the bubbles is complex and hard to characterize, design and scale up can be more difficult [35, 38], and their lower volumetric oxygen transfer can be insufficient for fast growing organisms and high-density cultures [30].

Airlift bioreactor Airlift bioreactors are a particular case of bubble column bioreactors, in which the gas is released in only a part of the vessel: the riser section, where the fluid moves up, is separated from the rest of the vessel, the down-comer section where the fluid is pushed back down [31, 37]. The riser can be an internal or external loop [30], and is separated by an extra wall, the most simple of which is a tube concentrical with the reactor chamber [37]. These typically have a higher aspect ratio (10 to 100:1) [31].

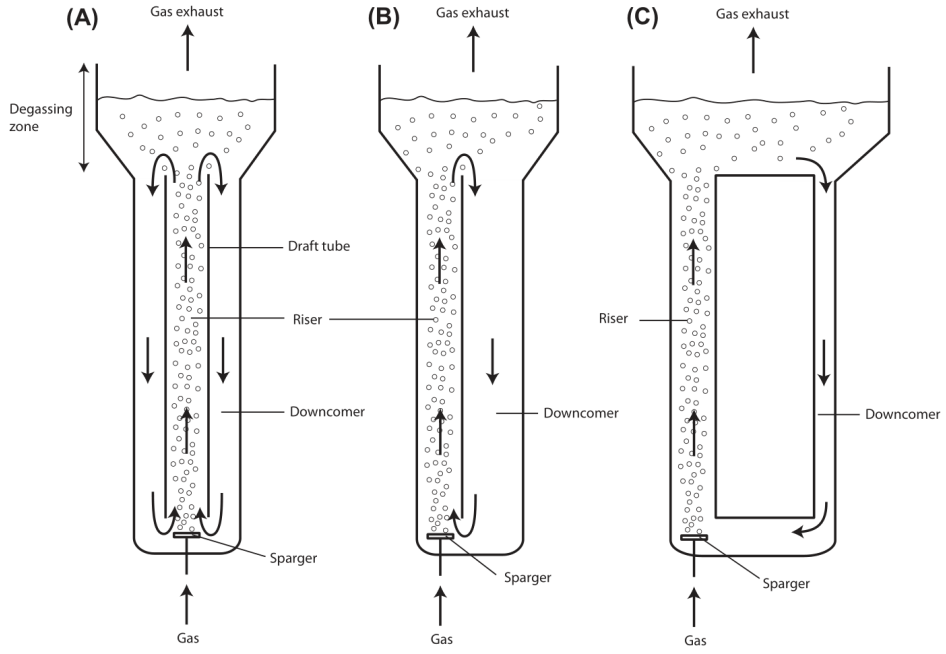

Figure 1.6: Schematic representation of various bubble column bioreactor designs. Adapted from [36].

Solid-state fermentators Solid state fermentation is defined as the growth of microorganisms in a moist solid phase, either particulated or in a matrix, and in the absence or near absence of free water [39–42]. The solid phase can also function as a nutrient source [39, 41].

While some works have noted that this type of reactors can be adapted for bacteria growth, its conditions are usually unsuitable for this type of organisms, so that it is mostly used for the growth of fungi or yeast [39, 40, 42], and usually limited to small scale or very specific industrial applications [40, 43].

Nevertheless, the decision for a specific bioreactor design should always take into account the

downstream processing required. The volume and equipment size should be paired in a realistic way, that is, the equipments used for downstream processing should be able to cope with the volumetric rates of the bioreactor used [30].

1.3.4 Modes of operation

Other than the type of bioreactor, its mode of operation is also a key aspect of the process. A bioreactor can operate in one of three modes: batch, fed-batch, and continuous operation.

1.3.4.1 Batch

Batch, or discontinuous mode, operates as a partially closed system. The substrate is added in the beginning, the products removed at the end, and no material is added or removed in between [32, 44, 45], other than gas exchange to keep oxygen levels within certain limits, and pH control solutions [32, 44]. This means that while it operates at a constant volume, its conditions change over time [32, 44].

Its the most common mode of operation for commercial use [44] due to its simplicity and low potential for contamination [45]. However, running multiple batches requires the process to be restarted each time, with a high downtime between batches [32]. This cost can be decreased if the operations can be performed faster, or the fermentation accelerated [44]. Finally, since it operates as a close system with changing conditions, the growth conditions might not be optimal throughout the entire process [45].

1.3.4.2 Fed-batch

In fed-batch or semi-continuous mode, one or more nutrients are added during the process, depending on the microorganism requirements [32, 45]. The growth rate of the organism can be controlled by the substrate concentration, keeping the oxygen demand within the mass transfer capacity of the bioreactor [44]. This mode is also used to bypass the growth inhibition effect of some substrates, so as to keep the specific growth rates close to their maximum value [32, 45]. While able to reach higher cell densities, this mode also requires greater operator skill for design and operation, and a more detailed understanding of the metabolism and biochemistry of the target organism [32].

1.3.4.3 Continuous operation

Continuous mode is characterized by a constant input of one or more nutrients, and a constant removal of cell, products and other residues, while keeping a constant volume [32, 44]. It can can be further divided in one of two modes, chemostat or turbidostat, depending respectively on wether the chemical composition of the medium or the ammount of biomass concentration are kept constant [32, 44, 45].

Regardless of the type of bioreactor, or mode of operation, if the final goal is to produce a specific molecule or product, this has to be collected, concentrated, and purified.

1.4 Downstream processing

Focused on the capture, isolation and purification of a target bioproduct, downstream processing is a critical step in the manufacturing process, and usually represents the bulk of the final cost of the product [1, 3].

The first stage after the production of the biological product is usually the cell harvesting. Several solid-liquid separation techniques can be used for this, like filtration, sedimentation, and centrifugation. In the case of intracellular products, the following step is to release it from the cell, by disrupting the cell through one of several possible methods. The disrupting method is chosen considering the organism used and its characteristics, the characteristics of the product and its location, and the overall costs of the process [2].

Having extracted the product from the cell, a purification stage follows. This is not so much a step, as a sequence of different techniques. Recovery, Isolation, Purification and Polishing (RIPP) is a commonly used scheme in bioseparation, that uses a sequence of low resolution methods (precipitation, filtration, centrifugation, and crystallization), for the first recovery, and high resolution methods (affinity separation, chromatography, and electrophoresis) for the purification and final polishing [10].

1.4.1 Cell lysis

For decades, the importance of microorganisms as sources of enzymes, proteins, and other commercially useful products has been recognized and, combined with new advances in molecular biology and genetic engineering, have made biotechnology a fast growing industry [13, 14]. These products can be divided into two main types: extracellular, that are secreted onto the growth medium, and intracellular, that accumulate inside the cell's cytoplasm [13, 46]. A significant part of microbial products of interest is still intracellular despite the recent developments in bioengineering, so that effective techniques for their extraction are required [13–15]. In particular, when it comes to the products of recombinant DNA technology or the overproduction of certain proteins, that are predominantly intracellular, the product release methods used can greatly affect the extent of product recovery, the purification process, or the quality of the final product [16]. Furthermore, the method used can also have a large economical impact on the final cost of the product, by affecting the ammount of impurities that need to be removed downstream.

Disruption processes for small, laboratory scale productions have been well characterized for many years, however, not all can be applied in larger scale productions. While non-mechanical means are commonly used at laboratory scale, preference has been given to mechanical methods for large scale operations, due to their lower costs and processing [16, 47].

As mentioned earlier, different types of bacteria present different challenges for disruption, and it is important to take into account the cell wall structure when selecting a disruption method [15]. Figure 1.7 presents a classification of different processes available for cell disruption.

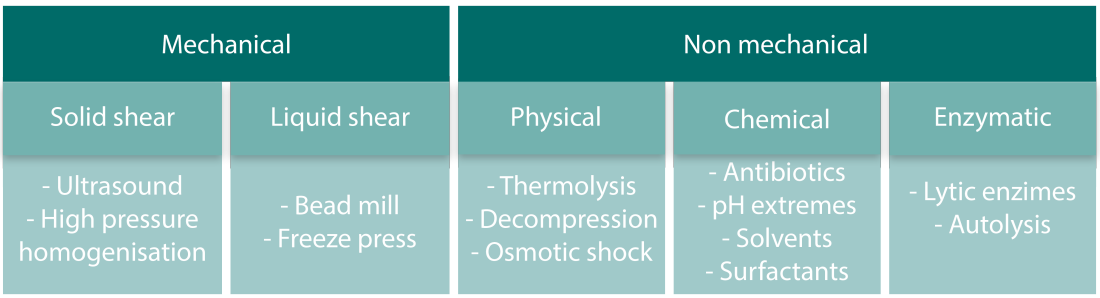

Figure 1.7: Cell disruption methods classification [13–15]

1.4.1.1 Mechanical disruption

The oldest and most common method used for cell disruption, mechanical disruption can involve both solid or liquid shear stress. While simple and effective, both the equipment and energy consumed can increase the costs, and shear stress and heating can some times cause protein inactivation if unchecked [48]. This type of cell disruption will cause the release of all cell components, including host proteins and nucleic material, and may create very fine particle debris, which can difficult the purification processes downstream [49, 50].

1.4.1.2 Solid shear

High speed bead mills First adapted from the pigment and dye industries [13], this method causes cell disruption by the grinding action of the inter-particle collisions [15], and can be used both at a laboratory and industrial scales [13]. While various designs exist, they all consist of a grinding chamber containing rotating disks or impellers moving glass or plastic beads [15]. An efficient cooling system is required since large amounts of heat are generated by the grinding particles. Its effect is mainly dependent on the residence time at larger scales [51], and the beads/cell concentration ratio at laboratory scale [52], but can also be affected by other factors [52, 53].Smaller bead diameters tend to be more effective, however increasing the bead size can allow for the selective release of periplasmic products without full cell disruption [54].

Freeze Press In this highly efficient method for full cell disintegration a cell suspension is frozen and forced through a small slit or orifice under high pressure. By forcing a state change in the ice crystals through this method, the abrasive action of the crystals and the plastic flow cause extensive cell rupture, with high efficiency even in single passes. This method also creates larger cells fragments than other methods, which can make them easier to remove later in the process [14].

1.4.1.3 Liquid shear

Ultrasonication Very common and established technique at a laboratory scale for microbial cell disruption due to its simple requirements, it uses sonic vibrations over 20 MHz to create liquid shear stress[16, 47]. Since it can fully disrupt the cell, it is used to recover intracellular products. It works by

cavitation, in a process where the formation, growth, and collapse of vapour cavities due to local reductions in pressure result in highly energetic elastic waves in the solution [13, 14]. Protein release is directly proportional to the acoustic power [47], and this method can be applied to very large biomass concentrations, depending on both the growth phase of the organism and the mean cell volume.It can operate continuously, however high localized temperatures can cause enzyme inactivation at larger scales, in fact presenting contradictory results depending on the heat stability of the product of interest [47]. This can be explored when the goal is to destroy the bacteria, and has been used for microbial disinfection [55]. It usually produces very fine cell debris which can hinder the downstream processes.

Hydrodynamic cavitation A proven method for large scale applications, in it a cell suspension is forced through a narrow constriction, increasing the velocity to the point of cavitation. A single pass can be sufficient for adequate cell disruption, and if necessary increased pressure and temperature can be used to enhance the effects [55]. It can also be used in combination with different pre-treatments to further decrease the energy requirements, and presents the same effects as ultrasonic sonication, with less energy input and heat generated. Additionally, depending on the location of the product of interest, a selective release can be achieved by adjusting the cavitation conditions so that only the bacterial wall is affected. [55].

High pressure homogenisation Another method commonly found in large scale applications, it consists on pushing a cell suspension through a narrow constriction, at high velocity, and impinged against a stationary phase. The nozzle is decisive for the efficiency of disruption [48, 55], independently of biomass concentration, so high efficiency can be achieved for high concentrations [51].

The main drivers for this type of cell disruption are the viscous shear stress and cavitation [15], with periplasmic products being released faster [51, 54]. Gram-positive bacteria, with their thicker peptidoglycan layer, need a higher pressure before disruption occurs, compared with gram-negative bacteria, however, other factors can also be involved [51, 54].It usually requires expensive equipment [48].

Finally, this method can be used in conjunction with chemical methods that weaken or destabilize the bacterial wall, as well as freeze-thaw cycles that break the cells. This combination can achieve the same release yield, with less passages and lower pression, or even higher release than this method could achieve alone [16, 50].

1.4.1.4 Non-mechanical disruption

Physical disruption

Temperature extremes Freezing and thawing is a common technique at laboratory scale. Cell disruption is achieved by the formation and melting of ice crystals, so that slow freezing cycles that increase crystal size can improve the process. The process can be enhanced by grinding and is

mostly dependent on the density of the cell suspension. Nevertheless, this is a slow process, with limited yields, and loss of enzyme activity has been reported [52].

On the other hand, thermolysis has been shown to be an effective method for DNA isolation [56], and protein release on some microorganisms [49], with short high temperature shocks proving the most effective, compared to longer low temperature treatments. For heat resistant proteins, also called hyperthermophilic proteins, this method can act like an extraction and purification process since most of the native proteins will denaturate at the temperatures used and cell structure is not fully destroyed facilitating the downstream processing [15, 49, 56]. In some cases it may be possible to selectively release a product based on location. Most proteins of interest are highly sensitive to temperature, so that this method has seen limited applications for larger scale uses, and mostly used for genetic material products [49], where it is a valid method for the recovery of plasmid DNA, avoiding the use of organic solvents that can affect the genetic material, or chaotropic agents that increase the final cost. It allows for recovery levels similar to those obtained with the more traditionally used alkaline lysis, while presenting less plasmid degradation, and being scalable [56].

Decompression One of the simplest methods, in it cells are put into contact with a pressurized sub-critical or supercritical gas. By rapidly releasing the pression, the expanding gas disrupts the cell wall. It is an extremely gentle technique, creating large debris that are easier to remove, and largely dependent on the rate of pressure release and the time of contact between cells and gas, even if usually presenting a low efficiency [13, 15].

Osmotic shock Commonly used in laboratory settings for small scale product extraction, it has limited application with microbial cells, and is usually used in combination with other methods. It consists on the rapid dilution of a cell suspension after equilibration in a high osmotic pressure solution, causing a rapid inflow of water that can increase the pressure until the cell is disrupted. Given the cell wall structure of microbial cells, this method is only effective on releasing periplasmic proteins from Gram-negative bacteria, and the cell walls must be weakened if the product is located in the cytoplasm. Finally, the contamination with high concentrations of the agent causing the osmotic pressure can affect the downstream processes, and the high cost of the additives limit its applications to small-scale operations [15].

Chemical methods

Antibiotics Particularly effective at lysing growing bacteria in small scale, several types of antibiotics are know to induce lysis by different mechanisms [15]. The β-lactam class of antibiotics affects the peptidoglycan synthesis and incorporation by interacting with penicillin binding proteins, blocking the correct formation of the cell wall and leaving it vulnerable to osmotic pressures that eventually disrupt it [13, 15, 57].

There are also several types of antibiotic peptides and toxins that alter the cell wall enough to

cause lysis. These can be divided by mechanism of action: (1) some peptides create pores across the lipid bilayer of the cell by acquiring an helix conformation within it; (2) others act like detergents and bind to the membrane, damaging it. Their action also depends on the type of bacteria, for example, citropin and aurein peptides affect mainly Gram positive bacteria by the second mechanism, while maculatin affects the same type of bacteria by creating pores [57]. Polymyxin, on the other hand, is known to act on most gram-negative organisms by the second mechanism, and can be used in combination with lysozyme to release cytoplasmic proteins [15, 58].

However, the use of antibiotics for larger scales has been avoided for several reasons: their effectiveness depends on the state of the culture, they are generally expensive [15], and most importantly, the recent increase of multi-drug resistant bacteria due to the over and misuse of antibiotics has led to crescent pressure to avoid their use [59].

pH extremes First developed and used for the laboratory scale preparation of DNA extracts, alkaline lysis acts by saponification of the cell wall lipids [15, 60]. In this method the cells are subjected to an alkaline solution like NaOH, that can be combined with a detergent and high temperatures. This leads to the total disruption of the cell wall, that usually is accompanied by an increase in viscosity [56, 60]. The harsh conditions of this method have limited its application since most products cannot handle them [15, 56], although some methods have exploited this as a scalable method for extraction and pre-purification of plasmid DNA [60].

Chaotropic agents and solvents Chaotropic agents such as urea and guanidine hydrochloride have been mentioned as mediators in product release from bacteria [15, 49, 50, 54, 61]. By disorganizing the structure of water, making it less hydrophilic, normally hydrophobic species like membrane proteins can be dissolved, destabilizing the cell membrane [50, 54]. Guanidine hydrochloride acts by inhibiting the cross-linking of peptidoglycan and cell wall synthesis, while solubilising membrane proteins, and is used in combination with Triton X-100 for its synergistic effects [50]. Since this combination allows for lower concentrations to be used, it has the potential to be used in larger scales [15]. Nonetheless, the high costs and non-optimal efficiencies have limited the use of chaotropes for lysis to small scale applications [15, 50].

On a different note, solvents can present very different effects, from full cell disintegration to full separation of cell wall from cell membrane. For example, toluene has been described as affecting the cytoplasmic membrane of bacteria, and was used as a method for RNA extraction, while chloroform has been used for the release of periplasmic proteins from gram-negative bacteria. Still, their toxicity made the food and biopharmaceutical industries avoid their use, while the need for their recovery post-use, and nefarious effects on the products of interest, further limiting their application to small bench scale processes [15].

Surfactants Surfactants can interact with both water and lipids, and act on the cells by solubilizing their membrane and membrane proteins [15]. The treatment of bacterial cells with different types

of surfactants is a recognised scalable method for the release of cellular components in molecular biology. Depending on the type of surfactant used, they can solubilize the membrane, proteins, or hinder protein-lipid interactions, thus either destroying the cell, or weakening it enough to improve the effect of milder methods. Some products are greatly affected by this method, like inclusion bodies, so that their extraction can instead be improved by combining it with other methods like sonication [16].

Overall, surfactants can be divided in three main categories: anionic, like SDS, cationic, like some ammonium salts, and non-ionic, like Triton X and Brij. SDS and Triton X-100 are of particular interest, particularly regarding *E. coli*. In the absence of Mg^{2+} ions, both SDS and Triton X-100 can solubilise inner and outer cell membranes. On the other hand, in the presence of these ions only the inner membrane is affected by Triton X-100 [54], an effect that can be used for the selective extraction of some products on this type of bacteria. The synergistic effect between Triton X-100 and the chaotrope Guanidine-HCl [50, 54] can also be used to lyse cells while using lower amounts of surfactants.

Several commercial lysis solutions based on non-ionic or zwitterionic detergents have also been created, and a brief overview of some is described in table 1.2. Used for small scale processes, most of these were developed to avoid the harvesting and concentration steps usually performed before lysis, so that they can be used directly on fermentation samples. However, the compounds used might affect the downstream processing [53], which can be difficult to account for when the nature of the solutions is proprietary. Still, for a more effective process, most of these are used in combination with other processes, like enzymatic attack by lysozyme.

Table 1.2: Commercial cell disruption reagents and enzymes. Adapted from [53]

Vendor	Reagents	Cell types	Vendor web site
EMD Chemicals - Novagen	BugBuster®, Yeast-Buster™, Cyto-Bus™, PopCulture®, rLysozyme™, Benzonase®, Lysonase™, M-Pek, S-Pek	Bacteria, yeast, insect, mammalian	www.emdbiosciences.com
Epicenter	EasyLyse™, Omni-Cleave™, ReadyLyse™	Bacteria	www.epicentre.com
Promega	FastBreak™	Bacteria	www.promega.com
Roche	Complete™ Lysis (B,M,Y)	Bacteria, mammalian, yeast	www.roche-applied-science.com
Semba Biosciences, Inc.	Recombinant Lysozyme, Benzonase®, Liquisonic™	Bacteria	www.sembabio.com
Sigma Aldrich	CelLytic™ (B, IB, M, MEM, MT, NuClear™, P, PN, and Y)	Bacteria, mammalian, plant, yeast	www.sigmaaldrich.com
Thermo Fisher-Pierce	POP-PERS® (B-, I-, M-, NE-, P-, and Y-Per®)	Bacteria, insect, mammalian, plant, yeast	www.thermofisher.com

EDTA As briefly noted on the previous section, Mg^{2+} and Ca^{2+} ions can have great effects on the stabilisation of the outer membranes of Gram-negative cells by cross-linking adjacent lipopolysaccharide molecules, thus this membrane can be destabilised by chelating these ions with ethylenediaminetetraacetic acid (EDTA). It has been shown to be effective in releasing periplasmic proteins from *E. coli* [15], as well as improving the effect of mechanical disruption methods [50]. It can also be combined with surfactants or enzymes for greater effect [15, 56].

Enzymatic methods Greatly used on the extraction of nucleic acids, lytic enzymes have also been used as a method to extract recombinant proteins from bacteria [62]. While these are highly specific and gentle methods, that do not generate shear, high temperatures, or oxidative damage, the optimal conditions for the enzymes can affect some sensitive products, and the presence of the enzyme itself can hinder the downstream processing [53]. Enzymatic cell lysis can be divided in three categories, dependent on the mode of action and type of enzyme used:

Foreign lytic enzymes The most used enzyme in commercial applications is hen egg white lysozyme [62], and several commercial lysis solutions include it in their compositions (Table 1.2) [48, 53].

It acts by catalysing the hydrolysis of β-1,4-glycosidic bonds, thus disrupting cell walls containing peptidoglycan. This makes it more effective on gram-positive bacteria, since they lack the lipopolysaccharide layer of gram-negative bacteria. For these, a combination of Triton X-100 or EDTA can be sufficient, as well as other types of enzymatic lysis [15, 62].

While it is a good method for the isolation of most soluble proteins, it is not the best method when trying to recover protein on the form of inclusion bodies, since it can form agglomerates between these and cell debris, that increases the difficulty of the downstream processing [16].

Autolysis The method of choice to lyse gram-positive lysozyme resistant bacteria, autolysis is the self-digestion of the cell wall by peptidoglycan hydrolases named autolysins [62, 63]. While part of several biological processes in Gram-positive bacteria, the recent developments on the understanding of their mechanisms and functions have allowed for their increased exploitation in medical and biotechnological applications [62].

It can be triggered by osmotic-imbalance, nutrient limitation, and certain antibiotics, however, since it depends on the metabolic activity of its host, it is most effective on growing cells [15, 63].

Phage lysis In this method the cells are lysed by the action of a bacteriophage, through endolysins, lytic enzymes similar to autolysins but encoded in phages [62]. The lytic activity peaks at the terminal stage of the reproductive cycle of the phage. So as not to break the cell prematurely, the enzyme accumulates in the cytoplasm until a different enzyme, holin, disrupts the membrane and allows for access to the peptidoglycan layer [62, 64]. These systems have seen increasing attention given their high specificity and activity.

1.4.2 Separation and purification

Most of the bioseparation techniques used are based on chemical separation processes, and have been used to purify antibiotics, amino acids or vitamins among other low molecular wheight compounds. Among these we can find liquid-liquid extraction, packed bed adsorption, evaporation, and drying, with almost no adaptation needed for use with biological substances. On the other hand, the purification of more complex molecules such as proteins, lipids, carbohydrates or nucleic acids, requires severe modifications to the procedures, or the creation of completetly new separation methods.

The separation of biological products presents must account for some key issues [10, 11]:

1. Very low product concentrations in the starting material may require that large volumes be processed to purify small quantities of pure product;
2. The starting feed may be severely contaminated by impurities with physicochemical properties similar to the target product, increasing the need for highly selective processes;
3. Therapeutical bioproducts present extremely tight quality requirements in terms of both active product content and impurities;
4. Highly sensitive and easily degraded bioproducts require methods that avoid extreme physiochemical and hydrodynamic conditions, as well as the use of organic solvents;
5. Multiple types of contaminants turn the separation into a multi-step procedure where the interaction between the various stages must be taken into account.
6. Scale up principles for the full process, and total cost and economics

Considering this, biological products can be concentrated and purified by exploring their different properties when compared to the unwanted products, as described in table 1.3.

Table 1.3: Overview of properties differences used to separate products from contaminants

Size and shape	**Density**	**Polarity**	**Solubility**	**Electrostatic charge**
Filtration	Centrifugation	Chromatography	Precipitation	Adsorption
Membrane separation	Flotation	Adsorption	Crystallization	Membrane separation
Centrifugation				Electrophoresis

Volatility	**Partition coefficient**
Distillation	Liquid-liquid extraction
Pervaporation	Partition chromatography

1.4.2.1 Types of separation

A separation process can be roughly categorized based on the type of physical separation:

1. Solid-Liquid separation - Includes any method used to isolate particles from a liquid medium (e.g. to remove cells/cell debries from culture medium) Common methods include filtration and membrane separation, sedimentation and centrifugation.

Table 1.4: Common examples of bioseparation techniques

High Throughput	High Resolution
Cell lysis	
Precipitation	Ultracentrifugation
Centrifugation	Chromatography
Liquid-liquid extraction	Affinity separation
Filtration	Electrophoresis
Adsorption	

2. Solid-Solid separation - When the goal is to separate between different particles in suspension (e.g. isolate a specific sub-cellular organelle, or between different types of DNA). Modified forms of centrifugation and filtration can be used.

3. Solute-Solvent separation - Multiple variants, can be used to concentrate a product by removing a solvent from a product solution, to remove dissolved impurities from a product solution, or to replace the solvent in which a product is disolved by a different one. Evaporation and distillation can be used, or filtration, adsorption and precipitation for temperature sensitive applications.

4. Solute-Solute separation - Can be complex due to similarities between the solutes being separated, it is used to isolate a particular solute from a solution containing others (e.g. isolating a serum protein from others). Uses liquid-liquid extraction or different membrane filtration methods.

5. Liquid-Liquid separation - Used to separate between different types of liquids. The methods use can range from simple phase separation and decantation to the use of membrane distillation and pervaporation.

1.4.2.2 Bioseparation techniques

While a variety of new bioseparation techniques are continuously being developed, most processes rely on multiple effects and combine different techniques to obtain the final product. A common strategy is the RIPP scheme, that focuses first on concentrating the product of interest using low selectivity techniques, that can process large volumes of material in a shorter time, at the expense of selectivity, followed by high-selectivity techniques, capable of isolating a target product with high selectivity, at the expense of throughput, to obtain the pure and polished final product. Some examples are noted on table 1.4

Precipitation This method forces one or more components to become insoluble in a complex mixture, precipitating. This precipitate can then be removed using solid-liquid separation methods. Precipitation can be caused by various factors, either the addition of different salts and pH modifiers to the solution, the use of different solvents, cooling the mixture, or using biospecific reagents as in the case of immunoprecipitation. A specific type of precipitation is crystallization, in which by using highly controlled conditions it is possible to slowly induce the formation of crystals.

Centrifugation Centrifugation can separate particles and macromolecules based on size, shape, and density, by applying artificially induced gravitational fields. Depending on the characteristics of the material to separate, different types of centrifugation have been created based on the scale of the gravitational field they create. Typical laboratory scale centrifuges usually have a range of 1000-20000 RCF and can be used for volumes up to 5 L, while larger scale preparative centrifuges are designed to be operated in continuous or semi-continuous modes, to process thousands of litres.

Adsorption Adsorption uses the binding of molecules to the surface of solid materials to separate molecules from a complex mixture, or a solute from its solvent. The adsorbent material can be grafted with specific ligands to improve the selectivity of the process. Naturally, this binding process should be reversible in order to retrieve the molecules adsorbed. The process depends on the molecular weight, size and shape of the solute, the shape of the ligand and binding site, and the polarity and electrostatic charge of the adsobent and the target molecule. Commonly used in the purification of several biomolecules, such as proteins, nucleic acids, or antibiotics, as well as in biomedical analysis, and in some types of chromatography. It can be further classified based on the type of interaction used.

Chromatography Chromatography is a technique for solute fractionation, that exploits the different interaction of different molecules present in a mobile phase and a binding stationary phase. The stationary phase can be composed by small particles or fibers packed into a confined space, or a structure polymerized in-situ, also called a monolith. In either case, the mobile phase permeates the stationary phase at constant velocity. It can operate for analysis of complex mixtures, analytical chromatography, or as part of a manufacturing process in preparative chromatography. Besides the adsorption mechanisms, the use of packed columns also allows for a different separation mechanism, size exclusion, separating molecules by their sizes.

Filtration In this process a solid-liquid suspension is pushed through a porous medium, a filter, which allows the filtrate to flow through, while retaining the solid particles. It can be divided in cake filtration, when the suspension has a high solid content that accumulates in what is called a cake, clarification, in the case of suspensions with very low solid content, or cross-flow filtration, where the liquid flows parallel to the filter. Particles can be retained at the surface of the filter, surface filtration, or trapped in the pores of the porous medium, depth filtration. The filter itself can be made of different materials, ranging from fibers and paper to ceramic and metallic meshes. The process is driven by a pressure differential between both sides of the filter, which can be created using either positive or negative pressures.

Membrane bioseparation A particular case of filtration, in membrane separation the filter is replaced with a thin semi-permeable barrier, usable for different types of separation: particle-liquid, particle-solute, solute-solvent and solute-solute separations. These can separate by solute size, elec-

trostatic charge, diffusivity, or solute shape. This type of application usually contains no solid particles, and its pores can range from $0.1\,\mu m$ to $20\,\mu m$ in the case of microfiltration, to under $1\,nm$ in the case of nanofiltration.

Extraction Extraction processes are Liquid-Liquid separation methods that explore the differential partitioning of a solute between two immiscible or partially miscible phases [10, 11].

While a large number of components can be used to form this type of systems, they can be categorized based on the chemical nature of its phases [11, 65]:

1. Polymer-polymer systems
2. Polymer-salt systems
3. Ethylene oxide (EO-propylene oxide (PO) (EOPO) polymer-water systems
4. Alcohol-salt systems
5. Polymer-ionic liquid systems
6. Surfactant-water systems

Regardless of the nature of the system, the extraction process typically follows three stages [10]: a mixing stage, to allow for a sufficient transfer of solute between the two phases of the system, followed by phase separation in which the system is allowed to equilibrate, where the solute concentrates in one of the phases, and finally phase collection, where each phase is collected as a separate stream.

The distribution of the solute between the phases of the system is given by the partition coefficient K:

$$K = \frac{C_E}{C_R} \tag{1.1}$$

Where C_E is the concentration of the solute in the extraction solvent (kg/m^3), and C_R is concentration in the original solvent (kg/m^3), in equilibrium. This value is independent of the solute concentrations for a given system, although it can deviate linearity for certain systems under high solute loadings [10].

While most of the previously described methods present excellent performance in the laboratory, they create significant challenges when scaled up. From issues with the integration between processes, efficiency losses with increased scale, mass transportation limits, and even the cost of the equipments required, the new challenges have far outpaced the rate of development of new solutions and processes. These issues have been further increased with the improvements achieved on the upstream stages, with increased fermentation cell densities and product titers. On the other hand, liquid-liquid extraction methods are mostly devoid of such issues, showing great promise for bioprocessing applications [11, 65].

While non-aqueous polymer systems are already in industrial use for the separation of various pharmaceuticals [11], the particular case of aqueous two-phase extraction (ATPE) has become one of the most researched for its characteristics.

Aqueous two-phase extraction Aqueous two phase extraction is a particular case of liquid-liquid extraction in which only aqueous solutions are involved. The fact that both phases are of an aqueous nature makes this a particularly well suited method for biological molecules extraction, not only due to its gentle environment, but also because the majority of the phase-forming components used can have a stabilizing effect on the structure of the bioproduct [65–67].

ATPS are spontaneously created when two solutions of incompatible solutes are mixed above a critical concentration [66, 67]. There are two main types of systems depending on the composition of their phases, polymer-polymer systems, with the most common being PEG-dextran, or polymer-salt systems, typically PEG-phosphate or PEG-citrate [65, 66]. These systems are easily emulsified with gentle agitation, where one of the phases is suspended as droplets into the other. These droplets will rapidly coalesce into a larger phase, so that the denser phase will rapidly sediment, while the rate of demixing depends on the phase ratio, their viscosities, and the height of the chamber. This dependence on height, instead of volume, means that even large volume systems can rapidly separate in an appropriate chamber [11]. While the phase separation mechanism in aqueous mixtures is not readily understood [66], this type of systems has been thoroughly studied over the past 30 years [11, 67], so that it is now possible to better model and predict the partition behavior of an ATPS for optimization [65].

The composition of an aqueous two-phase system is commonly referred in the form of (X, Y), where X and Y are the total system concentration of each component in % w/w. The phase separation of the system can be described in a phase diagram (Figure 1.8), combining a binodal curve (B) and the corresponding tie lines with specific tie line lenght (TTL) values [66, 68]. The binodal curve is the border between compositions were only a single phase is formed, and were two immiscible phases start to form. A tie line joins the points in the binodal curve corresponding to the composition of each of the phases formed, and every point in the tie line will create systems that separate into a top and bottom phases with the same compositions at variable volumes and phase ratios. The point where the TTL is equal to zero is called the critical point, where the composition and volumes of both phases are equal [66, 68]. It is important to note that the higher the TTL, the more different the physicochemical properties of the two phases formed [68].

The phase diagram is an essential tool for the design and optimization of a particular system, however the binodal and tie-line determination can be challenging to determine [65, 68]. The best way is to determine the composition of each coexisting phase in multiple systems with varied concentrations [66], however this can be a laborious process. While less precise, this is typically achieved by cloud point determination, in which one of the solutions is added dropwise into the other until turbidity appears, at which point the composition of the mixture is determined. This turbidity signals that the system is about to enter the two-phase are, and by repeating the process for multiple compositions it is possible to map the binodal curve [66]. This method has now been adapted and automatized in the form of high throughout robotic systems, and different microfluidic applications [65]. This evaluation becomes even more relevant since the phase diagram can be altered by pH, temperature, the molecular weights of the components used, as well as any other component loaded into the system

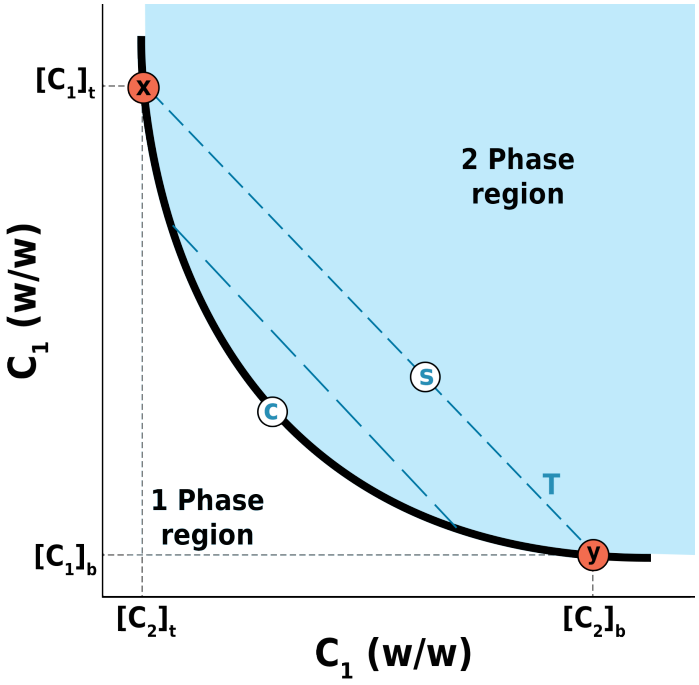

Figure 1.8: Representative phase diagram for an ATPS composed by C_1 and C_2. The binodal curve is represented in black, with corresponding tie-lines in blue. X and Y are two nodes of tie-line T, S corresponds to the composition of a particular system in that tie-line, and C corresponds to the critical point of this system.

Table 1.5: Partition coefficients of different proteins in various polymer-salt systems. Adapted from [67].

Molecule	System composition	K	Reference
β-Galactosidase	6.9% PEG 4000 – 10.6% potassium phosphate	17.00	[69]
Recombinant thaumantin	12.0% PEG 6000 – 13.0 % potassium phosphate, 8.80% NaCl	1.50	[70]
Recombinant cytochrome b_5	19.7% PEG 1000 – 17.7% KH_2PO_4/K_2HPO_4	760.00	[71]
Recombinant cutinase	30% PEG 1000 – 10% potassium phosphate	300.00	[72]
Penincilin acylase	PEG 1000 – sodium citrate	0.16	[73]

[68].

The possibility to easily create two different, biocompatible, water based phases, with very different physicochemical properties, has obviously become a point of interest for these systems, in particular for the potential to selectively partition molecules between these phases. Different molecules will present different affinities for each phase, depending on their properties, quantified by adapting equation 1.1:

$$K = \frac{C_t}{C_b} \tag{1.2}$$

where C_t and C_b are the concentrations of the target molecule on the top and bottom phases, respectively. While some progress has been made in predicting the K values based on the properties of the target molecules and of each phase, in most cases the optimization process is still empirical.

These systems have been shown to not only present remarkable selectivity, even for very similar peptides, proving their potential for purification applications, but they can also be used for their concentration effects, where concentrations factors of two to three orders of magnitude have been registered [68]. A few examples of their application are described in table 1.5

All the advantages of ATPS have made it a method of interest by the scientific community, with increasing attention by the industry. The fact that it uses mostly cheap materials and simple equip-

Table 1.6: Qualitative comparison of various downstream separation and purification methods. Adapted from [65].

Property	Method				
	Packed Bed Chromatography	Crystallization	Precipitation	Pol-Pol ATPS	Pol-Salt ATPS
Complexity	-	?	+/-	+	+
Integration with other operations	+	?	+/-	+	+
Processing capability	-	-	+	-	+
Heavy load processing without dilution	NA	?	+	+/-	-
Affordable without material recycling	-	+	+	+/-	+/-
Clarification without centrifugation	-	NA	?	+	+
Inexpensive and nontoxic reagents	-	?	+/-	+/-	+/-
Requires extra downstream steps	+	+	?	-	-
Allows unconditioned sample loading	+/-	-	+	+	+

ments, with straightforward scale up, while maintaining high selectivity and biocompatibility, and the potential for continuous applications, have made it one of the most promising technologies under development. In fact, by comparing with other downstream processing methods it becomes obvious that, while not solving all of the current issues, it does answer many of the current pitfalls (Table 1.6).

1.5 Microfluidics

Microfluidics is the science and technology of systems that use small channels (tens to hundreds of micrometers) to process and manipulate small (10^{-9} l to 10^{-18} l) volumes of fluids [74, 75].

Microfluidics hold the potential to revolutionize how modern biology is performed in the same way that microfabricated integrated circuits revolutionized computation, by reducing the space, labour and time required for experiments. In this case, microfluidics open the door for large-scale automation, and the possibility of performing numerous parallel assays, with very little reagent consumption. In fact, this miniaturization and automation already started to impact biosciences by allowing for easier and faster whole genome sequencing and analysis [6], while the development of Lab on Chip (LoC) systems is increasing on the biology and chemistry fields by performing biochemical analysis faster than the standard methods, while using lower volumes [7]. These LoC systems hold a great potential not only in the research fields, but can also be a key feature in future personalized medicine treatments.

Thus, it is important to understand how this technology works and what are its advantages and drawbacks, in order to better adapt it for different purposes and create new processes not available at a larger scale [9]. While microfluidics have been used extensively for different areas such as physical sciences and display technology [6], this chapter will focus mainly on those applications that regard biology, medicine and biotechnology.

A key aspect of microfluidic applications is the non-linearity of several fundamental physical concepts, and how they change as the scale decreases into the nanoliter [6]. This makes these systems interesting since effects that usually are negligible at larger scales can now become dominant. The combination of these phenomena in a particular system can be mostly described by a series of dimensionless numbers, some that are scale dependent, and others that while not depending on the scale still carry significant weight on the behaviour of the system [6].

1.5.1 Fluid physics at a microscale

While there are multiple dimensionless numbers that can characterize a microfluidic system with sufficient detail, it is important to first understand what exactly they are describing. Fluids are continuum materials, and thus discrete quantities like force or mass are replaced with continuous fields like force density f and density ρ, defined by unit volume. In Newtonian fluids, the velocity field is described by the Navier-Stokes equations, the rough equivalent of $F = ma$ defined per unit volume:

$$\rho(\frac{\partial u}{\partial t} + u\nabla u) = -\nabla p + \nabla(\mu(\nabla u + (\nabla u)^T)) - \frac{2}{3}\mu(\nabla u)I) + F$$

where u is the fluid velocity, p is the fluid pressure, ρ is the fluid density, and μ is the fluid dynamic viscosity. This equation combines the inertial forces ($\rho(\frac{\partial u}{\partial t} + u\nabla u)$), pressure forces ($-\nabla p$), viscous forces ($\nabla(\mu(\nabla u + (\nabla u)^T)) - \frac{2}{3}\mu(\nabla u)I)$), and external forces applied to a fluid (F). While the Navier-Stokes stokes equations represent conservation of momentum, conservation of mass is represented by the continuity equation

$$\frac{\partial \rho}{\partial t} + \nabla(\rho u) = 0$$

with both being required to solve any fluidic problem with these equations.

For slowly flowing, non compressible fluids like water, the continuity equation yields

$$\nabla u = 0$$

In the particular case of microfluidic flows and applications the Navier-Stokes equations can be reduced to

$$0 = -\nabla p + \nabla(\mu(\nabla u + (\nabla u)^T))$$

since gravity can be neglected there are no external forces, and a low Reynolds number means that inertial forces are so small compared to the viscous forces that they too can be neglected [76].

1.5.1.1 Reynolds number

One of the most significant dimensionless numbers used in microfluidics, the Reynolds number Reynolds number (Re) describes the relation between inertial and viscous forces [6], and can be used to describe the fluid flow regime as laminar or turbulent [9]. While one of the most mentioned numbers, almost all microfluidic devices function in a laminar flow regime, low Re, so that inertial effects usually become irrelevant [6]. It can be calculated by:

$$Re = \frac{\rho v D_h}{\mu}$$

where ρ is the fluid density, v is the characteristic velocity of the fluid, D_h is the hydraulic diameter, and μ is the fluid density. D_h depends on the channel's cross-section geometry [6, 9, 77]. A $Re < 2300$ usually indicates a laminar flow regime [9], while in microfluidics the normal values are far lower.

It must be noted that while inertial effects are small enough that they can usually be ignored in microfluidic applications, some works have presented new ways to exploit them in order to concentrate cells and particles in flow, by using high viscosity fluids and curved structures.

Laminar flow A laminar flow regime is characterized by a deterministic flow velocity in a fluid stream. A consequence is that multiple streams flowing in contact will only mix by diffusion, although the diffusion rate can be non-uniform in the microchannel [6, 9].

The typical microfluidic channel presents a parabolic velocity profile, where the fluid moves faster the further away it is from any of the channel walls (Figure 1.9).

This is a result of the no-slip boundary condition that states that the velocity of a viscous fluid at a fluid-solid interface is equal to the velocity of the solid boundary [76]. This holds true while the interactions between the fluid particles and those of the solid boundary, that is their adhesion force, are stronger than the interaction between the particles of the fluid, their cohesive forces. While this phenomena is not significant for the majority of microfluidic applications, so that the average fluid velocity can safely be used in the modeling stage, it can affect the diffusion profile of molecules inside the channel, and should be taken into account when using these devices for diffusion studies.

1.5.1.2 Diffusion and mixing at a microscale

Diffusion describes how a group of particles that starts concentrated in a predefined space distributes and evenly occupies all the available volume, by Brownian motion. [9]. While usually not important in large scales where mixing is mostly driven by turbulence or convection, the very short distances present within microchannels give diffusion effects a significant impact in microscale. Predicting and controlling this effect is thus essential to be able to create complex concentration gradients for different applications [6, 9].

Depending on the application, it might be important to mix fluids as efficiently as possible, for example in the case of chemical reaction applications where a slow mixture can greatly impair the reaction, but it can also be desirable to avoid and delay any mixing effects, as is the case when trying to separate products from a stream. A useful tool in the study of the diffusion behaviour of a particle or molecule inside a particular microfluidic channel is the Péclet number (Pe), which describes the importance of convection relative to diffusion

$$\frac{U_0 w}{D} \equiv Pe \tag{1.3}$$

where U_0 is the fluid velocity, w is the channel width, and D is the diffusion coefficient of the particle or molecule [6, 77]. This can be roughly understood as the ratio between the channel width, and the corresponding channel length necessary for a molecule to fully diffuse, that is, the number of channel widths required for full diffusion.

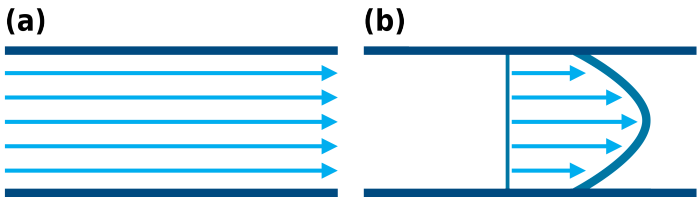

Figure 1.9: Basic representation of (a) laminar flow and (b) parabolic velocity profiles within a microchannel

Considering the dependency of the Pe regarding fluid velocity, from 1.3, it now becomes more clear how and why the non-slip condition can affect diffusion within a microchannel. The lower fluid velocity near the channel walls means that these areas can present a very different diffusion profile than the bulk of the channel, which might need to be taken into account depending on the application.

Given that the diffusion time for any particular molecule or particle in a channel is a function of distance and fluid velocity, it can be tempting to design very narrow channels when very fast mixing is desired. While this is effective, to some degree, it should also be noted that the no-slip boundary effects become increasingly more significant with the decrease in channel width, so that the pressure required to move the fluids also increases very fast.

1.5.1.3 Fluidic resistance

From the Navier-Stokes equations it is possible to determine the flow rate induced within a microchannel by a given pressure by

$$\delta P = QR$$

where Q is the flow rate, ΔP is the pressure drop across the channel, and R is the channel resistance. From this, it becomes clear that, for the same pressure drop, the flow rate will decrease for any resistance increase. This channel resistance is dependent on the the geometry of the channel. This can be applied to, for example, the shape of a blood vessel, where its resistance is given by:

$$R = \frac{8\mu L}{\pi r^4}$$

where μ is the fluid viscosity, L is the length of the channel, and r the channel radius [77].

On the other hand, if we consider a commonly used rectangular microchannel with a low aspect ratio, that is, with a height similar to its width, the resistance is given by

$$R = \frac{12\mu L}{wh^3}[1 - \frac{h}{w}(\frac{192}{\pi^5}\sum_{n=1,3,5}^{\infty}\frac{1}{n^5}\tanh(\frac{n\pi w}{2h}))]^{-1}$$

where w is the channel width and h the channel height. This is simplified for channels with high aspect ratio:

$$R = \frac{12\mu L}{wh^3}$$

1.5.1.4 Surface area to Volume ratio

While the previous section noted the effects that the channel surface has on the resistance, this is not the only parameter affected by changes to the surface. An important factor at microscale, and one of the big advantages in microfluidic structures, is the high surface to volume ratios. Because surface area does not scale linearly with total volume, it is not unusual to find increases by several orders of magnitude [77].

This effect can be used for applications that require the adsorption of molecules at the surface of the channel. This can greatly increase the efficiency of an assay by combining an increase in contact area with the shorter diffusion distances of a microfluidic channel [78–80]. Nevertheless, it must be

noted that this effect can also become an issue in assays where surface adsorption is not desired, and it can even lead to the depletion of a particular analyte if its concentration is sufficiently low [77].

A secondary aspect related with the surface to volume ratio of a microchannel is how it relates with surface tension forces of fluids within it. These result from the cohesion between the molecules of a liquid at a liquid/gas interface, and while they are usually inconsequent at large scales, their effect becomes significant at microscale. This has been used to create capillary flow based, autonomous liquid insertion and circulation mechanisms, that have a high degree of miniaturization and control. Since the distance that a fluid can travel by capillarity is directly related with the surface energy of the fluid and the radius of the capilar, it becomes possible to create complex flow profiles within a channel by using different surface treatments to create virtual walls and pumping mechanisms [9, 77, 81].

1.5.2 Manufacturing methods

A multitude of techniques have already been employed on the fabrication of microfluidic structures. While it can be argued that most have been adapted from the semiconductor industry [82], many have been specifically developed to address particular issues in microfluidic applications.

1.5.2.1 Micromachining

One of the first methods ever used was micromachining, using glass or silicon [83, 84]. This is a group of techniques directly adapted from the microelectronics world, and encompasses all the processes that deposit, etch, or define a material were the minimum feature size is in the micrometer range or less [83].

A typical micromachining process can include:

- Thin-film deposition - usually made by oxidation, chemical vapor deposition (CVD), physical vapor deposition (PVD), or electrodeposition, depending on the material and requirements, and can be used for masking, isolation, or structural purposes;
- Lithography - used to transfer the desired pattern onto the substrate by selectively exposing a photoresist using a photomask. This photomask can be a hard-mask, usually a glass plate covered with a previously patterned thin chromium layer, or a soft-mask, where a focused beam is used to expose the selected areas, in what is called direct write photolithography (DWLii, Heidelberg Instruments) (DWLii) when a laser is used, or electro beam lithography, when an electron beam is used [83].
- Chemical etching - this step can be performed using either a liquid or a gas. The etchant used is selected based on two main characteristics: selectivity for the material to be etched, and directionality, that is, the profile at which the etchant removes the material. Etchants that attack the material in all directions at the same rate are called isotropic, and create semi-circular profiles under the resist mask, while those that have different rates of etching in specific directions are called anisotropic, and can be used to create straight or angled walls as shown in Figure 1.10

[82].

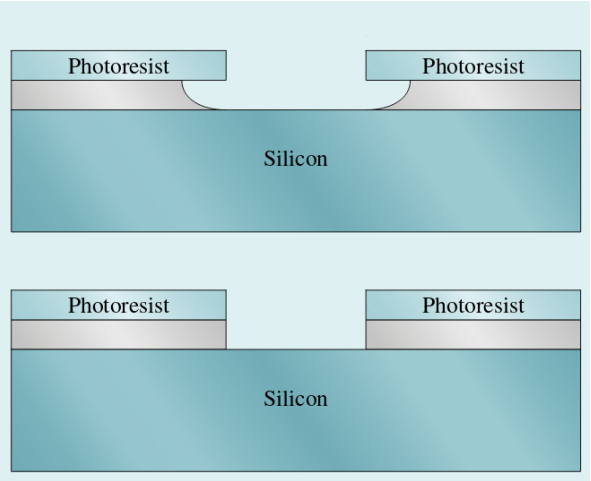

Figure 1.10: Profile for isotropic (top) and anisotropic (bottom) etching, through a photoresist mask. Adapted from Ziaie et al. [85]

- Substrate bonding - depending on the final objective, it might be required to bond the final structure to a different substrate to create more complex structures. This tipically relies on one of two methods. Direct bonding, between two silicon substrates, involves the hydrophilization of both surfaces by using hydrofluoric acid, or boiling nitric acid. The substrates can then be compressed together, usually under high-temperature, creating a strong bond at an atomic scale. Or silicon-glass anodic bonding. With this method a glass wafer is placed on top of a silicon wafer, and both are heated to 300 °C to 400 °C. The bonding occurs by applying ~1000V to the wafers, with the cathode connected to the glass. The movement of sodium ions within the glass creates a depletion layer at the interface, that creates an electrostatic force strong enough for covalent silicon-oxygen bonds to occur at the interface (Figure 1.11) Ziaie et al. [82].

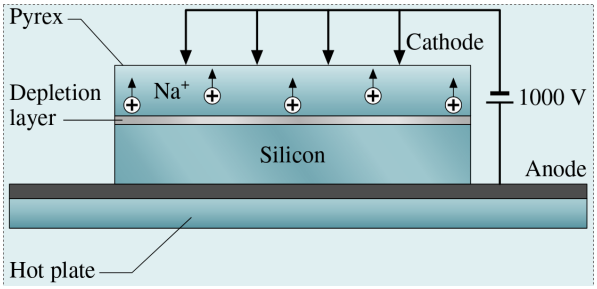

Figure 1.11: Setup for glass-silicon anodic bonding. Adapted from Ziaie et al. [85]

These base steps can be mixed and repeated with different materials to create complex structures [82, 83].

While silicon micromachining can be used to create highly complex systems with nanometre sized structures, it has now been mostly abandoned for microfluidic aplications, in favor of cheaper and

faster methods, usually involving the use of polymeric materials. Its opacity, high manufacturing cost driven by the need for highly specialized skills, equipment and installations, and less than ideal surface properties for biological applications, have mostly limited these techniques for microeletromechanical systems (MEMS) manufacturing. Nevertheless,they have still found use in specific microfluidic applications where the high temperature or pressure resilience, high aspect ratios, or circuit integration are required [9, 84].

1.5.2.2 Soft lithography

Given the limitations of micromachining, research turned to the use of other fabrication techniques to fabricate microfluidic structures, mainly using polymers. Glass and silicon were mainly replaced by PDMS, polymethylmethacrylate (PMMA), paryelen, cyclic olefin copolymer (COC) or polycarbonate, since they are cheaper and simpler to handle [86].

The most widely used method to fabricte microfluidic structures is soft lithography, which mainly consists of molding or embossing methods [82]. The material of choice for microfluidics is PDMS, a two part polymer with great gas permeation for biological applications, impermeable to water, and that presents great chemical and thermal stability while presenting a chemically modifiable surface [77, 83]. With these techniques, the structure of the microfluidic device is defined by a mold, so that the precision and quality of the final structure depends on the precision with which the molds are fabricated. As such, while micromachining can still be used when specific mold features are required, photolithography is the mainly used process to create multidimensional mastermolds [9, 77].

Photolithography The photolithographic process is, at its core, very similar in steps to micromachining fabrication, wherein a substrate is coated, patterned, and etched to reveal the final structure. The substrate used is typically a silicon wafer, which is coated in a photoresist. The most commonly used photoresist is SU-8, an epoxy-resin-based negative photoresist, that can be spun in thick layers ($>500\,\mu m$), and patterned with simple photomask/UV lithography, while still achieving vertical sidewalls [83]. There are a variety of photoresist options depending on the final profile desired, as well as positive or negative photoresists, which vary by how they react to light. A positive photoresist reacts to light by becoming soluble after exposure, while a negative photoresist will become insoluble. After a brief etch, in the case of SU-8 molds using propylene glycol methyl ether acetate (PGMEA) as liquid etchant, the final microfluidic mold is revealed. These steps can then be repeated multiple times, with different photoresists if needed and with different heights, to create more complex structures [87].

With the final microfluidic mold ready, it can then be used to create multiple replicates of the same microfluidic structure. The most used method consists of pouring a PDMS mixture over the SU-8 mold (Figure 1.12) that is then be cured by temperature. After curing, it can be peeled of the mold and sealed against a PDMS membrane or a glass slide, and the mold reused to create more copies of the same structure [9, 82, 83].

In a further effort to reduce costs and time for production, some recent works have described the use of commonly available laser printers to create molds, avoiding the use of photoresists and clean

room facilities, even if limited to shallow structures [88, 89].

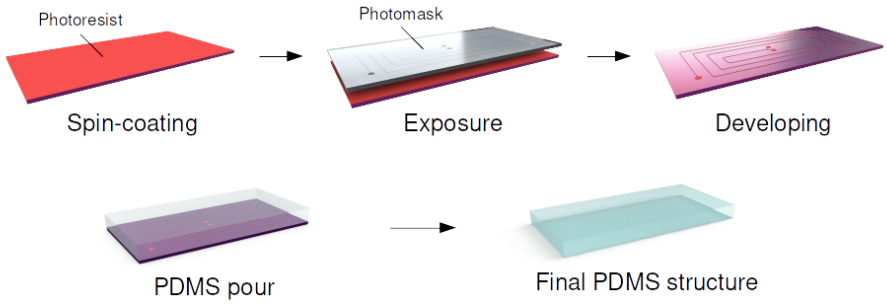

Figure 1.12: Overview of a soft lithography process used to create a microfluidic structure

Hot embossing and Micromolding Alternative applications for molds created by soft lithography can also include hot embossing and micromolding techniques. With hot embossing the structure is created by heating and pressing a master mold against a pliable plastic sheet, usually PMMA. The heat and temperature force the plastic to conform to the structure of the most, maintaining its shape after cooling. These can then be bonded to plastic sheets to create the microchannels, and the molds reused to create more structures. This method can be used to produce large volumes of microfluidic chips in a very short time, at a very low cost. On the other hand, changing any part of the structure is costly and time consuming, requiring the fabrication of a new master mold. It is thus more appropriate for the mass production of fully designed devices [9]. On the other hand, micromolding works by applying the principles of injection molding to microstructured molds. A melted thermoplastic is injected into a cavity containing the master mold. After a quick cooling, the part is ready. Since its molds are made in the same fashion as hot embossing, it also presents the same limitations and can also present lower resolution depending on the materials used. Still, it presents economic advantages for increased scale production given its faster process [9, 82].

1.5.3 Microfluidic components

While it can be argued that the microchannel is the most important part of a microfluidic device, other components are required in order to properly explore all the advantages that the method presents. There is already an extensive body of knowledge describing each possible microfluidic component in great detail, be it valves[90–93], pumps [93–96], mixers [97–99], or sensors [100–103]). Thus only a brief overview of each is given below, with some examples of their use.

1.5.3.1 Actuators

Valves Microfluidic valves are used to control fluid flow, and can be classified based on their modes of operation: passive require no energy, instead actuating based on fluid direction or pressure, while active valves require energy input in order to operate. Their use depends on the type and amount of control needed for each application [9].

Passive valves are one of the simplest forms of fluid control. These can exploit the surface properties of the channel as a way to control the liquids, or rely on the liquid movement itself. Jeon et al. [104] developed two types of passive PDMS check valves (Figure 1.13). By creating either a flap or

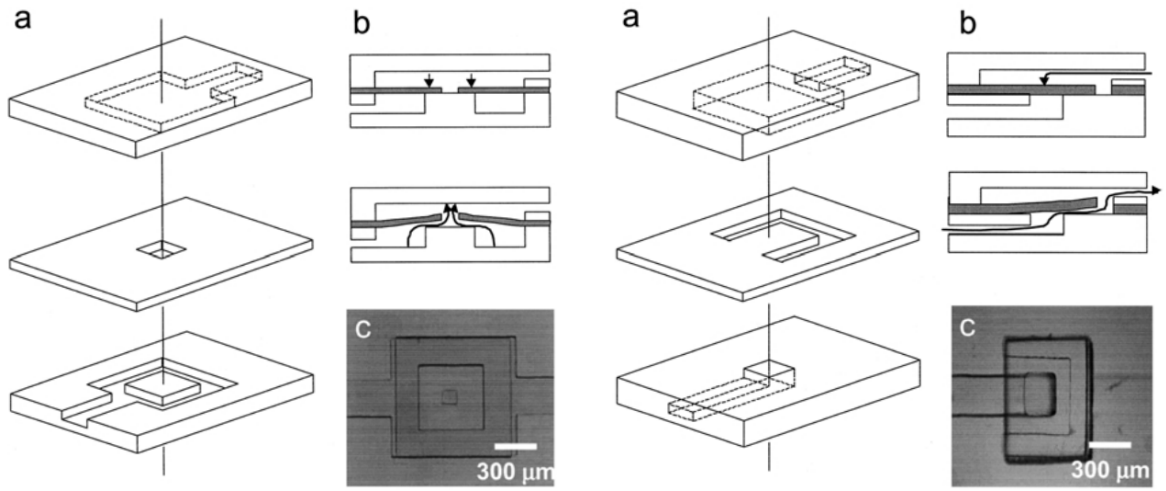

Figure 1.13: Schematic overview of two types of passive valves: diaphragm (left) and flap (right). a) simplified design, b) operational description, c) optical micrograph of the device. Adapted from [104]

diaphragm out of PDMS, the fluid is only allowed to flow in one direction, and any reversal will close the valve, blocking any movement without the need for external input. In a different approach, Feng et al. [105] developed passive valves based on hydrophobic microfluidics. By creating the structures out of hydrophilic silicon dioxide over glass, and selectively modifying its surface to be hydrophobic, in combination with a narrower section, a passive microfluidic valve is created that will only allow water to flow if a certain pressure threshold is applied, in any direction.

On the other hand, while active valves can be actuated using different methods, the most common relies on the application of air pressure to function, although some designs have also been developed that can be actuated by temperature or local chemical reactions.

Some of the first microfluidic valves developed used glass and polymer membranes, such as the work of Grover et al. [106] that developed an air pressure actuated valve made of a glass-Teflon-glass composite (Figure 1.14). By varying between positive and negative pressure it was possible to control the flow of liquid within the channel, and even modulate it to some degree, with a practically instant actuation. However, this still required the use of glass microfabrication methods, which limited its application. Unger et al. [107] tackled this issue by creating a bilayer PDMS chip, that used 2 different molds to create a fluid channel and a control channel, separated by a PDMS membrane. When the control channel is pressurized, the membrane is pushed against the fluid channel, closing it. This method avoided the use of complex fabrication techniques, instead relying on the relatively simpler soft-lithography methods, and went on to become one of the most used pneumatic micro valve designs.

While microfluidics valves are more commonly actuated using air pressure, it is possible to use different methods for fluid control. Satarkar et al. [108] developed a hydrogel nanocomposite valve that

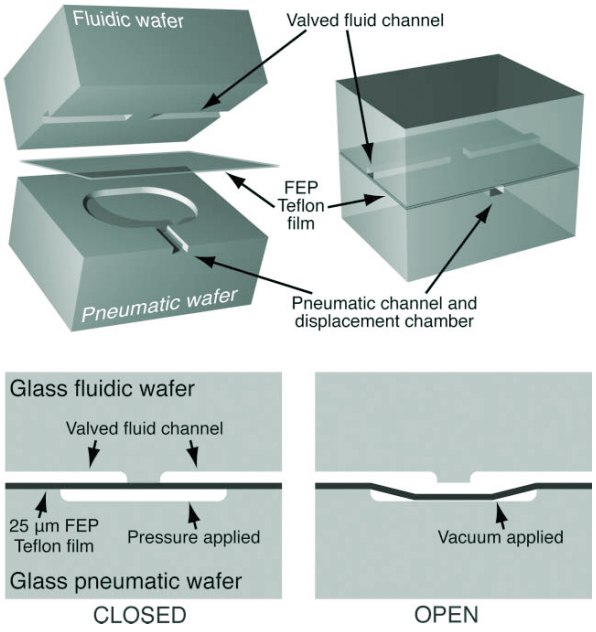

Figure 1.14: Exploded and assembled schematic of an air pressure actuated valve (top), and a cross-sectional view detailing the functioning (bottom). Adapted from Grover et al. [106]

is thermally actuated. The hydrogel is encased in a pocket underneath a membrane. When exposed to an alternating magnetic field, nanoparticles in the temperature responsive hydrogel release heat, causing the structure of the hydrogel to collapse, opening the valve. After cooling, the hydrogel recovers the initial structure, closing the microchannel.

The obvious next step after being able to control the flow of liquids within the microchannel is to integrate a pumping mechanism in the microfluidic device, so that the use of external pumps can be avoided.

Pumps There has been increased interest in the development of new micropumps for microsystem integration, not only in an attempt to decrease the overall size of the system, avoiding external pumps, but also because having closed systems can be advantageous for several analysis, protecting both user and sample.

While they can be further divided by mode of actuation, micropumps can be divided in two categories [94]:

- Mechanical displacement micropumps - these pumps move fluid using oscillatory or rotational pressure forces, either through solid-fluid interaction, like peristaltic or rotary pumps, or fluid-fluid interaction, like phase-change and gas permeation pumps.
- Electro and magneto-kinetic micropumps - this type of pumps can generate a constant/steady flow, and work by a direct energy transfer to pumping power. Electroosmotic and electrodynamic pumps are some examples commonly used in microfluidics

Some of the most commonly used are diaphragm pumps. These combine a pumping chamber with inlet and outlet valves for flow rectification.

Previously, van Lintel et al. [109] devised a piezoelectric pump based on micromachined silicon. Using the piezoelectric element as a diaphragm to create positive and negative pressures to fill the pumping chamber, the authors report flow rates up to $8\,\mu L\,min^{-1}$. Still, the need for high voltages and the complexity of manufacturing of these pumps have limited their applications.

Grover et al. [106] combined one way valves with a Teflon film that acted like a diaphragm. By switching between positive and negative air pressures they could reach a flow rate of $1.1\,\mu L\,s^{-1}$ within the microchannel. Jeon et al. [104] used a similar method to create a manually actuated pump. Using check valves and a reservoir, they devised a construction that could be actuated by manual pressure on the reservoir. Although limited, this approach can be sufficient for devices that need to transport limited amounts of fluid, avoiding the use of any external equipments for fluid flow.

Finally, after the development of the single, easy to manufacture, pneumatic valve by Unger et al. [107], the researchers noted that multiple valves could be used in sequence to create a peristaltic motion. This peristaltic pump was capable of a flow rate of $2.35\,nL\,min^{-1}$. Liu et al. [110] reported an interesting system that took a diferent approach to the peristaltic motion. The authors embedded a magnetic material into a layer above the microchannel, separated by a thin PDMS membrane (Figure 1.15). By rotating a magnet under the microchannel, the membrane would be pushed by the magnetic material, creating a constriction that can then be moved, forcing the fluid within the channel to move. Flow rates up to $50\,\mu L\,h^{-1}$ could be achieved, while the entire system is of relatively simple construction and low cost. On a different note, Takamura et al. [111] used electroosmotic flow as

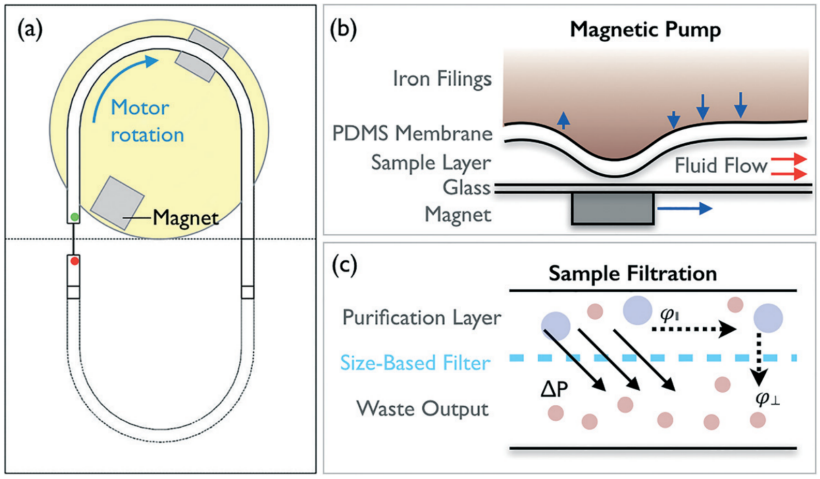

Figure 1.15: Mechanism of operation of a magnetically driven peristaltic pump used for microfluidic filtration. Adapted from Liu et al. [110]

pumping mechanism in their structures. The authors used narrower channels combined with salt-bridges as electrodes, and reached flow rates of $415\,nL/min$. This type of pumps is notable on the fact that the fluid moves like a plug, and can be controlled, even if the microchannel branches at some point, by the potential difference between inlet and outlets. Nonetheless, it faces large limitations on the choice and placement of electrodes, since its high voltages requirements can induce electrolysis, creating air bubbles in the channel. The electrodes can also be subjected to oxidation or otherwise become damaged. Another issue to take into account is the electrophoretic effect on the fluids, par-

ticularly in the case of chips for healthcare applications, where samples can contain several proteins and nucleic acids in suspension [111].

Juncker et al. [112] demonstrate a different approach to pumping fluids, by reporting an autonomous microfluidic capillary system. Their system includes a reaction chamber followed by a capillary pump. By simply depositing a solution at the inlet, it will flow by capillary action, until it reaches a capillary retention valve. By depositing a new liquid at the inlet the process is repeated, and they could perform multi-step immunoassays within the reaction chamber. A similar passive solution was used by [81], where the designed microfluidic device used capillary action to move fluid inside the channel at different flow rates along an assay, depending on the requirements of each step, without the need for any external actuation.

1.5.3.2 Mixers

As previously described in section 1.5.1.2, under laminar flow conditions mixing can only occur by diffusion. While this can be sufficient for some processes, or even exploited on some particular cases, it becomes a significant issue on those that require a proper mixture. Diffusion is a slow process, particularly when dealing with large particles like cells, thus several mixing mechanisms have been developed to address this issue [9].

Micromixers can be fundamentally divided into two categories, passive, which rely mainly on molecular diffusion and chaotic advection, or active, which use an external field to induce the mixing, be it pressure, temperature, electromagnetic effects or acoustics [97, 98].

Given that diffusion is limited by distance and particle properties, one of the simplest methods to improve mixing is lamination. By using the channel geometry to split and fold fluid streams, it is possible to increase the contact area of the different fluids, improving the mixing by diffusion [9, 98]. Some structures that make use of this are exemplified in Figure 1.16.

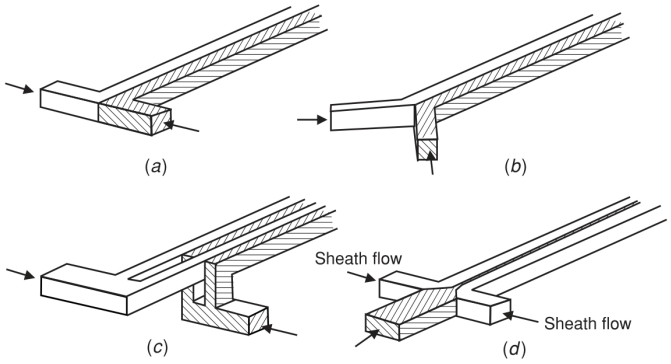

Figure 1.16: Various methods used for laminar mixing: a) T-mixer, b) Y-mixer, c) parallel lamination, d) hydraulic focusing. Adapted from Nguyen and Wu [97]

Another option is chaotic advection. Since advection is usually parallel to the flow of liquid in a channel, a way to improve it is by disrupting the laminar flow of the fluid, by using special structures like obstacles or combinations of carefully designed bends, ridges and constrictions[97].

Kumaran and Bandaru [113] demonstrated a simple way to disrupt the normal laminar flow con-

ditions of a channel, by making one of the walls of the channel soft. The instability created by this soft wall is enough to sharply increase the mixing in the structure, and the degree of mixing can be tuned by adjusting the flow rate of the fluid or the shear modulus of the soft wall. Fan et al. [114] showed another approach to mixing, by using simple sharp corners on the channel. When combined with relatively high flow rates, thin multilamellar fluid structures are created in these areas, that accelerate mixing in a very short time. A different method is presented by Hong et al. [115]. In their work, the authors used Tesla valves, a structure normally used as a one way valve, and combined them to create a device that combines convection and diffusion to achieve a thorough mixing, while being simple to fabricate and completely passive (Figure 1.17). On the other hand, active mixing methods

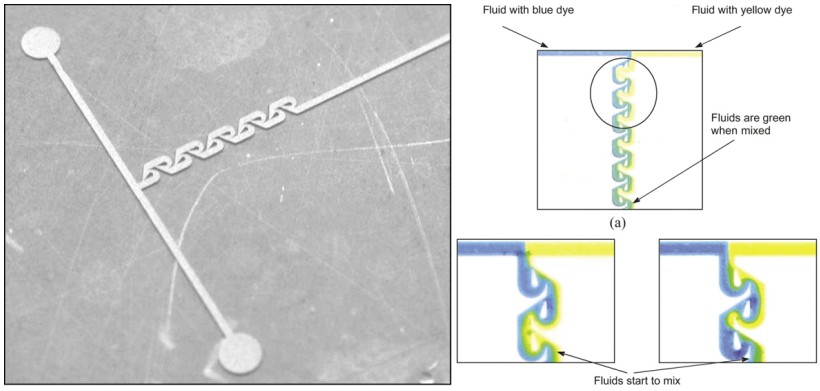

Figure 1.17: SEM micrograph of a micromixer mold using Tesla valves (left), and captured video frame of the micromixer in use, demonstrating the mixture of two differently coloured fluids (right); Adapted from Hong et al. [115]

rely on external inputs to induce mixing. The most obvious way is to integrate a microstirrer in the mixing channel, in a process similar to bench top magnetic stirrers, however this is not trivial to implement given the dimensions of the channels. Ballard et al. [116] devised a magnetic microstirrer, using magnetic microbeads and an external permanent magnet. First, the authors patterned nickel/iron poles on the channel floor. Then, by applying an external magnetic field, in the form of a permanent magnet, and injecting magnetic microbeads in the channel, the beads are attracted to the poles. At this point, by rotating the permanent magnet, and thus rotating the magnetic field, the particles rotate around the poles, effectively creating a large number of magnetic stirrer bars within the microchannel. This method was able to mix even still liquids much faster than diffusion alone, at the cost of higher complexity of fabrication, with the need for moving parts inside the channel.

An alternative method is to use serial segmentation. While the lamination method divides the fluids to increase the contact area and shorten the diffusion distance, this method achieves the same by using alternate injection of the fluids, creating plugs that then mix by diffusion and Taylor dispersion along the channel. This method was adapted and improved on the work of Cortelezzi et al. [117]. Here the authors used 3 inlets, two for a carrier solution, and one for a medication they wished to mix, connected to a mixing chamber with an obstacle at the middle. By keeping a steady flow on the medication inlet, and injecting the carrier solutions harmonically in time, but in opposition of phase, the solutions created serial lamellae of opposite concentrations, that in combination with a large mixing

chamber that stretched them further, allowed for a fast mixing effect.

Regarding the application of acoustic methods, the simplest application consists in the use of piezoelectric transducers to create acoustic waves and streams within the channel. While this has proved to be a very fast and effective method, it also has serious limitations for biological or chemical applications, since the use of high frequencies can cause cavitation, and the acoustic energy added to the system can cause temperature increases that can affect the samples [97, 98]. An example of this is the work of Cui et al. [118], where the authors created a thin-film piezoelectric resonator that used ultra-high frequency acoustic fields, achieving a 87% mixing efficiency in $1\,\mathrm{ms}$.

Nonetheless, the choice of mixer is always dependent on the type of system used, since their efficiency can depend on the flow rate and the type of reagents used [9].

1.5.3.3 Sensors

While the small scale of microfluidic devices does present great advantages, it is not without limitations. One of them is the extraction of useful data from the devices, where the small sizes used can become a problem for signal transduction and sensor integration. By using lower volumes, the amount of material to be detected is also reduced, increasing the need for higher sensitivity. This is a current challenge for microscale applications, with increased research efforts being put into creating more responsive and smaller sensors, as well as in creating different methods with responses measurable by current sensors.

The current methods used in microfluidic devices can be divided into three main categories:

- Electrochemical - Measures conductance, resistance, or capacitance; Can provide real-time detection, with low fabrication costs. However, they present a short life either in shelf and when in use, and require a good control of ionic concentrations before use [119].

  An example is the common three-electrode setup, that has been adapted for modern microfluidic application. Dungchai et al. [120] developed an electrochemical biosensor with a working and counter electrodes made from carbon ink, and a silver/silver chloride ink as reference electrode. This sensor could simultaneously measure glucose, lactate and uric acid in biological samples, as well as small molecule markers when modified with enzymes, in about $100\,\mathrm{s}$. The measurements were done using chronoamperometry, and the sensor showed limits of detection and quantitation of $0.21 \pm 0.02\,\mathrm{mM}$ and $0.70 \pm 0.06\,\mathrm{mM}$, respectively, for glucose, $0.36 \pm 0.03\,\mathrm{mM}$ and $1.19 \pm 0.11\,\mathrm{mM}$, for lactate, and $1.38 \pm 0.13\,\mathrm{mM}$ and $4.60 \pm 0.43\,\mathrm{mM}$ for uric acid. Also, a limit of detection of $3.6 \pm 0.3\,\mathrm{mM}$ and a limit of quantitation of $11.9 \pm 1.1\,\mu\mathrm{M}$ were achieved for H_2O_2, using oxidase enzymes.

  MicruX shares a similar design in their commercial microsensors, incorporating microfluidic channels with thin-film electrodes. These can take amperometric measurements, and are sold already bonded to a microfluidic structure, or as single chips to be replaced after use with an external device. The electrodes are made from a layer of $150\,\mathrm{nm}$ of either gold or platinum, with different possible configurations and surface areas [121].

While electrochemical detection does present some key advantages for miniaturized analytical systems, like high sensitivity, good precision, low cost and power consumption, and their easy incorporation into microfluidic chips, they can still present large variations from shifts in temperature, pH, and ionic concentrations [119].

- Mechanical - This type of sensor works by measuring variations in resonant frequency or surface stress, for example caused by protein adsorption to a surface. They can be extremely sensitive, with limits of detection in the order of fento to picograms [122]. However, while they can be integrated as a monolithic sensor, with very fast detection time and label-free detection, these sensors can be complex to fabricate, and have found limited applications in liquid samples due to damping effects [119].

  These sensors can usually be divided in cantilevers and bridges, although other types of mechanical sensors also exist, like quartz crystal microbalances. They are mainly operated in one of two modes: a dynamic mode, in which the sensor oscillates with a particular resonance frequency that is changed when the target molecules interact with its surface, or in static mode, where this interaction causes surface stress on the sensor, deflecting it. This deflection can be measured by laser reflection, piezoresistive measurements, or capacitance changes [123].

  Gfeller et al. [124] described the use of these sensors as a method to test for antibiotic susceptibility by measuring bacterial growth. Cantilevers where functionalized with agarose, which was submerged in LB Broth inoculated with *E. coli*. They then measured the frequency of the cantilever by reflecting a laser on its tip, using a position sensitive detector. The sensor could detect mass changes equivalent to $\approx$ 100 *E. coli* cells, sufficient to detect the antibiotic susceptibility within 2 hours. However, although these experiments where performed under high humidity conditions (37ºC, 93% humidity), they are still limited to conditions where the cantilever is exposed to air, and not submerged. Due to this fact, several steps are required during the functionalization and cell inoculation to keep the system in working conditions.

  On the other hand, other researchers tried to develop mechanical systems that could be used in liquids. For example, Leahy and Lai [125] have demonstrated a system capable of real-time *E. coli* cell detection in liquid, by combining a cantilever design with electrokinetic effects. In short, the authors designed a cantilever with a micron-sized gap between its free-end and a wall. By applying an AC voltage across the cantilever and the wall, they were able to induce an electroosmotic flow, as well as dielectrophoretic collection of cells in the region. The cantilever frequency is measured with the use of a reflected laser, and shifts with the presence or absence of cells in the gap. This system was capable of detecting cell concentrations as low as 100 cells/mL. Nonetheless, it required careful preparation of samples, and the non-specific response given by the deposition of particles across the gap are still critical points that require improvement.

- Optical - Detects variations in light intensity, refractive index sensitivity, or interference pattern. It can provide real-time detection, with minimal sample handling and preparation. However, the instrumentation required can expensive and complex to set-up, if not already available in the

laboratory.

It is the most used detection method in microfluidic platforms, relying on optical detection of biomolecules to achieve a high sensitivity, while using optical instrumentantion comonly available in most laboratories (optical and fluorescence microscopes) [119]. These techniques can either detect the light emitted by fluorescent markers attached to the molecules of interest, their absorbance in the ultraviolet range, or detect bio/chemiluminescent signals [7].

Chemiluminescence is particularly useful in detecting biomolecules in microsystems when compared with fluorescence or colorimetry, since it does not require an external light source nor excitation light filter. This relative simplicity makes it easier to integrate in a fully portable system. Also, when combined with sensitive optical sensors such as photodiodes, very low limits of detection can be achieved while keeping a small form factor for integration. Santos et al. [126] described such a system, where two different types of optical sensors were integrated in a microfluidic device, and used to measure several biological parameters without the need for a microscope.

While fluorescence has been used to measure temperature, cell functions, flow velocity, flow profiles, and polymer dynamics, the fluorescent molecule used can interfere with the process studied, and not all experiments allow for the use of fluorescent chemicals.

1.5.4 Microfluidic Applications

Considering all the development done on different microfluidic modules and components, it becomes obvious that this type of systems hold the potential to accelerate the development of new industrial processes for biomanufacturing applications. As such, it is important to note how microfluidics is already being applied to all stages of biomanufacturing, from the upstream stage, with the creation of microbioreactors, to the downstream stage, where multiple large scale processes have already been miniaturized and the devices used for condition screening and process optimization.

1.5.4.1 Microbioreactors

As already noted in section 1.3, the first stage of a biomanufacturing process includes the selection of the best performing microbial strain, as well as the optimal cultivation conditions for the production of the target product. This can require several rounds of experiments before the optimal conditions are found, increasing the time and cost of the process. Microfluidic techniques have been proposed as a potential solution to this issue by enabling high-throughput breeding and screening of microbial strains, using parallel and scalable culture and detection chips that can be integrated and tested [127, 128].

Various microfluidic chips capable of bacterial suspension cultures have been described, with the most common approach using a chemostat and turbidostat type of reactor for screening, with other types of reactor more commonly found for biomass production or for analytical applications.

As mentioned in section 1.3.4.3, a chemostat is a culture vessel in which microbial cells reach

Table 1.7: Overview of microbioreactor platforms and their essential characteristics

Reactor type	Material	Volume (µL)	Sensors and control	
Batch	PDMS/Glass	50	DO, pH, OD	Zanzotto et al. [130]
Chemo and turbidostat	PDMS/PC	1000	DO, pH, OD	Lee et al. [98]
Batch Array	Polystyrene	250	DO, pH, Temperature, OD	Maharbiz et al. [131]
Batch	PMMA/PDMS	1000	pH, OD	Buchenauer et al. [132]
Batch	PDMS/PMMA	150	DO, pH, OD	Zhang et al. [128]
Turbidostat	PDMS	n.a.	Pneumatic valve and fluorescence intensity	Luo et al. [133]
Batch	PDMS	50	DO, pH, OD, fluorescence and luminescence	Zanzotto et al. [134]
Fed-Batch	PEEK, polyimide, PDMS	700	pneumatic valve control, pH, OD,	Buchenauer et al. [135]
Batch and Fed-batch	PMMA/PDMS	500	pH, OD, DO, fluorescence,	Funke et al. [136]
Batch	PDMS	100	OD, DO, pH	Lee et al. [137]
Batch	PMMA/PDMS	150	OD,DO,pH	Szita et al. [138]

a steady state condition, with biomass production, substrates, and product concentration remaining constant [128]. First described by Novick and Szilard [129], a steady stream of nutrients is flown into the culture tank, at the same rate that bacterial suspension is removed, with the goal of keeping the bacterial population growing at a reduced rate for an indefinite period of time.

Regardless of the type of reactor used, multiple approaches have been taken in trying to create a functioning small scale bioreactor, with different materials, volumes, and integrating a variety of sensors, and an overview of these works can be observed in Table 1.7.

One of the first microfluidic chemostats was developed by Balagaddé et al. [139], a 6 chamber, 16 nL reactor (Figure 1.18).

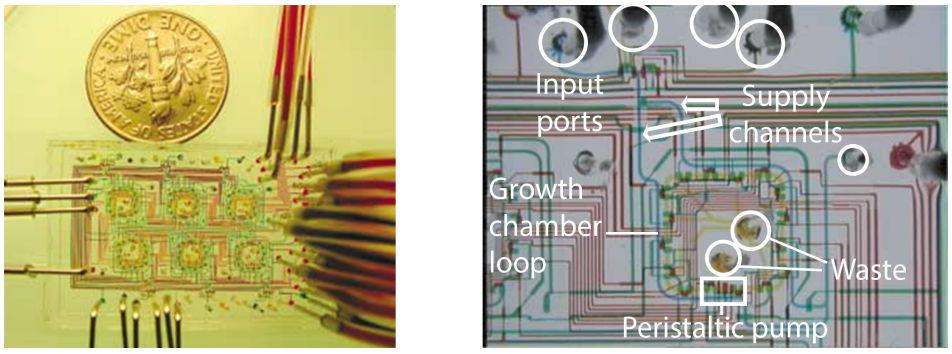

Figure 1.18: Optical micrograph of a parallel chip containing six parallel chemostats (left), Detail of a single microfluidic chemostat and its components (right); Adapted from Balagaddé et al. [139]

Each growth chamber had 16 addressable segments, with integrated peristaltic pump, and valve actuated medium exchange, waste removal, and cell recovery. The device was used to test different growth media, temperature, and dilution rates, with a different set of conditions in each of its 6 chambers, paving the way for a faster and cheaper screening of culture conditions. However, the device is highly complex in both construction and control, with several PDMS layers for valves and channels. It also lacked any type of integrated sensor, instead requiring the use of image capture and analysis equipment and software to collect useful data, limiting its applications.

On the other hand, Zhang et al. [128] described a microchemostat with optical density, pH and dissolved oxygen real-time measurements, for continuous culture of *E. coli*. With a working volume of 150 µl, the microdevice was able to test different steady state conditions in a short period of time, and could function without contaminations for over 180h. Still, while this device is simpler in construction compared to the previous example, it still requires six layers made from different materials, and several

different bonding methods to create the final structure. In addition, while it integrates several sensors for a better control of the conditions of the culture, it still required large external equipment for data acquisition.

On a different note, Luo et al. [133] focused on the development of a turbidostat, a device that maintains long time bacterial cultures at constant optical density. The microfluidic structure uses an agarose filter to allow nutrient exchange without loss of biomass, and pneumatic valves, optical microscopy and a computer controlled loop to maintain a constant cell density within the culture chamber. However, the very small culture chamber limited the system to low cell densities, while still being constrained by the need for large devices for control.

As noted, increasing the number of reactor chambers and control structures in a microchip can increase its complexity to the point of making its use prohibitive, particularly for scaling up. Focused on the scalability of microreactors for high throughput bacterial suspension culture, Gan et al. [127] developed a microchip with 8 independent bioreactors, that can be controlled with only three control channels. The chip, represented in figure 1.19, integrated a micropump capable of manipulating the flow through all chambers, and allows for the direct comparison of up to eight different medium conditions, with equal dimensions and flow rates in all the chambers. The system was also tested with different organisms. Several approaches have been taken in trying to apply the existing large scale

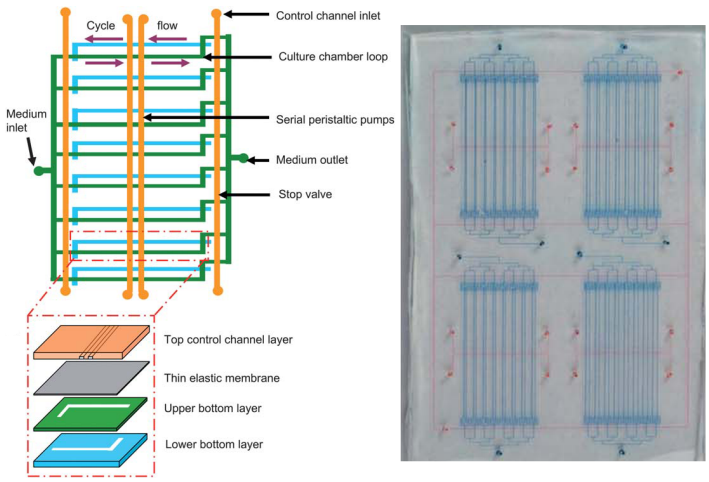

Figure 1.19: Schematic representation of a multi reactor chip, with the overall design and layered detail (left); Photograph of the chip with 4 identical loops (right). The control channels are filled with a red solution, and the culture chamber loops with a blue solution; Adapted from Gan et al. [127]

technologies to microscale reactors. However, while most of the technical challenges in creating and maintaining an adequate environment have been overcome, most of the systems developed still rely on large scale devices and actuators to maintain these conditions. Also, they are compromising between ease of manufacture, assembly and use, that are highly complex for the microscale devices presented, and the possibility of screening several conditions faster and cheaper. Nonetheless, there has been limited applications of these systems to current problems, and little work as been done in relating the findings at the microscale with the large scale behaviours of bioreactors, where these microscale optimizations could have significant economical impact. Finally, the potential to use these devices as a representation of the upstream stage of a larger bioprocess remains to be explored, with

most works focusing solely on the reactor, and not on how it can be integrated with other operations or devices.

1.5.4.2 Cell lysis

If the goal of integrating complete bioprocesses in a microfluidic chip is to be achieved, cell lysis has to be scaled down, so that intracellular products can be recovered.

In the same way that not all methods are usable at larger scales, some methods scale down better than others [48]. Thermal, chemical and electrical lysis are more commonly used in microchips, since they are easier to miniaturize, however mechanical lysis has also been used at these scales.

Table 1.8 presents an overview of some works developed in this topic. It is possible to observe that

Table 1.8: Microfluidic lysis summary table

Author	Type	Target mol.	Organism	Lysis Effic.
Aly Saad Aly et al. [140]	Chemical	DNA	M.luteus, K.rosea, P.putida, E.coli	Not quantified
Buser et al. [141]	Electromechanical	Lysis	M.marinum, S.epidermidis	∼50%/compared to benchscale bead
Rosa and Kaler [142]	Electrical/Enzymatic	Lysis	E.coli	Up to 80%
Hwang et al. [143]	mechanical/chemical	DNA	S.aureus/MRSA	Not quantified
Jiang et al. [144]	Chemical	DNA	K.pneumoniai, C.koseri, S.aureus, E.coli, P.aeruginosa, E. faecalis	Not quantified
Kim et al. [145]	Mechanical	DNA	E.coli	∼65% compared to standard protocol
Kulinski et al. [146]	Chemical/Mechanical	DNA	E.coli	Not quantified
Lee et al. [147]	Electrochemical	DNA	S.epidermidis, E.coli, P.putida, S.mutans	Not quantified
Mahalanabis et al. [148]	Chemical/Mechanical	DNA	E.coli, B.subtilis, E.faecalis	Not quantified
Privorotskaya et al. [149]	Thermal	Lysis	L.monocytogenes v7	>90%(at the surface)
Tandiono et al. [150]	Mechanical	GFP/DNA	E.coli	∼100%
Tsougeni et al. [151]	Thermal	DNA	S.typhimirium, E.coli	∼100%
Van Heirstraeten et al. [152]	Chemical/Enzymatic	DNA/RNA	S.pneumoniae, S.aureus, H.influenzae	Not quantified
Wan and Yeow [153]	Chemical	Lysis	E.coli	90%@30min, 95%@45min, 100%@60min
Wang et al. [154]	Electrical	Lysis	E.coli	∼95%

most techniques have been developed and tested as methods to extract genetic material, for on-chip

amplification or otherwise. A consequence of this is that there has been limited attention to lysis as an extraction method for the development of biotechnological applications. Nonetheless, some of these can potentially be adapted for different goals.

It is also worth noticing that, even though some lysis methods are simpler to miniaturize than others, it is possible to find examples of chemical, mechanical, and physical lysis adapted to microfluidic systems.

For example, Schilling et al. [155] developed a method to lyse bacterial cells for large protein extraction, shown in figure 1.20. A cell suspension and commercial chemical lytic agent are injected

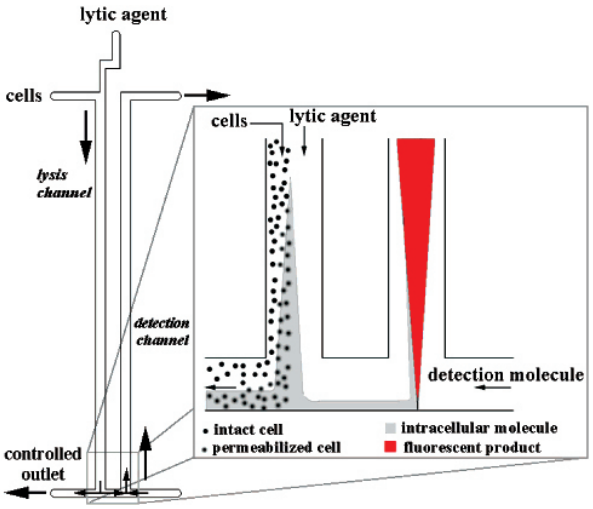

Figure 1.20: Representation of a microfluidic device for cell lysis and detection of intracellular components. Adapted from [155]

in parallel in a straight channel, mixing by diffusion, and the lytic agent causes the protein to be released to the surrounding liquid within 190 seconds, where it can then be extracted. Still, the goal of the device was to give a rough estimate of the concentration of the protein, and not to achieve full cell lysis nor product recovery.

On the other hand, Bao and Lu [156] created a device for rapid electrical lysis. By using small isolating beads to capture and concentrate the cells, the fluid area was also largely decreased, which increase the local electrical field for improved lysis. Very fast lysis was observed after the electric pulse was applied, with full protein release in about 50 seconds. The main microfluidic device can also be reused after replacing the microbeads. While not able to operate in continuum, this makes it an excellent system for simple single point protein release, such as those found in some analytical procedures. A similar system was also developed by Wang et al. [154] using continuous DC voltage, avoiding the use of a cell concentration step. A cell feed is moved through a microfluidic channel by DC electric field. The microchannel contains a constriction in width, which causes the electric field intensity to increase locally. This allowed for continuous cell lysis at lower field intensities, avoiding problems like water hydrolysis.

Finally, Kido et al. [157] developed a plastic disk based system for sample homogenization and cell lysis, that uses bead-beating and mechanical stator-rotor lysis in a semi-disposable system. While it can be integrated with centrifugation, and lyse all types of cells, the need for specialized equipment,

and the structural complexity of the device have limited its application.

1.5.4.3 Separation in microfluidics

Not only has the separation of biomolecules acquired a new importance in microfluidics by allowing very small volumes or low analyte concentrations in pathological conditions to be studied and analysed, but the fast and relatively inexpensive results obtained at microscale can sometimes also be translated into larger scale processes. This means that microfluidic applications can have a screening function, rapidly accelerating the development of new processes. Almost all types of separation have now been scaled down into microfluidic applications.

After the release of an intracellular product, this product needs to be concentrated and purified. Current microfluidic solutions for protein purification have mostly focused on chromatography, affinity capture and electrophoresis [122, 158–160]. Malmstadt et al. [161] used a smart polymer bead conjugate to create a stationary affinity chromatography matrix within a microchannel. The system demonstrated good binding and elution capacity using biotin-streptadivin complex, in a temperature dependent fashion, without the use of harsh chemical eluents. On a different approach, Pinto et al. [159] developed a nanoliter-scale system for analysis and optimization of multimodal chromatography. This microdevice allowed for the optimization of the process using reduced reagent volumes <$50\,\mu l$, with low ammount of resin (about $70\,nl$), and the very fast assay ($<1\,\mathrm{min}$) allowed a wide range of pH and conductivities to be tested in a very short time. This system was later adapted to screen several sets of conditions in a very short time, by integrating thin-film photosensors for detection and pneumatic valves for adsorption/elution automation [162].

Nevertheless, most of these techniques operate in batch, and require multiple steps in each process. This goes contrary to the current interest in moving to continuous processes, with greater productivity and lower costs [163]. A potential approach in this regard is the use of ATPS, a common approach for protein separation and purification that can be used at both bench and laboratory scales.

As mentioned in section 1.4.2.2, this type of system allows for protein extraction with good yield and selectivity and can eliminate most of the contaminants such as cell wall debris or nucleic acids in a single step. It becomes of interest when combined with the laminar flow profile of microfluidic devices, that facilitates the formation and stabilization of two-phase flow [158]. Previous works have demonstrated that microfluidic devices can be used as a simple and fast method to characterize an ATPS [164], and also a tool to optimize affinity-driven partition conditions for specific products [165].

1.6 Thesis outline

This work is divided into four main sections: the first section started by giving a brief overview of what encompasses a biomanufacturing process and how it is divided, with a mention of the most common approaches for the different stages at the macroscale. This is followed by a short introduction to the world of microfluidics, starting with an overview of the physics at small scale, followed by common microfluidic components and their manufacturing processes, and finally ending with a short

review of previous microfluidic applications and how they could or were used for the development of bioprocesses.

The second section mainly concerns the development and characterization of a microfluidic bioreactor, focusing on the design, manufacturing and testing of each module, and finally the integration into the final device and fermentation testing.

The third and forth sections focus on the downstream processing of cell samples, describing the development of a microfluidic cell lysis chip for screening and optimization of product release from chemical and enzymatic lysis, and its integration with a second microfluidic module used for the optimization and screening of continuous protein separation and concentration conditions.

Finally, this thesis ends with overall conclusions and potential lines of future work, as well as the list of publications and presentations that resulted from this work.

2

Microbioreactor development and characterization

2.1 Introduction

This chapter focuses on the development of a microbioreactor for the growth of *E. coli* cells. Biotechnological manufacturing processes begin with the production of a molecule of interest, using the metabolic machinery of an organism. As such, the efficiency of these processes depends on the selection of the best performing strain and optimal culture conditions. While this area has been the subject of the largest advances in the biomanufacturing process, it still is an important stage that can include a variety of experiments and optimizations, which can further delay the development of new processes. As such, there is a need for the development of faster, high throughput methods that can accelerate the creation of new and reliable bioprocesses.

The application of microfluidics to this problem has led to the development of new microreactors. These microdevices exploit the advantages of microscale, with reduced reagent consumption, increased safety, high surface-area-to-volume-ratios, and improved mass and heat transfer control, while still creating reliable information regarding larger scale applications. In particular, microbioreactors that can operate in continuous, such as microchemostats, present the increased potential to accelerate the development of new processes, given their ability to rapidly change conditions and observe its effects without performing multiple parallel experiments. This means that it is possible to perform multiple assays in a single device, in continuous, with almost immediate feedback and control.

The development process of this type of devices follows the engineering design-build-test-evaluate cycle for each component of the bioreactor, which is also applied to the final integrated system. The final goal of this work is the development of a functioning microchemostat, capable of rapid testing of different conditions in continuum.

At its core, a microchemostat can be divided into 5 main components: a vessel where the cells are contained, an actuation mechanism to move liquids into and out of the reaction vessel, a temperature control mechanism to maintain optimal temperature throughout the experiments, integrated sensors to monitor the progression and extract useful data from the experiments, and finally a control system that connects to all the other components, collects data and changes conditions as needed.

2.2 Materials and methods

2.2.1 Chemicals and biologicals

LB Broth and LB Agar cell culture mediums were obtained from Nzytech. Tris-buffer, *E. coli* bacterial strains BIVU0811 harboring the pMAB1-GFP-C-lytA plasmid were kindly supplied by Biomedal (Seville, Spain). A Milli-Q® water purification system was used to supply water for all experiments (Millipore, Bedford, MA, USA).

2.2.2 Microfluidic structure design and fabrication

The final microfluidic device is composed by two main components, a fluid layer, containing the microreactor channel, and a control layer, that integrates all the actuation components.

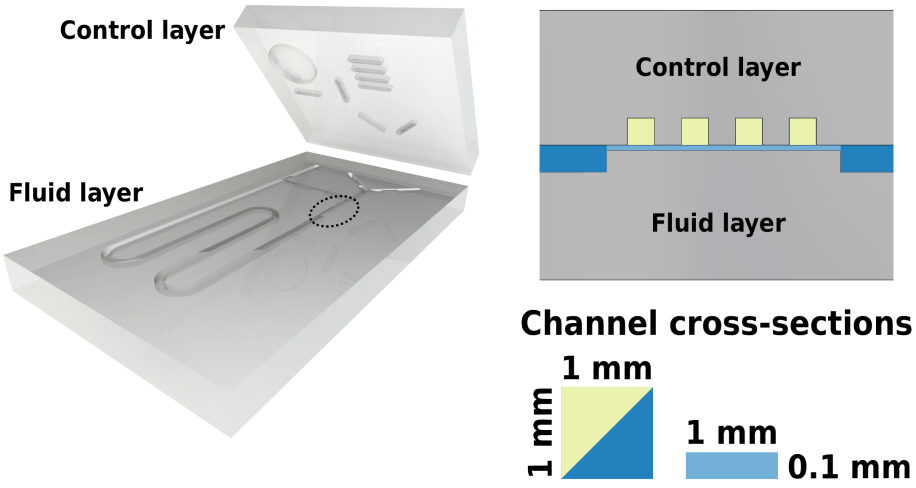

Figure 2.1: Channel design, cross-section, and overlapping profile of the fluid and control layers. Microfluidic channel is represented in blue, while the pneumatic valves are represented in yellow.

2.2.2.1 Fluid layer design

The first stage of designing a microchemostat is defining its final application, and the constrains and specifications that it should adhere to. In this case, the goal is to develop a continuous bioreactor where *E. coli* cells can grow to an optimal density, produce a product of interest, in this case GFP, and that can then be used to feed other microfluidic devices downstream for process optimization. It should be able to provide a constant outflow of about $2\,\mu L\,min^{-1}$ to $20\,\mu L\,min^{-1}$ of cell suspension for this purpose. In addition, it should provide a simple mechanism to change the growth conditions during use by injection of different components into the medium.

The design needs to take into account the basic characteristics of the organism to grow, in particular its optimal growth conditions, and corresponding growth rate. In the case of the *E. coli* strain used in this work, these correspond to a temperature of $37\,°C$, under agitation, in LB growth medium. The typical doubling time for this type of cells is about $20\,min$, which corresponds to a specific growth rate of about 2.

The theoretical model for a chemostat operation determines that, under steady state conditions and with no washout, the dilution rate will be equal to the growth rate, and from this it is possible to calculate that a total volume of about $90\,µl$ would be sufficient for operation under the determined conditions. This value was doubled to account for mass transport limitations that are known to decrease the actual growth rate in chemostat operation.

With the preliminary parameters determined, the vessel was designed with a total volume of about $150\,µl$, and a channel cross-section of $1\,mm \times 1\,mm$ (Figure 2.1(a)). The design included a single outlet for sample collection, and two inlets for multiple liquid insertion. It also accounted for multiple valve sections for fluid flow control and pumping, as described in the following section.

2.2.2.2 Control layer design

While a bioreactor can operate without any input or output of liquid, chemostat operation requires a continuous input and output.

Considering the various microfluidic valve designs have been described in the literature, as detailed in section 1.5.3.1, the simplest valve mechanism requires two distinct and perpendicular channels, separated by a thin PDMS membrane, also known as a Quake valve. By applying a positive pressure on one of the channels, the membrane will deflect, collapsing the other. The degree to which this type of valve can completely stop the flow of liquid in a channel will depend on the existent pressure inside each of the channels and the actuation pressure being used, the thickness and flexibility of the PDMS membrane, and the cross-section profile of the channel to be closed.

Each valve was designed as a $1\,mm$ wide channel, to be perpendicularly sealed against the vessel channel, so that the cross-section of both results in a $1\,mm \times 1\,mm$ square (Figure 2.1(b)). Since the performance of a valve can be affected by multiple factors, different combinations of valve channel widths, membrane thickness and flexibility, and valve separation space, were designed and tested regarding the minimum air pressure required for actuation, the ability of the membrane to return to the original position after actuation, overall durability and, in the case of the combined peristaltic pump, their effects on the total flow rate achieved. This optimization work of the valve assembly was previously performed in collaboration with an exchange bachelor student (data not shown).

During the design stage, various valve structures were created by milling a piece of PMMA, creating grooves corresponding to the valve channels, with metallic air inlets glued in place. This allowed for the rapid manufacturing of multiple valve designs that could be tested by creating a mechanical seal by pressure against the microfluidic channel.

2.2.2.3 Microfluidic structure fabrication

Given the relative large dimensions of the designs, typical photolithographic processes cannot be used for the fabrication of this type of structures. Instead, Computer Numerical Control (CNC) milling was used to rapidly create accurate PMMA molds directly from a Computer Assisted Design (CAD) file, which were then be used to create the final PDMS structures. The rapid turnaround time of this manufacturing method also allows for a faster iterative optimization of multiple parameters, from testing new designs to improve liquid flow and hydraulic resistance, to testing different milling parameters for optimal surface properties on the final mold.

A key aspect for mold production is the surface finishing. The final microfluidic structure is fabricated by pouring PDMS on a PMMA mold, curing it for $90\,\mathrm{min}$ at $70\,^{\circ}\mathrm{C}$, and sealing the cured structure against a thin PDMS membrane. As a consequence, the sealing surface of the PDMS structure will replicate the roughness of the mold, which can impair the sealing effectiveness if the final surface presents large imperfections. Previous works have described that the final surface roughness of machined PMMA depends mainly on the feed rate [166, 167], with slower feed rates creating smoother surfaces. However, slower feed rates can dramatically increase the time needed to fabricate a single mold, specially when large areas need to be machined. Considering the size of the features in the final design, a $2.5\,\mathrm{mm}$ endmill was selected for the machining, in order to cover the largest possible area in each passing, while still defining the full structure without artifacts. Multiple molds were then manufactured varying the feed rate between $600\,\mathrm{mm\,min^{-1}}$ to $100\,\mathrm{mm\,min^{-1}}$.

PDMS structures were prepared by first mixing a 1:10 mixture of PDMS:curing agent (Sylgard 184 silicon elastomer kit, Dow-Corning), adding a black pigment (40 Ivory Black, Pigmenti Puri CP0147AO, Ferrario S.P.A) at a 1:20 ratio, with vigorous mixing, followed by degassing before pour, creating an opaque PDMS mixture as previously described [168]. Each mold was filled with this PDMS and test sealed against a $150\,\mu\mathrm{m}$ thin PDMS membrane.

The final molds for the fluid layer were produced using a feed rate of $100\,\mathrm{mm\,min^{-1}}$, at 7500 rpm, while the control layer was manufactured using a $1\,\mathrm{mm}$ endmill with a $100\,\mathrm{mm\,min^{-1}}$ feed rate, at 10000 rpm.

2.2.3 Valves control and addressing

The control channels were filled with de-ionized (DI) water using capillary tubing, connected to a compressed air line and subjected to a pressure of $100\,\mathrm{kPa}$ overnight. This is done to prevent the diffusion of air through the PDMS during actuation, which can create bubbles inside the channel.

Two 4-port solenoid air controllers were used to control the airflow into the control layer. Each port was connected to a control channel through plastic tubing, and controlled through a custom circuit.

2.2.4 Microfluidic peristaltic pump flow rate characterization

In order to characterize the behavior of the peristaltic pump regarding its flow rate in function of the actuation frequency, a piece of capillary tube was cut and marked at $1\,\mathrm{cm}$ intervals using a caliper.

The reactor channel was then filled with DI water, and the pump actuated at a known frequency, timing how much time was required for the liquid to cross each marking. Since the inner dimensions of the capillary tube are well defined it is thus possible to calculate the flow rate induced by the pump.

2.2.5 Heating element

One of the key elements in maintaining a cell culture is temperature. Temperature variations can modify the growth rate of several organisms, and it is one of the parameters used to change between maximum biomass and maximum productivity when it comes to the production of some biomolecules in bacteria. Given the relatively small size of the chemostat being developed, and the added complexity and equipment requirements added with the use of a large incubator, the use of thin film heaters that can be easily custom manufactured for a particular design becomes an adequate solution.

2.2.5.1 Design and modeling

The main requirements for the heating element were ease of integration with the chemostat system and vessel, and ability to maintain a stable temperature in the $37\,^{\circ}\text{C}$ to $40\,^{\circ}\text{C}$range. In addition, given its integration with the system, it should be able to sustain repeated uses and structure handling on its surface without degradation, to avoid constant repair which could involve a full disassembly of the system. Finally, while most of the area can be opaque, avoiding the need to use transparent conductive metal oxides, it should contain at least one spot where light is allowed to go through, not to hinder later optical measurements.

A Titanium-Tungsten (TiW) thin film was selected for its appropriate electrical properties as a resistive heater, as well as its resistance to scratching and overall stability.

The simplest resistive heater design is a long, evenly spaced serpentine, exploiting the Joule-heating effect to increase the temperature of a trace by passing electrical current through it. While simple and effective in creating a relatively uniform temperature profile in the center of the device, this type of design has previously been shown to present a temperature profile where the edges of the serpentine present lower temperatures than the middle, due to the faster heat dissipation by conduction [169]. Given that this issue is localized along the edges of the heating element, it is possible to dimension it so that the PDMS structure of the chemostat only occupies the center portion of the thin film heater, where the temperature is more uniform. Given the overall dimensions of the microfluidic structure, this corresponds to a $4\,\text{cm} \times 4\,\text{cm}$ heating area.

While the spacing between traces of the serpentine affect the temperature gradient, due to heat dissipation, the dimensions of each trace also have to be carefuly considered. With Joule-heating effects, the power of heating generated (P), that is, the temperature of the conductor is proportional to its resistance (R), and the square of the current (I)

$$P \propto I^2 R$$

. The resistance of a trace can be determined by

$$R_{trace} = \rho_{res} \frac{L_{trace}}{A_{trace}} (1 + \alpha_{res}(T_{trace} - T_{ref}))$$

where ρ_{res} is the resistivity of the material at T_{ref}, L_{trace} and A_{trace} are the length and cross-sectional areas of the trace, respectively, α_{res} is the temperature coefficient of resistivity for the material, T_{ref} is the reference temperature for the resistivity of the material, and T_{trace} in the average temperature of the trace.

The height of each path is determined by the thickness of the film deposited, in this case 1500 Å, T_ref is 25 °C. While the heater should maintain a temperature range of 25 °C to 40 °C, the previous equation does not account for power losses, diffused heat, nor the thermal mass of the substrate, which can all affect the final temperature. Due to this, the target temperature T_{trace} was set at 50 °C. Combining both equations, and considering that $P = VI$, it is possible to determine an acceptable trace width and length that can provide an adequate heating power, while being powered by an off-the-shelf 24 V power supply, in this case, a 45 cm long, 6 mm wide trace, that was designed as a serpentine with 6 mm wide gaps (Figure 2.2).

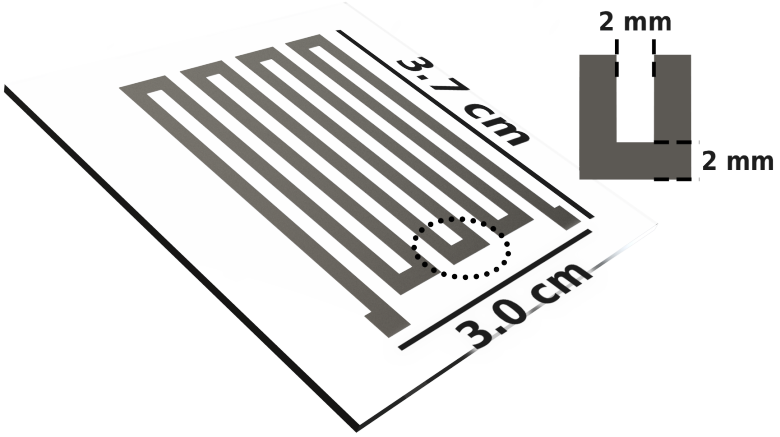

Figure 2.2: Heating element dimensions and characteristics

2.2.5.2 Heater manufacturing and assembly

The final heater design was fabricated by depositing a 1500 Å thin film over a clean Corning 1737 glass substrate by DC magnetron sputtering, patterned by DWLii, and etched by reactive ion etching.

To be able to apply voltage to the device, a conductive epoxy paste was used to bond a conductive wire to both device pads, that was then terminated with a quick disconnect coupler for ease of use. Hot glue was used for added rigidity, given the brittle behavior of the epoxy paste.

To and create a rough profile of the temperature across the PDMS structure, small cuts were made on its sides so that a thermocouple could be inserted. The temperature was then measured in multiple points using a multimeter. This was also used during batch operation to register the temperature in a single point.

Since the heating power generated by an electrical conductor is proportional to the square of the voltage running through it (in direct current (DC)), the heating element was first tested with increasing

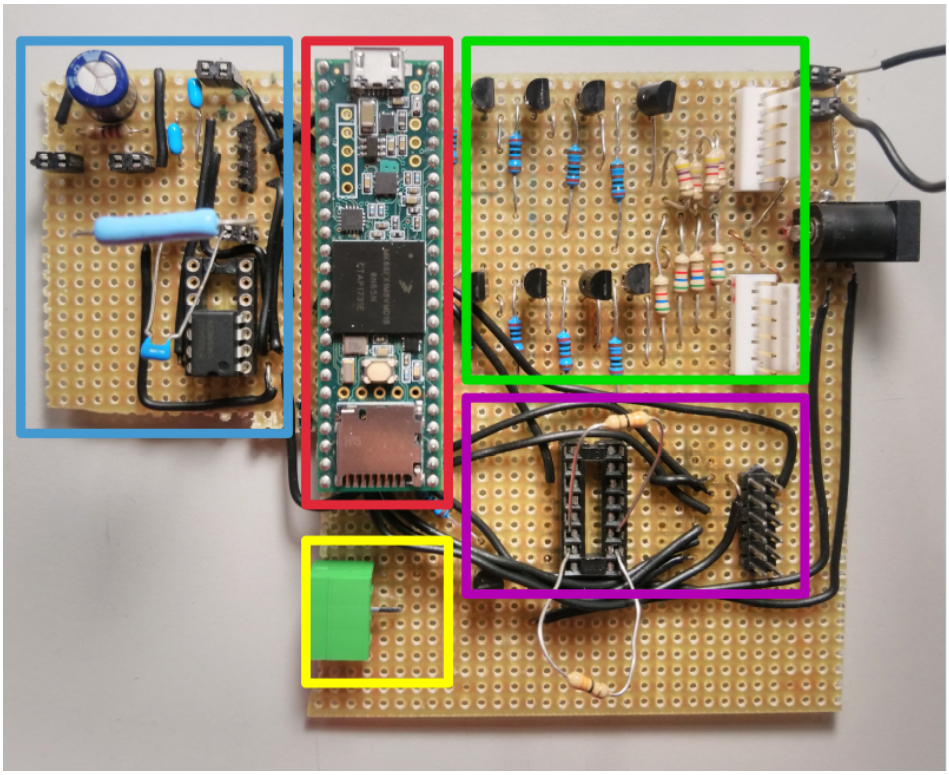

Figure 2.3: Perfurated board circuit integrating a microcontroller(red), transimpedance amplification circuit (blue), and valve blocks and heater controllers (green and yellow, respectively). The purple section contains the basic setup for the integration of a thermistor based temperature monitoring system, not currently in use

voltages and single point temperatures noted after 5 min. To analyze the steady state at 24 V, the power supply was set for 30 V for 15 min, and then decreased to 24 V for 2 h. Temperature measurements at the various points were collected at this stage.

2.2.6 Circuit components and assembly

In order to create a functioning and automated valve system, the solenoid valves need to be actuated with a well defined pattern and time scale. To facilitate this, a custom control circuit was designed, supplied by a 24 V, 1.5 A power source, connected through a transistor to each individual valve. Each transistor is controlled by an output pin of microcontroller, in this case a Teensy 3.6, where specific patterns and actuation frequencies can be programed to facilitate testing.

The same transistor design is used to control the power delivered to the heating element, as it uses the same power supply as the solenoid valves.

A transimpedance circuit was also coupled to a photodiode, and connected to the microcontroller. This used a LMC6482 CMOS high precision opamp to amplify the very small signal produced by the photodiode to a value that the 12-bit Analog to Digital Converter (ADC) of the microcontroller could detect. The full assembly can be observed in Figure 2.3. The full circuit design and bill of materials is detailed in appendix B.

2.2.7 Optical density measurements

An EG&G FFD-100 photodiode was selected as sensor for in-channel optical density measurements. This was coupled to the previously described circuit for amplification, and connected to the microfluidic structure on a previously designed space. A $5\,\mathrm{mW}$ red laser was used as light source, shining at a predefined angle from the edge of the device. This increases the optical path that the light needs to cross before hitting the sensor, at the same time acting in the same way as an optical fiber, and increasing the light variations caused by the changing cell concentrations in the channel.

2.2.8 Cell culture and calibration samples

Recombinant, GFP producing, *E. coli* strains were cultured according with the supplier protocol (Biomedal, Spain). In short, a pre-inoculum was cultured overnight at $37\,^{\circ}\mathrm{C}$ in LB medium, with ampicillin ($100\,\mathrm{mg\,l^{-1}}$), under constant 270 rpm agitation. This culture was then used to inoculate $250\,\mathrm{ml}$ of cell medium, at an initial OD600=0.1, that was then cultured under the same conditions until and OD600=1 was reached. Cell samples were then collected for further assays. Optical density was measured using a spectrophotometer (T70 UV/VIS Spectrophotometer, PG Instruments), and samples with optical density ranging from 0.1 to 1 where prepared by dilution with LB medium for microfluidic optical density measurements.

2.2.9 Microbioreactor batch operation

Before operation, the microfluidic system was fully assembled, and the fluid channel, reservoirs, and capillary tubes where filled with 70% ethanol for $30\,\mathrm{min}$. These were then flushed and rinsed twice with LB medium. The heater was turned on, and the system allowed to reach a stable temperature, before the reactor was inoculated with a culture sample at an OD600=0.1. Data acquisition started at this point, with OD measurements being collected each second. The peristaltic pump frequency was fixed at $10\,\mathrm{Hz}$.

2.3 Results and discussion

2.3.1 Temperature measurements

To first test the behavior of the heating element, the supply voltage was sequentially increased from $5\,\mathrm{V}$ to $30\,\mathrm{V}$ and the temperature allowed to stabilize for $5\,\mathrm{min}$. Steady state behavior at $24\,\mathrm{V}$ was tested by lowering the supplied voltage from $30\,\mathrm{V}$ to $24\,\mathrm{V}$ after $15\,\mathrm{min}$, and maintained for $2\,\mathrm{h}$. These results are shown in Figure 2.4. As noted in section 2.2.5.1, the dissipated power of a resistive heater is proportional to the square of the current flowing through it. As such, it was expected that the measured temperatures would increase with the voltage increase, as was observed. Considering that the model used in section 2.2.5.1, while designed with a target temperature of $50\,^{\circ}\mathrm{C}$, did not account for heat dissipation towards the atmosphere, nor the thermal mass of both PDMS structure and glass substrate, the final steady state temperature of about $40\,^{\circ}\mathrm{C}$ demonstrates that the heating

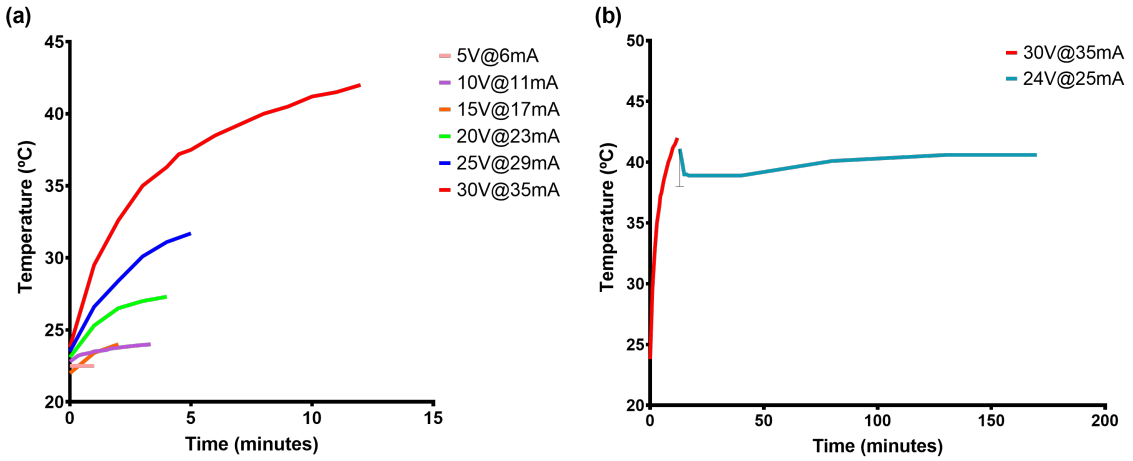

Figure 2.4: (a) Measured temperature of the PDMS structure for different applied voltages. (b) Steady state temperature behavior at fixed voltage

device presents a suitable behavior for the purpose of cell growth. It should also be noted that this system can thus avoid the use of any control mechanism, maintaining a stable temperature in the optimal range without any external input.

Various point temperature measurements across the structure were then used to create a temperature profile, as can be observed in Figure 2.5. A temperature gradient can be noted between the

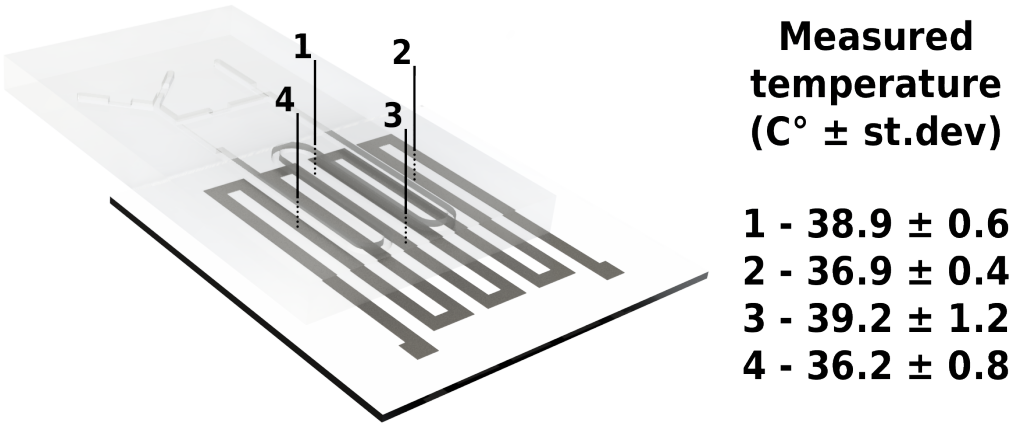

Figure 2.5: Temperature profile of the PDMS structure induced by the heating element. Each point was measured in duplicate

outside and the inside areas of the structure, with higher temperatures being present in the middle of the heater. This has been previously noted by [169], and is a result of the faster heat dissipation by conduction at the edges of the material, whereas the inside regions are shielded and can better contain the generated heat. Nevertheless, all regions maintained a temperature in the range of 36 °C to 40 °C, an adequate temperature range for the growth of *E. coli* in this system.

2.3.2 Microfluidic peristaltic pump flow rate

Pumping rates for the microfluidic peristaltic pump were quantified by measuring the time needed for liquid to fill a predefined length of capillary tubing, for each frequency. A capillary tube with $0.86\,\mathrm{mm}$ inner diameter was marked at $1\,\mathrm{cm}$ intervals. Knowing the dimensions of the tube, it is possible to calculate its volume, and deduce the flow rate achieved from the previous time measurements. These results can be observed in Figure 2.6. It is possible to note that the maximum flow rate achieved was

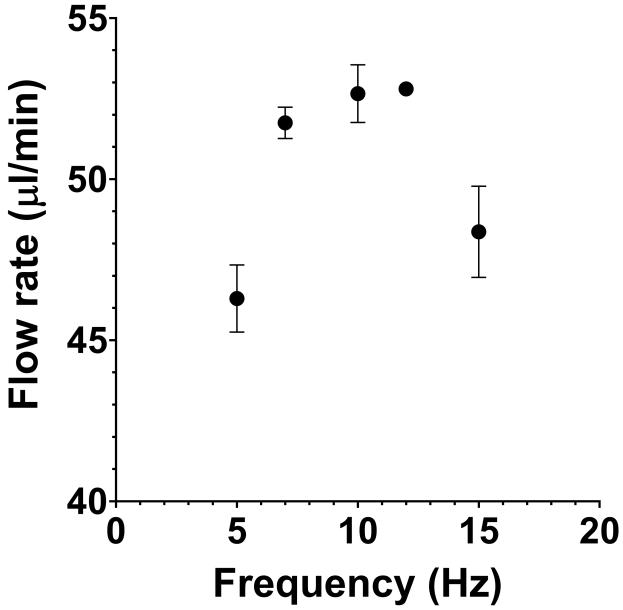

Figure 2.6: Pumping rate of the peristaltic micropump in function of actuation frequency

about $53\,\mu\mathrm{L\,min^{-1}}$, at a frequency of $10\,\mathrm{Hz}$, with the flow rate rapidly decreasing for lower and higher frequencies. This behavior was previously described by [107], and can be correlated with the valve actuation speed. The flow rate achieved increases with the actuation frequency, by increasing the number of pulses per second, until the point were the pump cycle does not allow the valves to fully open and close, leading to a decrease in the flow rate.

2.3.3 Integrated optical density measurements

2.3.3.1 Optical density calibration curve

In order to properly measure the OD of a cell suspension in the channel, the optical sensor should be calibrated using samples with known OD, creating a calibration curve that can be used to correlate a measured OD with the corresponding cell density. Microfluidic OD was calculated as $OD = log_{10}\frac{ADC_0}{ADC_{meas}}$, where ADC_0 is the analog converted value measured a the blank sample (clear LB medium, OD$\bar{0}$), and ADC_{meas} is the analog converted value measured for each sample.

For this, cell samples with specific OD were measured, and the results compared with the corresponding macro-scale measurements, as observed in Figure 2.7. From the Lambert-Beer law, OD is only linearly correlated with concentration for low sample concentrations, with cell sample OD

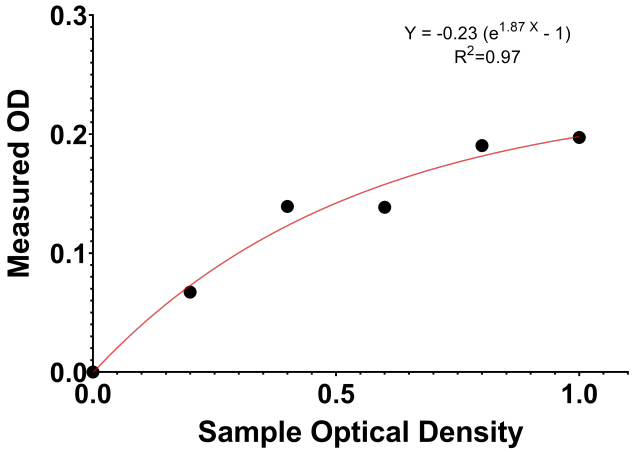

Figure 2.7: Calibration of the microfluidic OD measurements against macroscopic measurements

measurements not being directly performed on samples with OD>1 without dilution for this reason. This same behavior was observed for measurements where OD>0.6. In addition, the smaller dimensions and short optical path of the microfluidic channel shifted the range of measured OD to between 0 and 0.2. Nevertheless, it was possible to correlate the measured values with the corresponding macroscale OD, extracting a calibration curve that allows for the calculation of the OD of a cell sample using the integrated optical sensor.

2.3.4 Control Software and Graphical User Interface

Microfluidic bioreactors have the potential to rapidly accelerate the development and optimization of new processes, by testing the effects of multiple variations to the growth conditions and growth medium, with a decreased response time virtue of their smaller size. In addition, this faster response time also makes them prime candidates to test the effects of other perturbations, such as the effects of different antibiotics in an organism. However, these improvements are nullified if the device requires constant manual adjustment for operation. In this regard, automated control systems can greatly improve the ease of use of this type of microfluidic systems, allowing for a coordinated control of multiple device components, like the frequency of the peristaltic pump or the heating element, as well as immediate responses to pre-defined triggers.

A control system was designed that makes use of the Teensy microcontroller, connected to a separate computer for parameter setup. The software developed is thus separated into two parts, one used in microcontroller to actuate the multiple parts and collect data from the sensors, and a second, running on a separate PC, where the conditions of the system can be defined and altered as needed, and where the various parameters of the experiment can be visualized in real time. Figure 2.8 presents the interface that the user interacts with for device setup. In this way, the user can not only easily define the starting conditions for a specific experiment, they can also rapidly change them if required, as well as follow the experiment in real time.

Figure 2.8: Graphical user interface used to define the experimental parameters to test, and real time data display. Blue: multipurpose section for individual valve control or pump operation. Green: Toggle options for the heating element, optical sensor, and temperature sensors if present. Red: Real time data plot, where the current and historical optical density measurements are displayed.

2.3.5 Microreactor batch operation

Figure 2.9 shows the integration of all the systems previously described into the final device. As

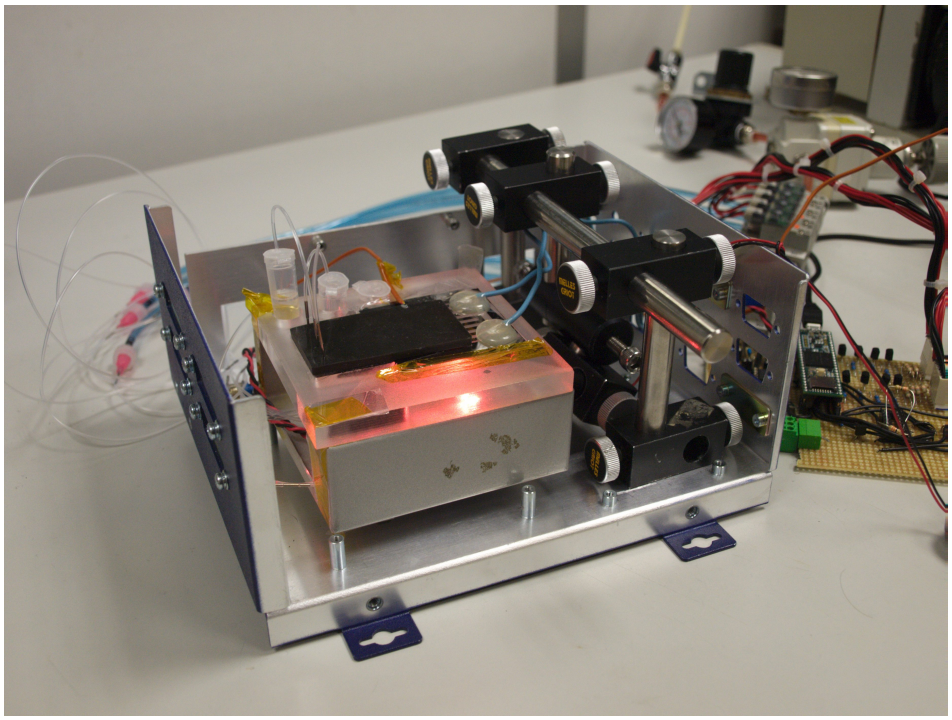

Figure 2.9: Final device assembly. It is possible to note the PDMS structure on top of the heating element, the 3 containers for medium input as waste retrieval, the integrated circuit, the laser assembly, and the two 4 port solenoid valve blocks

described in section 2.2.9, the microreactor was inoculated using a cell sample with OD=0.1, and left

running with a fixed 10 Hz pump frequency. OD measurements were collected every second, and can be observed in Figure 2.10. It can be observed that the culture roughly followed a Gompertz growth,

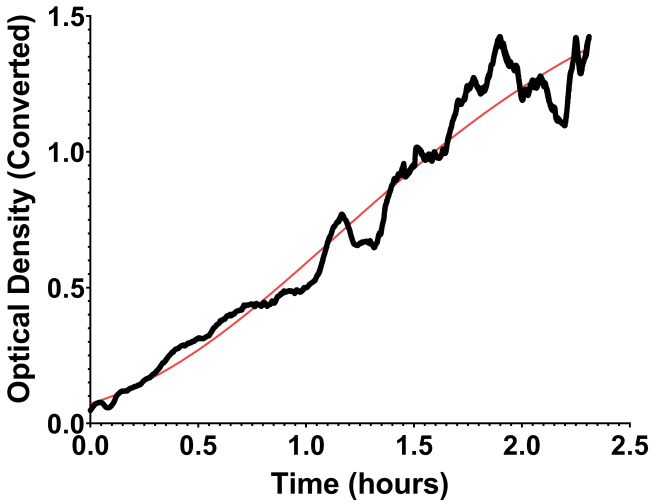

Figure 2.10: Bacterial growth as function of time, measured by OD. Reported OD values were converted using the calibration curve from section 2.3.3.1. The data was fitted using a Gompertz curve fit, with $R^2 = 0.97$

where the growth rate decays exponentially as the population approaches it maximum. Without any addition of growth medium, a typical batch operation growth curve is characterized by a lag phase, when cells are adjusting to the environment, an exponential growth phase, where the number of cells increases logarithmically, and a stationary phase, when the organisms are using all the available nutrients in the medium, and this in addition to the accumulation of waste materials causes the rate of cell division to balance with the rate of cell death. Analyzing the data in Figure 2.10, it can be argued that the lag phase of the system was very short, if non-existent, showing that the culture conditions presented by the system can closely resemble those of a culture flask, since barely any adaptation time was required for the cells to return to their normal growth. It can also be noted that the growth rate appears to be tapering off after about 2 h, when the culture could possibly be entering a stationary phase. This can possibly be caused by either the accumulation of waste materials and metabolites, or nutrient deficiency, since no cell medium was added to the culture. Both of these conditions can become a potential issue in microfluidic applications where the low volumes used can create less favorable conditions very rapidly.

2.3.5.1 Specific growth rate

From the fitted equation from Figure 2.10, it is possible to calculate the maximum specific growth rate achieved during the batch run. Considering the 1 h interval around the inflection point of the curve at 1.04 h, the culture maintained a maximum specific growth rate of $\mu = 1.28$, which corresponds to duplication time of about t_d=0.54 h^{-1}=32 min. While acceptable, this value is shifted when compared with the typical t_d=20 min for *E. coli*, an indicator that a limiting factor can be present, from mass transfer limitations of oxygen through the PDMS to nutrient limitations from the rapid growth in a confined space.

2.4 Conclusions

This chapter focused on the development and integration of various modules to create a functioning microbioreactor. Starting with the microfluidic structure and actuators, the channel dimensions were calculated based on the growth characteristics of *E. coli*, and the device design was chosen to maintain ease of use and integration with the remaining modules, while integrating a peristaltic pump and four fluid control valves. The system achieved a maximum flow rate of about $55\,\mu l\,min^{-1}$ which provided sufficient mixing for cellular growth to occur. However, while adequate for batch operation, if directly used for continuous operation this flow rate would likely result in washout, emptying the bioreactor. Considering the integrated valves along the microchannel, a future work can further explore their automated control to create an actuation pattern that continuously switches between replacing part of the fermentation broth with fresh medium and recirculating the bioreactor content. In this way, it could be possible to obtain an overall output of $2\,\mu L\,min^{-1}$ to $20\,\mu L\,min^{-1}$ from short bursts of a higher flow rate peristaltic pump. Another possibility is redesigning the valves of the peristaltic pump for lower flow rate, by decreasing their widths and corresponding actuation surface, although this could have unpredicted effects on the performance of the device.

A thin film resistive heater was also designed and fabricated, capable of maintaining a sufficiently uniform temperature across the device for the cells to maintain growth. *E. coli* cells typically have an optimal growth temperature in the $37\,°C$ to $40\,°C$ range, with the integrated heater varying between $36\,°C$ to $39\,°C$ in the different regions measured. This was achieved without any form of active control, meaning that the steady state temperature of the heater/bioreactor assembly is close to that of the target temperature for bacterial growth, and that the assumptions used in the modelling stage were correct. Nevertheless, while providing adequate conditions for the fermentation, considering that the temperature gradient of the heater is mostly dependent on width and separation of its traces, the device could be further improved by modifying the design to balance the heat dissipation on the edges of the reactor, in order to normalize the temperature in all regions.

In order to follow the cellular growth with time, a photodiode and laser were coupled with an opaque PDMS structure to measure the optical density of the cells inside the channel, with adequate correlation with macroscale measurements. By focusing a laser at an angle relative to the microchannel, it became possible to increase the optical path of the measurement, allowing for optical density measurements that would not be possible by measuring directly across the channel. The use of an opaque PDMS structure for both the fluid and control layers also meant that all light hitting the photodiode would have to have crossed the fluid in the channel, greatly increasing the signal to noise ratio of the measurements. However, while functional, the system is still highly sensitive to movement and adjustments, requiring precise fixtures for the correct functioning. A possible improvement would be the integration of a fixed angle laser fixture with the current assembly, to maintain a fixed alignment at the correct angle and position regardless of handling.

Finally, the entire system was used in batch fermentation mode to prove the concept, demonstrating that it was capable of creating and maintaining adequate conditions for bacterial cell growth, with

the combined operation of the various modules maintaining a specific growth rate of about 1.28, with a duplication time of 32 min, compared with the typical 20 min for *E. coli*. While this shows that the combined system can be used for bacterial fermentation, it would be relevant to determine what is decreasing the rate of growth of the organism. Further studies could focus on the effect of different temperatures, different medium concentrations, and different flow rates, in order to better characterize the system. This could be coupled with improvements on the control systems to add further automatic operations based on environmental and cellular density triggers, for example injecting an inductor when a pre-determined cell density is reached.

3

Microfluidic cell lysis screening and optimization

3.1 Introduction

Whether the objective is to release a product, or simply to obtain an analyte for further detection, cell lysis typically follows cells production. Several methods exist at large and bench scales, as described in section 1.4.1, and while not all of them are, at first glance, simple to integrate into a small scale, most of them have been scaled down in some form. However, most of the lysis techniques developed so far have been used as methods to extract genetic material, for applications such as on-chip amplification, and are typically focused on sample pre-treatment for Lab-on-Chip devices. As consequence, limited attention has been given to lysis as an extraction method for the development of biotechnological applications in microfluidics.

This chapter focus on the development of a diffusion-based microfluidic device for the rapid screening of continuous lysis conditions, using *E. coli* as model host and GFP as model product.

The main goal of the device was to determine the efficiency of different lysis conditions for the release of an intracellular protein from bacteria, that is, to measure the effect of different lysis solutions, contact times, and cell to lysis solution volume ratios, through the analysis of protein diffusion effects. In this way, a rapid screening of multiple lysis conditions becomes possible by simple fluorescence analysis. A simplified numerical model was used to aid in the design, and diffusion assays were performed to validate the assumptions. This microfluidic lysis process can operate under continuous conditions, to allow for the future integration with other microfluidic bioprocessing modules.

3.2 Materials and methods

3.2.1 Chemicals and biologicals

LB Broth and LB Agar cell culture mediums were obtained from Nzytech. Tris-buffer, lysozyme from chicken egg white, and sodium salicylate were purchased from Sigma-Aldrich. B-PER® was purchased from Thermo-scientific. *E. coli* bacterial strains BIVU0811 harboring the pMAB1-GFP-C-lytA plasmid were kindly supplied by Biomedal (Seville, Spain). A Milli-Q® water purification system was used to supply water for all experiments (Millipore, Bedford, MA, USA).

3.2.2 Microfabrication

The microscale experiments were performed using PDMS microfluidic devices, fabricated as previously described [170]. In short, an aluminum hard mask was fabricated by first sputtering Al (2000 Å; Nordiko 7000 magnetron sputtering system) on a glass slide (Corning Eagle XG Glass). The Al layer was then coated with a thin layer of photoresist (PFR7790G) and patterned using a direct-write lithography system (Heidleberg Instruments DWL II) and etched using an aluminum etchant solution (Gravure Aluminum Etchant; Technic, Microchemicals). This hard mask was then used to fabricate a $50\,\mu m$ SU-8 mold. A clean, $5\,cm \times 5\,cm$ silicon substrate was first coated with a $50\,\mu m$ thick SU-8 layer (SU-8 50 formulation, Microchem). The previously made hard-mask was then used to selectively expose the SU-8 layer to UV light (λ = 254 nm, 400 W). A negative mold of the final structure was obtained after a final baking and development. The SU-8 spin and bake times used were obtained from the manufacturer's data sheets. The SU-8 molds were used to fabricate several copies of the microfluidic device, using PDMS prepared at a 1:10 ratio with the respective curing agent (Sylgard 184 silicon elastomer kit, Dow-Corning). This mixture was degassed, poured over the mold and baked for $90\,min$ at $70\,°C$. The resulting structure was then cut, the inlets and outlets punched using a blunt syringe tip (Instech Solomon, Plymouth Meeting, PA, USA), washed, and irreversibly sealed against a $700\,\mu m$ thick PDMS membrane, which was prepared following the same procedure. An oxygen plasma was used for the sealing by exposing both surfaces for $1\,min$ with a power of $11\,W$ (Harrick Plasma PDF-002-CE).

3.2.3 Cell culture and sonication

Recombinant, GFP producing, *E. coli* strains were cultured according with the supplier protocol (Biomedal, Spain). GFP-Lytag fusion protein was used as a model protein. Lytag, the C-terminal region of the lytic amidase present from *Streptococcus pneumoniae*, can interact with PEG molecules and facilitate product separation downstream. In short, a pre-inoculum was cultured overnight at $37\,°C$ in LB medium, with ampicillin ($100\,mg\,l^{-1}$), under constant 270 rpm agitation. This culture was then used to inoculate $250\,ml$ of cell medium, at an initial OD600=0.1, that was then cultured under the same conditions. When an OD600=1 was reached, gene expression was induced through the addition of $1\,mM$ sodium salicylate, and cultured for 5 hours at $30\,°C$, 200 rpm. Cell samples were then collected for further assays. Optical density was measured using a spectrophotometer (T70 UV/VIS

Spectrophotometer, PG Instruments). An ultrasonic homogenizer was used in order to obtain samples with different and known percentages of cell lysis (Sonoplus HD 3200, Bandelin). The previously collected cell samples were centrifuged at 4000 g for 15 min, at 4 °C, and resuspended in 250 mM Tris-HCl buffer, pH 7. These solutions were then homogenized by sonication, under ice-water bath, for specific times (15, 30, 45, 60, 120 and 300 seconds). The same protocol was used for raw samples, were the cells were lysed in the fermentation broth. The homogenized samples were then cultured overnight in solid agar plates (LB agar, with ampicillin ($100\,\mathrm{mg\,l^{-1}}$), at 37 °C, with different dilutions (1:1, 1:10, 1:100, 1:1000, 1:10000). The percentage of live cells remaining in each sonicated sample was determined by counting the number of colonies present in each plate, in triplicates, and compared against non-homogenized samples subjected to the same procedure. The remaining of each sample was then used for the microfluidic experiments.

3.2.4 Lysis solutions

Two different lysis solutions were selected: A commercial lysis solution, B-PER®, based on non-ionic surfactants, and an enzymatic solution of lysozyme ($100\,\mu\mathrm{g\,mL^{-1}}$ in 50 mM Tris-HCl, pH=7.5). The selection was also based on their different modes of action. While B-PER® has been described to have a permeabilizing effect on the cells, releasing the product without full cell disruption, lysozyme releases the product by destroying the cell wall [155, 171, 172].

3.2.5 Microfluidic operation and image acquisition

Syringe pumps (New Era Pump Systems, NE-300) were used to inject the solutions into the microfluidic device through two inlets. The diffusion of fluorescent molecules and cells across the channel was then followed using a fluorescence microscope (Leica DMLM), equipped with a DFC300FX camera, at different positions along the length of the channel. A 100 W mercury light lamp coupled with a light excitation filter with a band-pass of 450 nm to 490 nm, and a long pass emission filter of 515 nm, was used for the fluorescence experiments. All fluorescence images were acquired with a 1 s exposure time, and processed using ImageJ (National Institute of Health, Bethesda, MD, USA), and GNU Octave (version 4.4.1). At least two micrographs were obtained for each assay, one close to the inlet, and one downstream at a measurement point at approximately 18 cm from the inlet. In the case of the diffusion assays, micrographs were acquired at 3 cm intervals from the inlet. The fluorescent signal was then analyzed using both ImageJ software and in-house GNU Octave scripts. In short, each image was first converted to 8 bits, vertically aligned to the microchannel walls, and the microchannel area profile was plotted. The area outside the channel was averaged and subtracted as background.

3.3 Results and discussion

The aim of this work is to design and develop a microfluidic device for rapid screening of continuous lysis conditions. First, the microfluidic device and the operation principles are described. Then, two

sets of experiments were carried out to characterize cell lysis in the microfluidic chips: (i) in the first set of experiments, a calibration was performed to obtain a correlation between the microfluidic fluorescence signals and the macro scale homogenization data; and (ii) in the second set, different lysis conditions and solutions were tested to highlight the applicability of the proposed microfluidic device for screening of lysis conditions.

3.3.1 Microfluidic device for rapid screening of continuous lysis

The proposed microfluidic device is based on the combined exploitation of the difference in the diffusion coefficient between whole cells and free protein, and of the laminar flow profile typical of microfluidics, which limits transversal mixing to diffusion effects. This results in the separation of the cells from the GFP released as a result of lysis, allowing for a method to quantify the amount of cell lysis that has occurred.

In order to define the microchannel cross-sectional dimensions, the effect of the aspect ratio of the channel, i.e., the ratio between the height and width of a microchannel, on the diffusive behavior in a microfluidic system was analyzed [173]. In a system where a high and a low concentration solutions of a diffusible analyte are injected side by side, the parabolic velocity profile of the fluid within the channel will change the diffusion profile of the analyte, altering the shape of the interdiffusion zone. Given the lower velocity near the channel walls compared to the center of the channel, the diffusion interface acquires a butterfly shape, with increased diffusion occurring near these regions due to the increased time for diffusion, and this effect becomes more pronounced with increasing aspect ratios, affecting the overall performance of the system [173]. Since the goal was to achieve full interdiffusion of protein and lysis components, which depends on the diffusion distance, a square cross-section of $50\,\mu m$ x $50\,\mu m$ was defined. Smaller channels could present issues during fabrication, due to poorly defined structures, and during image acquisition, by presenting a smaller observable area requiring greater magnification which could introduce optical artifacts. On the other hand, larger channels would imply a larger interdiffusion distance, which would also increase the time needed for full diffusion, requiring a longer channel to achieve the same condition.

To start, the diffusion coefficients of the components of the solutions, namely whole cells, free GFP, free lysozyme, and (since the exact composition of the commercial solution is not known) small non-ionic surfactants were considered. In the case of *E. coli* cells, the diffusion was assumed to be like the diffusion of a $2\,\mu m$ spherical particle in water, at $25\,^{\circ}C$, calculated by the Stokes-Einstein equation (Equation 3.1) [174].

$$D = \frac{\kappa_B T}{6\pi\eta r} \tag{3.1}$$

Where κ_B is the Boltzmann's constant, T is the absolute temperature, η is the dynamic viscosity, and r is the particle radius.

Considering the channel dimensions described above, the average full diffusion distance can be approximated to half of the width of the channel, at $25\,\mu m$. Then, using the diffusion coefficients of each element, and using Einstein's equation of Brownian motion $x = (2D\tau)^{1/2}$, where x is the root-mean-square distance transversed by a particle ($x = 25\,\mu m$) during the time interval τ for a

given diffusion coefficient D, it is possible to predict the amount of time needed for each component of the solution to achieve full diffusion within the microchannel. To facilitate future integration with other microfluidic modules, total flow rates of 1.5, 3.0 and 4.5 $\mu L\,min^{-1}$ where considered in the calculations. These values can then be used to estimate the minimum channel length needed for complete diffusion in the channel and are listed in table 3.1. The main thing to note in Table 3.1 is

Table 3.1: Estimated values for the full diffusion time of each component of the solution, and corresponding minimum length for diffusion for each flow rate

			Diffusion length for each flow rate (cm)		
Compound	Diffusion coefficient ($cm^2\,s^{-1}$)	Diffusion time, τ (s)	$1.5\,\mu L\,min^{-1}$	$3.0\,\mu L\,min^{-1}$	$4.5\,\mu L\,min^{-1}$
GFP	8.7×10^{-7}[175]	3.6	3.6	7.2	10.8
Lysozyme	1.0×10^{-6} [176, 177]	3.1	3.1	6.3	9.4
B-PER®	1.0×10^{-6} [178]	3.1	3.1	6.3	9.4
E. coli	2.5×10^{-9}	1.3×10^3	1.3×10^3	2.5×10^3	3.8×10^3

that the predicted diffusion coefficients of GFP, the target product, and of lysozyme and B-PER®, the lysis components, are approximately 2 orders of magnitude higher than the diffusion coefficient of *E. coli*. This can be used to design a microfluidic device in which the cell solution and lysis solution can be inserted in two inlets, flow in parallel and while the cells do not undergo significant diffusion, both the active components of the lysis solution and GFP can diffuse across the channel. In such a device, it should be possible to monitor the effectiveness of the cell lysis, as described in Figure 3.1. Considering the values in table 3.1, a channel length of $30\,cm$ was selected to fulfill this condition. Figure 3.1(a) illustrates the operation of the microfluidic screening device which is comprised of a $30\,cm$ long channel, with a $50\,\mu m \times 50\,\mu m$ cross-section, two equidistant inlets and a single outlet. First, a solution with cells expressing GFP and either a test lysis solution or buffer are injected into separate inlets, both at $1.5\,\mu L\,min^{-1}$, using syringe pumps. The sharp contrast of the fluorescence profile in the micrograph (Figure 3.1(b)) at the inlet was used to determine the interface position within the channel (red lines). This position was then used in the captured fluorescence micrographs downstream, splitting the channel into "high fluorescence" (cell side) and "low fluorescence" (lysis solution side) regions. To be able to measure a fluorescence value for each channel region while avoiding interferences from both the channel walls and the diffusion interface, only the fluorescence value of the central 50% area of each region was averaged. These gray scale intensity values obtained thus correspond to the fluorescence intensity for each condition. In Figure 3.1(c), taken downstream (L = $18\,cm$) using a Tris-HCl buffer solution, no transversal cell diffusion was observed as evidenced by the continued existence of the sharp drop of fluorescence at the interface. In Figure 3.1(d), when a test lysis solution was used, a clear enhancement of the fluorescence in the "low fluorescence" region is observed, indicating some level of cell lysis and subsequent transversal diffusion of GFP.

Additional diffusion assays were performed by flowing a GFP solution (in Tris-HCl buffer, from cell lysate) in one inlet and Tris-buffer in the other, using the same flow rates used for the lysis assays ($1.5\,\mu L\,min^{-1}$, $3.0\,\mu L\,min^{-1}$ and $4.5\,\mu L\,min^{-1}$). Fluorescence images were acquired every $3\,cm$, and the diffusion was analyzed based on the fluorescence ratio within the channel.

The measured diffusion coefficient of GFP was $1.9 \times 10^{-7}\,cm^2\,s^{-1}$, a slightly smaller value than that

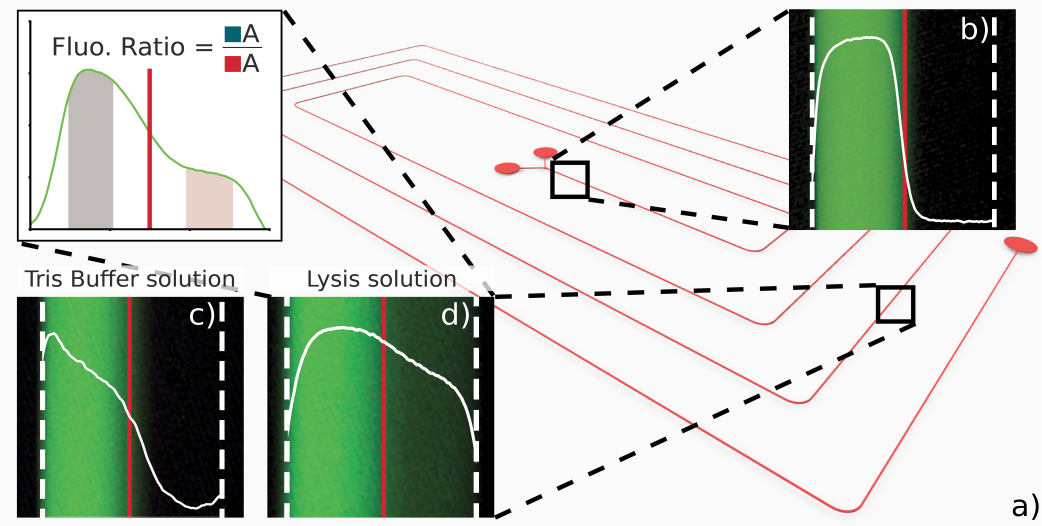

Figure 3.1: Schematics of the microfluidic device for rapid screening (in red, (a)). The interface position between the cell solution (*E. coli* expressing GFP) and either a buffer (50 mM Tris-HCl, pH=7.5) or non-fluorescent lysis solution is measured at the inlet (b) and is later used to divide the channel profile into high and low fluorescence areas (red line), that can be used to calculate a fluorescence ratio (c and d). The inset on the top left shows a schematic of the fluorescence profile across the channel. The fluorescence ratio is defined as the ratio of the fluorescence on the "high fluorescence side" to that on the "low fluorescence side". Fluorescence is measured only in the central 50% area of each region. The fluorescence in the low fluorescence region indicates cell lysis and subsequent GFP diffusion.

from literature (Table 3.1). This discrepancy can be attributed to various reasons. First, the pulsed profile of the stepper motor in the syringe pumps can cause slight shifts in the real flow rate within the channel. Also, it has been previously described that the effective diffusion coefficient can vary for microchannels with depths substantially higher than 10 µm [155], as is the case with this structure (50 µm). Finally, the model used values for distilled water at 25 °C to simplify the calculations, however it has been reported that the diffusion coefficients for biomolecules can be affected when dissolved in salt based buffers [176]. Nonetheless, since these experimental diffusion values were measured in the same device in which the assays are to be carried out, they can be used to recalculate the minimum channel length previously determined using literature values. While the corrected diffusion values result in an increase in the minimal channel length needed for full product diffusion ($\approx 30\%$ longer channel), the corrected lengths are still below half the total length of the channel, and well under the length for cell diffusion, thus still allowing for an accurate evaluation of the lysis effect by fluorescence diffusion.

3.3.2 Calibration of microfluidic lysis against standard macroscopic methods

A calibration curve was obtained by comparing the lysis efficiency of a macroscale method (sonication) quantified by solid culture colony counting (detailed in section 3.2.3), against the signal obtained in the microfluidic device, as can be seen in Figure 3.2. Cell samples were collected and subjected to

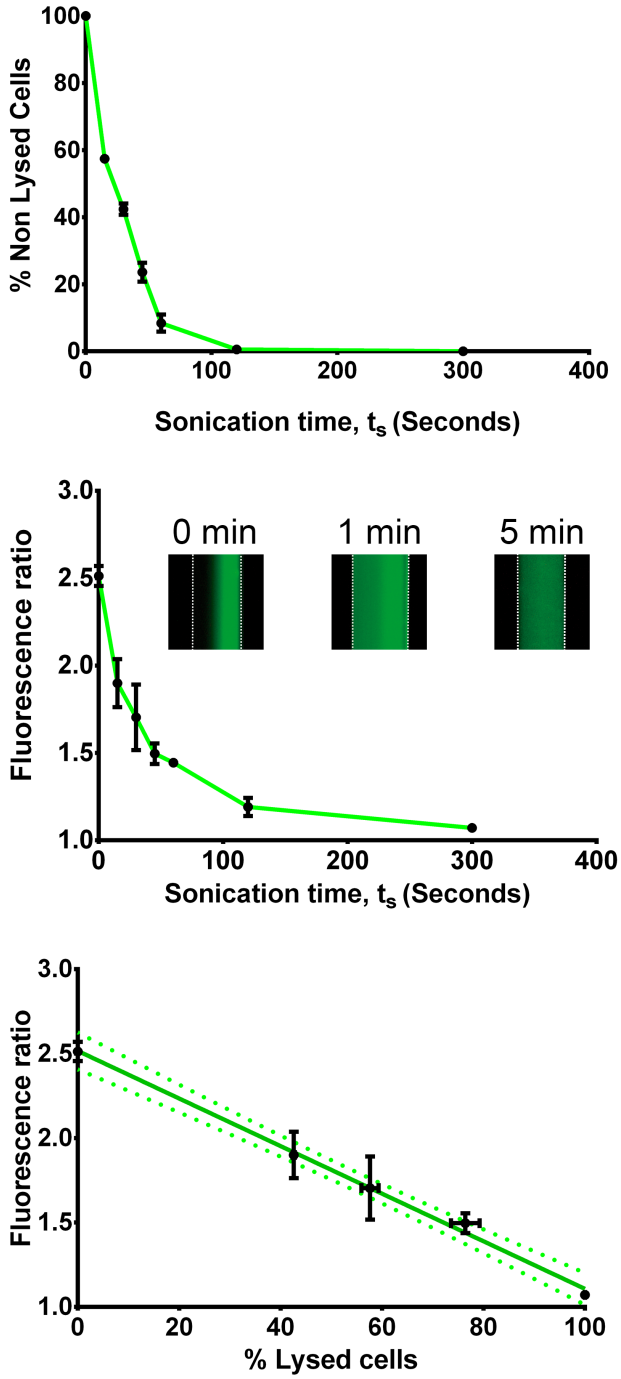

Figure 3.2: Calibration of the lysis in the microfluidic device against macroscopic sonication. (a) Percentage of non-lysed cells remaining for each sonication time (macroscopic measurements); (b) fluorescence ratios measured in channel, for each sonication time (microfluidic device). Micrographs represent the different fluorescence profiles obtained for increasing sonication times. Sonication was made prior to insertion into the microfluidic device; (c) correlation between fluorescence ratios and percentage of lysed cells. The dotted lines correspond to the 95% confidence interval.

different sonication times, before serial dilution and plate seeding for CFU determination. Plate counts could then be used to calculate the average percentage of dead cells for each sonication time. As expected, a rapid decrease in cell viability was observed with the increase in sonication time (Figure 3.2 (a)). Sonication has been a staple for bench scale lysis procedures, and by adjusting the time and power it was possible to obtain samples with a wide range of total lysed cells. This increase in the sonication efficiency with the increase in sonication time has been previously described in detail by Tandiono et al. [150] and Dehghani [179]. The next step was to use the previously sonicated samples (Figure 3.2 (a)) in the microfluidic chip, to obtain the different on-chip fluorescence ratios for each lysis efficiency (which was assessed via plate counts). Each sonicated sample was injected at a flow rate of $1.5\,\mu L\,min^{-1}$ in one inlet, with Tris-HCl buffer injected in the other inlet, and the fluorescence profile measured along the channel length. Due to the laminar flow inside the microfluidic channel which limits the mixing phenomenons to transversal diffusion, and considering that cells have a much lower diffusion coefficient than GFP, they will remain on the side of the channel where they were injected, while GFP will diffuse across the width of the channel. This will create a quantifiable fluorescence differential that can be correlated with the lysis efficiency. As can be observed from the fluorescence micrographs present in Figure 3.2 (b), a rapid decrease in the fluorescence ratios was observed with the increase in sonication time. This corresponds to higher concentrations of free GFP on the samples subjected to longer sonication times, and thus a higher percentage of lysed cells. Finally, it was possible to correlate the results of the previous two experiments (macro and micro), in order to obtain a calibration curve of the cell lysis efficiency as related to the fluorescence ratios measured in-channel (Figure 3.2 (c)). A linear correlation could be observed between the fluorescence ratios measured and the corresponding lysis efficiencies, and this calibration curve can be further used to quantify the effect of the different lysis solutions and conditions tested in the microfluidic device.

3.3.3 Rapid screening of lysis conditions

3.3.3.1 Lysis assays in isolated cells suspension

Lysis assays were performed using cell harvested by centrifugation ($OD600 = 1$), and resuspended in a Tris-HCl buffer solution.

Three different flow conditions of resuspended cells and either Tris-HCl buffer, B-PER® or lysozyme solutions were tested in the microfluidic system, corresponding to three different residence times, and the fluorescence ratios were measured and converted to lysis efficiency (Figure 3.3(a)). Confirming the previous observations (section 3.1), no significant diffusion of the resuspended cells occurs into the buffer, even for the lower flow rates, as the low diffusion coefficient causes the cells to remain in the half of the channel where they were inserted. When the commercial B-PER® solution is used, the lowest flow rate ($1.5\,\mu L\,min^{-1}$) presents the highest lysis efficiency in the chip ($\approx 100\%$). This result can be explained by the different residence times for each flow condition. At the lowest flow rate the residence time of $20\,s$ is sufficiently long to achieve full cell lysis and allow for full product diffusion, reaching a uniform fluorescence profile at the end of the channel, this does not occur for the other two flow rates tested ($3.0\,\mu L\,min^{-1}$ and $4.5\,\mu L\,min^{-1}$). In fact, a rapid decrease in the lysis efficiency could

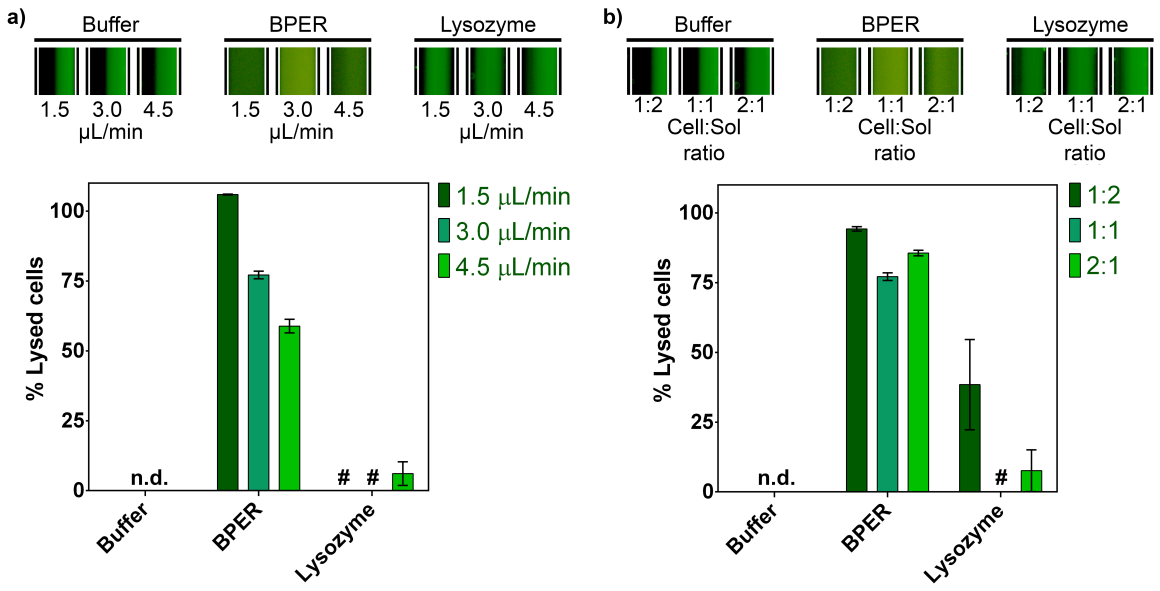

Figure 3.3: Percentage of cell lysis obtained for buffer resuspended cells, using Tris-HCl buffer, B-PER®, and lysozyme, measured by the corresponding fluorescence ratio in the channel. a) For different total flow rates (using the same flow rates of resuspended cell solution and buffer or lysis solution); b) for different flow rate ratios (keeping constant total flow rate of $3.0\,\mu L\,min^{-1}$). Micrographs represent the fluorescence profile obtained in the microchannel for each condition. Each point was measured in triplicate. n.d. - not detected, # - non measurable conditions

be observed with increasing flow rates, indicating a sensitivity to the contact time between cells and lysis buffer for B-PER®.

On the other hand, very different results were observed when lysozyme is used as the lysis solution. Only at the highest flow rate could a quantifiable lysis be observed; a prime example of how different lysis methods can affect the downstream processing steps. In this case, the lytic effect of the enzyme led to the rapid release of genomic material which created a viscous environment surrounding the cells, a consequence of rapid cell disruption previously described at macro and industrial scales [180]. This viscous phase encapsulating the cells tends to accumulate down the middle of the channel due to hydrodynamic forces, creating the profile observed in Figure 3.3(a) (lysozyme, flow rates of $1.5\,\mu L\,min^{-1}$ and $3.0\,\mu L\,min^{-1}$), showing a fluorescent band surrounded by two dark areas. In fact, this is a known issue for the bench scale lysis protocol, where it is usual to add a DNase to the lysis buffer in order to control the viscosity of the lysed solution, which can then sometimes increase the complexity of the sample treatment downstream [180, 181]. While this effect becomes an issue regarding quantification of the lytic effect, since the described quantification method is no longer applicable given the different fluorescent profile and diffusive behavior inside the channel, it still provides useful information in a screening assay. Of note, it allows for a rapid evaluation of the rheological properties of the lysate and highlights potential problems that could arise in the product separation and purification steps. Nonetheless, the small lytic effect measured for the highest flow rate condition could indicate that the corresponding residence time in the channel would be close to the minimum lysis time required to disrupt cells with this enzyme solution.

The lytic effect of different ratios of lysis solution to cell solution was then tested for comparison

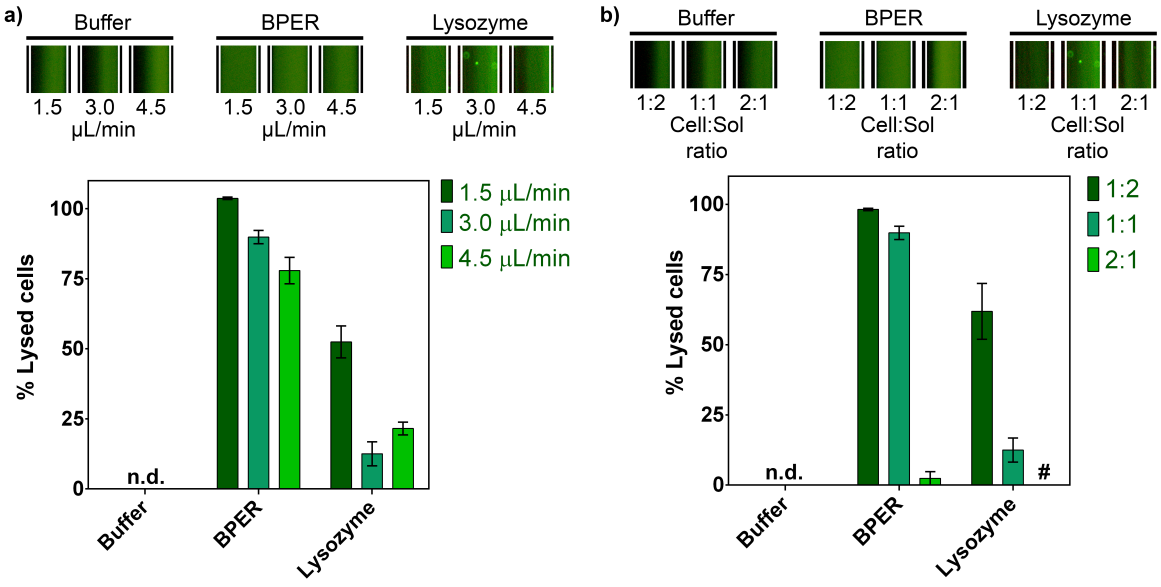

Figure 3.4: Percentage of cell lysis obtained from direct fermentation samples, using buffer, B-PER®, and lysozyme, measured by the corresponding fluorescence ratio in the channel. a) For different total flow rates (using the same flow rates of resuspended cell solution and buffer or lysis solution); b) for different flow rate ratios (keeping constant total flow rate of $3.0\,\mu L\,min^{-1}$). Micrographs show the fluorescence obtained in the microchannel for each condition. Each point was measured in triplicate. n.d. - not detected, # - non measurable conditions.

with the experiments described above by changing the flow rates of the two solutions being injected in the microfluidic system (cell solution in one inlet, and a buffer solution, B-PER® or lysozyme in the other inlet), while maintaining the overall flow rate fixed at $3.0\,\mu L\,min^{-1}$. Figure 3.3(b) shows once more that no cell diffusion can be detected at the end of the channel when co-flowing with the buffer solution. It is also possible to notice in the micrograph the relative shift in the interface position due to the different flow rates being injected in each inlet.

Testing the B-PER® solution, no significant changes in lysis efficiency where observed between the different flow rate ratio conditions (Figure 3.3(b)). Even when diluted to about 30% of the original concentration (2:1 cell solution to lysis solution ratio), the commercial solution still presented a lysis efficiency of about 75%, comparable to the assays performed with less diluted lysis solution. It is thus possible to conclude that lower amounts of lysis reagent can be used to achieve significant product release, not only lowering the overall cost of the process, but also decreasing the dilution of the product in the final sample, as well as the amount of surfactant that could need removal. However, it should be noted that this is observed under model conditions, where cells were resuspended in a buffer solution.

In the case of the lysozyme assays, the results shown in Figure 3.3 (b) follow the trend obtained using different flow rates (detailed in Figure 3.3 (a)), with low lysis efficiencies. In the previous experiments (flow rate series, Figure 3.3 (a)) it had already been observed that it was not possible to quantify the lysis for the standard 1:1 flow rate ratio, due to the increased viscosity in the channel. By decreasing the relative number of cells being injected, thus having a higher concentration of enzyme in solution, a small but measurable lysis effect (30-35% lysis efficiency) was obtained (Figure 3.3 (b)),

an effect similar to previously reported studies on lysozyme permeabilization of *E. coli* [172]. The lower cell volume also led to a lower viscosity after lysis, due to the lower amount of genomic material released. Finally, the enzyme activity could also have been affected, limiting the overall lytic effect, due to the increased concentration of inhibitory lipopolysaccharide (LPS).

3.3.3.2 Lysis assays in raw fermentation sample

To study the potential for a direct integration of the lysis microfluidic chip with a microfluidic bioreactor, raw fermentation samples, i.e., samples collected directly from the fermentation flask without any treatment, were also tested following the experimental protocol of the previous section (3.3.3.1). Similar to the results obtained with the isolated cell samples, when the crude fermentation sample co-flows with buffer, it is possible to observe two distinct transversal regions within the channel, with no cell diffusion to the buffer size (Figure 3.4(a)). However, it should be noted that the direct fermentation samples presented a slight fluorescence signal in this control condition. This is due to free protein present in the fermentation medium, resulting from cellular death during the growth phase, and which can diffuse to the buffer side. This background signal was accounted for and subtracted in all measurements on these samples.

The lytic effect of the commercial solution showed a dependence on residence time (Figure 3.4(a)), as already observed in the results from the buffer suspensions. Nonetheless, even for the highest flow rates tested, the lysis efficiencies remained above 75%, showing that this solution could be used for higher throughput microfluidic systems, where a rapid cell lysis is needed, even from raw fermentation samples.

When the lysozyme solution is used, a different lysis profile is observed compared to the commercial solution. When isolated cell samples were used (Figure 3.3(a)), the highly viscous cell mass obtained hindered the measurement, whereas significant lytic effect could be measured with the raw fermentation samples (Figure 3.4(a)). This difference can be attributed to the presence of LPS in suspension in the raw fermentation solution, a result of the natural cell death that occurs during the fermentation phase, and that can have an inhibitory effect on the enzyme [182]. As such, this is a case where a milder and slower lysis can improve the overall process. While requiring extra time, this situation may avoid the rapid release of genomic material. While the best lysis condition using this enzyme only reached about 50% cell lysis at $1.5\,\mu L\,min^{-1}$, this process could still be useful for the continuous extraction of sensitive products that could be affected by surfactants, as well as high value products where the downstream removal of a surfactant could make the process economically nonviable.

Assays at different flow rate ratios were also performed for the raw fermentation samples (Figure 3.4(b)). The large effect of the dilution resulting from the different solution ratios on the commercial lysis solution action should be noted, with the lysis efficiency sharply reduced for higher cell fractions. The lysozyme solution now appears as a relatively good lysis method, with a lysis efficiency above 50% for the sample with the highest amount of enzyme. The lower cell volume, combined with the inhibitory effect of LPS from the cell culture, resulted in a mild lysis without excessive genomic material

release, for a more controlled cell lysis along the channel. This allows for a controlled product release, without the addition of any surfactant to the solution, which could hinder the downstream processing.

Finally, it is possible to compare the current device against common techniques for the screening of bacterial cell lysis. Absolute lysis efficiency is not a trivial value to determine, and usually only its relative value is quantified. Current lysis quantification techniques typically rely either on the quantification of released protein and/or RNA/DNA, or on actual cell counting (by microscopic observation, or by agar plating and determination of viable cell numbers, the method used in this work for calibration)[7, 183, 184]. The first methods can be laborious, and rely on expensive equipment, limiting the number of conditions that can be tested in a given time frame. As an example, high pressure liquid chromatography (HPLC) is a common technique employed to assess cell lysis by measuring a leaked product. However, its setup and sample preparation steps can be complex and time consuming. While presenting relatively more simple setups, assays such as Picogreen™ or NanoDrop™ still require several sample preparation steps, and can suffer from interference due to other components present in solution [7, 180].

On the other hand, optical cell counting can be an extremely slow process, even when using recent computer assisted methods, and is mainly used for very low volume assays (for example in microfluidic chambers), while plate counting relies on culturing the tested sample, which could take anywhere from hours to days, depending on the organism. Lastly, flow cytometry can also be employed for this purpose. However it suffers from complex staining procedures, and requires extensive post measurement data analysis [180].

This microfluidic device eliminates the need for expensive equipment, using a common fluorescence microscope present in most biology laboratories. Furthermore, the fluorescent signal measured can also be measured by integrated photosensors, as previously described, completely avoiding the need for external, bulky equipment [78, 79, 159]. The fact that it provides almost instant results (in the order of seconds to minutes), and the flexibility that microfluidics provides regarding the testing of multiple solutions in a short time frame, give the device the ability to sweep a large range of lysis conditions for a single solution in a single assay, as well as the ability to test between multiple lysis solutions by simply changing a syringe. Overall, this allows this device to screen multiple lysis conditions in a fraction of the time of current techniques, with very little handling.

3.4 Conclusions

In this chapter, a simple and rapid microfluidic system for the continuous evaluation of liquid based chemical/enzymatic lysis conditions was demonstrated. The use of a fluorescent model protein, coupled with a one-time calibration that related cell lysis and fluorescence, allowed for the rapid quantification of the lysis efficiencies of different solutions and flow conditions in the microfluidic device. This device was successfully used to test the lytic effect of both an enzymatic and surfactant-based solutions, under different contact times and solution ratios, as well as the effect of cell supernatant on the lysis efficiency. The device also demonstrated the ability to detect potential problems such as

the increased viscosity due to the rapid release of genomic material that can arise for specific lysis conditions and hinder the performance of a bioprocess. Finally, different lysis solutions, concentrations and lysis times could be rapidly tested by changing either the solution injected, or the flow rates, which allowed for a very fast screening of the overall effect of each solution. While the present work used bacteria, it should also be possible to use this screening microfluidic device to study the lysis of other types of cells and products. Since most other cell types used for bioproduct manufacturing are typically larger, with lower diffusion coefficients, they should maintain the observed behavior under laminar flow conditions, where the cells tend to remain on the side of the channel into which they are injected, with essentially no diffusion across the channel. Nevertheless, future work should also be performed to assess the impact of the formation of inclusion bodies on the diffusive behavior being quantified in this work. The tendency of some proteins to aggregate in this type of structure can either create particles large enough to present much slower diffusion, artificially decreasing the measured lytic effect, or can change the fluorescence of the protein due to the close proximity of multiple molecules.

Maintaining the goal of process integration, the lysis microfluidic device was developed as a modular component. Considering the continuous nature of this process and the manufacturing techniques used, it is possible to integrate the lysis module with other microfluidic devices emulating both up and downstream processes. For example, it would be of interest to combine this module with the microreactor described in the previous section, using the output of the microreactor as a cell input into this device.

This type of micro-modular platform can also be combined with regime analysis and bioprocess models to predict industrial scale performance of bioproduct production processes. With this approach a preliminary evaluation of the conditions that influence both the production and the purification steps of bioproduct can be conducted much earlier in the development pathway of a bioprocess at lower costs, thus allowing for later large-scale trials to be more targeted. This work could thus be improved by larger scale studies using the same conditions determined in the microfluidic device, to better demonstrate the potential for early stage process optimization of this type of approaches.

4

Continuous microfluidic platform combining cell lysis and protein concentration for screening overall process conditions

4.1 Introduction

Following the results from chapter 3, this chapter focuses on the integration of the previously described lysis module with a separation and concentration module. In this way it becomes possible to screen for the best conditions not only for the product release, but also for the combined product separation. In fact, while the biomanufacturing process is usually viewed as a combination of single unitary operations, each processing step can have important effects on the subsequent ones, so that the optimal conditions for each operation do not necessarily correlate with the optimal conditions for the full combined process.

It was important to maintain the continuous nature of the microfluidic device described in the previous chapter, and focus was given to methods that allowed for continuous operation at this scale. The characteristics of ATPS made them an ideal method for this purpose, given that not only are they a common approach for protein separation and purification that can be used at both bench and laboratory scales, but this type of system also presents protein extraction with good yield and selectivity, eliminating most of the contaminants such as cell wall debris or nucleic acids in a single step. It becomes of particular interest when combined with the laminar flow profile of microfluidic devices, that facilitates the formation and stabilization of two-phase flow [158]. Previous works have already demonstrated that microfluidic devices can be used as a simple and fast method to characterize an

ATPS [164], and also a tool to optimize affinity-driven partition conditions for specific products [165].

4.2 Materials and methods

4.2.1 Chemicals and biologicals

LB Broth and LB Agar cell culture mediums were obtained from Nzytech. Tris-buffer, lysozyme from chicken egg white, sodium salicylate, PEG with 3350 Da molecular weight, and phosphate salts (K_2HPO_4 and KH_2PO_4) were purchased from Sigma-Aldrich. PEG stock solutions were prepared at 50% concentration (w/w), while phosphate stock solutions were prepared at 20% (w/w), with a 1:1.43 ratio of basic to acid forms of the salt, to obtain a solution with pH=7. B-PER® was purchased from Thermo-scientific. *E. coli* bacterial strains BIVU0811 harboring the pMAB1-GFP-C-lytA plasmid were kindly supplied by Biomedal (Seville, Spain). A Milli-Q® water purification system was used to supply water for all experiments (Millipore, Bedford, MA, USA).

4.2.2 Cell culture

Recombinant, GFP-LYTAG producing, *E. coli* strains were cultured according with the supplier protocol (Biomedal, Spain). Briefly, a pre-inoculum was cultured overnight in LB medium, with $100\,\mathrm{mg\,l^{-1}}$ of ampicillin ($37\,^{\circ}\mathrm{C}$, 270 rpm). $250\,\mathrm{ml}$ of cell medium were then inoculated from this culture, at an initial OD600 = 0.1, and cultured under the same conditions. Gene expression was induced at OD600 = 1.0 through the addition of $2\,\mathrm{mM}$ sodium salicylate, and cultured for 5 hours at $30\,^{\circ}\mathrm{C}$, 225 rpm. Cell samples were then collected for further assays. Optical density was measured using a spectrophotometer (T70 UV/VIS Spectrophotometer, PG Instruments). Lysate samples were obtained using an ultrasonic homogenizer (Sonoplus HD 3200, Bandelin).

4.2.3 Soft lithography of PDMS structures

PDMS microfluidic devices were fabricated using standard soft lithography processing as described in section 4.2.3. The final structure was then cut, the inlets and outlets punched using a blunt syringe tip (Instech Solomon, Plymouth Meeting, PA, USA), washed, and irreversibly sealed against a $700\,\mu\mathrm{m}$ thick PDMS membrane, prepared by spincoating a silicon wafer with PDMS, and polymerized using the same procedure. The structures were sealed using an oxygen plasma by exposing both surfaces for $1\,\mathrm{min}$ with a power of $11\,\mathrm{W}$ (Harrick Plasma PDF-002-CE).

4.2.4 Lysis module

The first half of the microfluidic channel is dedicated to cell lysis evaluation. The operational parameters of the lysis module have been previously described in greater detail for its single application [185]. In brief, this module exploits the difference in diffusion coefficients between whole cells and free, intracellular produced fluorescent proteins, to evaluate the efficiency of cell lysis occurring within a microchannel. A cell suspension and a lysis solution are injected side by side into a long channel. Since in microfluidics and in laminar flow conditions the only driving force for transversal mixing is

Table 4.1: Flow rate experimental conditions tested, with corresponding labels. Test solution refers to either a buffer solution, B-PER®, or lyzosyme solution

	Flow rates ($\mu L\,min^{-1}$)			
Label	1:2	1:1	2:1	1:1
Cell suspension	1.0	1.5	2.0	0.75
Test solution	2.0	1.5	1.0	0.75
Total flow rate	3.0	3.0	3.0	1.5

diffusion, it is possible to exploit the different diffusion coefficients of free protein and whole cells to measure the percentage of cell lysis by the fluorescence profile at the end of this stage. By varying the cell suspension to lysis solution flow rate ratio it becomes possible to test for different lysis solutions dilutions and cell fractions, and by varying the total flow rate it is possible to test different residence times, and thus contact times. Due to their lower diffusion coefficient, whole cells tend to stay on the side of the channel in which they are injected, while the higher diffusion of free protein allows them to occupy the entire channel. This creates a fluorescence profile that directly correlates with the percentage of product released with a specific combination of lysis conditions.

Since the extent of the diffusion in the channel is dependent on the channel length and cross-section, the device presented in this section uses the channel dimensions from the previous work (Chapter 3). The designed microchannel is $30\,cm$ long, with $50\,\mu m \times 50\,\mu m$ square cross-section. The output of this module is directly integrated as an input to the next microfluidic structure, the ATPS module.

Two different lysis solutions were tested: A commercial lysis solution, B-PER®, based on non-ionic surfactants, and an enzymatic solution of lysozyme ($100\,\mu g\,mL^{-1}$ in $50\,mM$ Tris-HCl, pH=7.5). B-PER® has been described to have a permeabilizing effect on the cells, releasing the product without full cell disruption, while lysozyme releases the product by attacking and destroying the cell wall [155, 171, 172].

The experimental conditions used for each tested solution are listed in table 4.1, so that all mentions of 1:2, 1:1, and 2:1 ratios are volume/volume ratios, defined by the ratio of the flow rates being injected into the system.

4.2.5 ATPS module

The other part of the device is a microfluidic module that performs PEG/phosphate ATPS for the separation of free protein from the cell lysate. Previous work has described the use of microfluidic devices for the characterization of the binodal curves of an ATPS[164], as well as multiplexed screening of affinity-driven partition systems [165], however none of these systems integrated ATPS with other operations. This section of the microfluidic device consists of a $30\,cm$ long channel, with a $150\,\mu m \times 50\,\mu m$ rectangular cross-section. A 20% phosphate solution and a 50% PEG solution are injected sequentially in a second set of inlets downstream from the lysis module, and allowed to diffuse along the microchannel. The output of the previous lysis module leads to an input in this module. This module was used for two functions: first, to characterize the binodal curve of the system for various

loadings, in order to study the effects that the different components present in the lysate could have on the partition, or on the formation of the system; and second, as a method for the screening of continuous protein separation conditions. A system composition was selected from the binodal characterization, which was then used to compare product separation from the various lysates obtained under different conditions. Micrographs were acquired at the outlet.

4.2.5.1 Microfluidic binodal curve determination

ATPS can be characterized by their phase diagrams and binodal curves, a representation of the space of conditions where two-phase separation occurs that, when combined with tie line measurements, also provides information on the volume fraction of each phase [66, 186]. While their determination is usually labor intensive and time consuming, microfluidic devices have helped accelerate this process. The binodal curve was determined at microscale using a previously described method [164]. In short, PEG and phosphate aqueous solutions were introduced into the second set of inlets, while either combinations of water, cell suspension and cell lysis solutions were injected at inlets 1 and 2. The presence or absence of two phases was registered at the outlet for the various compositions.

By varying the relative flow rates of three solutions (PEG, Phosphate, and the output of the lysis module which consisted of either water, a cell suspension, or a mixture of cell suspension and B-PER®), it was possible to rapidly test a wide range of concentrations inside the microchannel. Using optical microscopy it was then possible to differentiate between three different states at the outlet: i) the presence of an interface, indicating a condition above the binodal curve; ii) an unstable or intermittent interface, indicating a condition very close or overlapping the binodal curve; or iii) absence of any interface, indicating a condition below the binodal curve. Each data point was then plotted as a function of its corresponding PEG and phosphate concentrations, as well as the type of interface measured. The data points presenting unstable interfaces were used to fit a binodal curve and compared with macroscale data previously reported in the literature [66].

The same process was repeated using different loadings of cell suspension and test solutions relative to the total ATPS composition, in order to test the effect of the various solutions on the binodal.

4.2.5.2 Protein concentration from lysate

Having determined the binodal curve of the total system, the combined lysis and protein concentration modules were tested. A crude cell extract suspension was injected at inlet 1, while a chemical cell lysis solution under testing was injected at inlet 2, as described in section 4.2.4. At the same time, PEG and phosphate solutions were injected at inlets 5 and 6, as described in section 4.2.5.1. The protein extraction for various lysis conditions was tested by changing the lysis conditions of the first module, as described in section 4.2.4, while maintaining the relative flow ratio at inlets 5 and 6. The partition coefficients for the various conditions were determined by the ratio of fluorescence between the two formed phases, from equation 4.1:

$$K_p(x) = \frac{Fluo_{PRP}}{Fluo_{SRP}} \tag{4.1}$$

were $Fluo_{PRP}$ is the fluorescence value from the PEG rich phase, and $Fluo_{SRP}$ the fluorescence from the salt rich phase, both measured by grey value intensity from an 8-bit image, using ImageJ (National Institute of Health, Bethesda, MD, USA).

4.2.6 Microfluidic operation and image acquisition

The solutions were injected using syringe pumps (New Era Pump Systems, NE-300) through each of the 4 inlets. A fluorescence microscope (Leica DMLM) equipped with a DFC300FX camera was used to monitor the fluorescence diffusion across the first half of the microfluidic chip, and the protein partition in the ATPS at the outlet. For this, a 100 W mercury light lamp coupled with a light excitation filter with a band-pass of 450 nm to 490 nm, and a long pass emission filter of 515 nm was used. Fluorescence images were acquired with 1 s exposure time, and processed using ImageJ (National Institute of Health, Bethesda, MD, USA), and GNU Octave (version 4.4.1). In the lysis assays, images were acquired just before the point of injection of the PEG and phosphate inlets, while in the ATPS assays image acquisition was performed at the outlet. All acquired images were first converted into grey scale 8-bit images. In the lysis assays, the fluorescent signal was analyzed by vertically aligning to the microchannel wall, plotting the microchannel area profile, and calculating the fluorescence ratio. In the ATPS assays, the partition coefficient was calculated by extracting the average fluorescence value for the PEG rich phase and salt rich phases, and calculating the partition coefficient K_p using equation 4.1. The area outside the channel was averaged and subtracted as background for all pictures.

4.3 Results and discussion

4.3.1 Microfluidic platform combining two integrated modules: cell lysis module and ATPS module

The final microfluidic design and structure are detailed in Figure 4.1. To better characterize the system, each module was tested sequentially, and then combined to evaluate the integrated process.

4.3.2 Lysis module

The lysis module is used to screen extraction conditions for the product of interest, employing either chemical or enzymatic lysis. This module (Figure 4.1 (a)) exploits the difference in diffusion coefficients between whole cells and free protein which, when combined with the laminar flow profile inside a microchannel, results in the limited diffusion of whole cells, and on the full diffusion of the free protein, for a properly dimensioned microchannel. When combined with a fluorescent protein, such as GFP, this results in different fluorescent profiles that can be directly correlated with the percentage of cell lysis.

The mathematical modeling, dimensional optimization, performance characterization, and data analysis methods of a similar module have been previously described in Fradique et al. [185] and

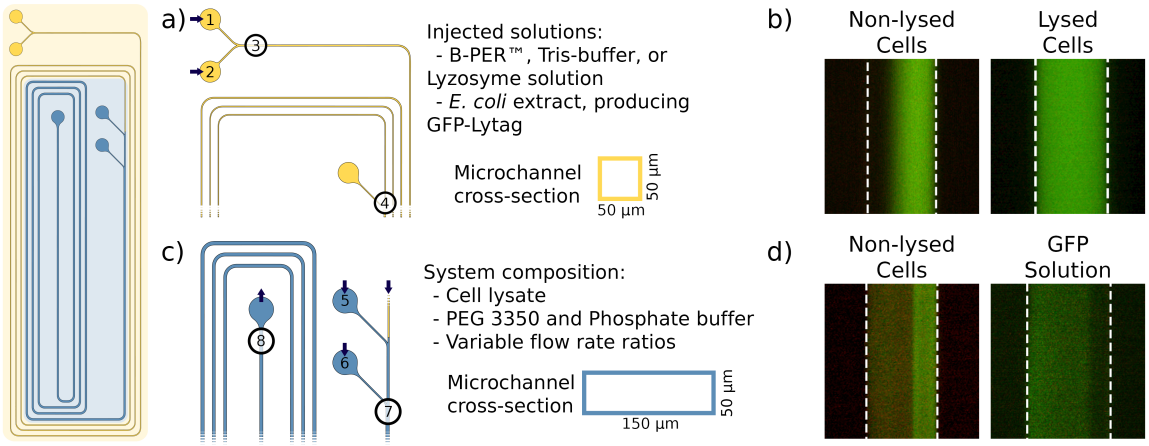

Figure 4.1: Schematic representation of the microfluidic structure, composed of two integrated modules. (a) The lysis module (yellow) is a 30 cm long, 50 µm × 50 µm square channel. A lysis solution and cell sample are injected at inlets 1 and 2, respectively. A fluorescence profile is measured at sections 3 and 4, after the inlets and just before injection into the second module, respectively. Typical fluorescence profiles for non lysed and lysed cells are represented in (b). (c) The ATPS module (blue) is a 30 cm long, 150 µm x 50 µm rectangular channel. 50% PEG and 20% phosphate solutions are injected sequentially at inlets 5 and 6, visually inspected in section 7, allowed to mix along the channel, and measured in section 8. Typical fluorescence profiles for non-lysed cell suspensions and free protein solutions are represented in (d)

these methods were used to quantify the cell lysis efficiency of each condition by correlation with the fluorescence ratio measured at the outlet.

Given the goal of being able to combine upstream and downstream processes into a single microfluidic chip, for example, in the form of a microbioreactor used as a cell suspension source, this work used crude extract samples from macroscale fermentations. The microfluidic module (in yellow in Figure 4.1) was used to test for 2 different residence times, using both chemical and enzymatic lysis solutions, with 3 different cell suspension:lysis solution ratios. Data was acquired at point 4 (indicated on Figure 4.1 (a)). Total residence times were determined by the total flow rate of the system. All tested conditions and obtained cell lysis efficiencies are included in Figure 4.2.

The first result to note is the absence of fluorescence diffusion in the cell samples co-flowed with buffer, presenting two distinct regions within the channel, characterized by a clear fluorescence separation, independently of the residence times and flow rate ratios used. The slight fluorescence present in the buffer region is expected, given the possible presence of free protein released during the fermentation as a result of natural cell death during the growth phase. This signal was measured and subtracted from all measurements. This result serves as control for the system showing the fluorescence profile of the microfluidic device when no lysis occurs.

By comparing the results obtained from the different flow rates, it is possible to observe that the lytic effect of B-PER® presented a dependence on the residence time, as noted by the increase in lysis efficiency observed in the lower flow rate condition ($1.5\,\mu L\,min^{-1}$) compared to that at the higher flow rate condition ($3\,\mu L\,min^{-1}$). The increased residence time allows for a longer interaction between the cell lysis solution and the cells, consequently achieving full cells lysis and product release along the length of the channel, as can be observed by the uniform fluorescence profile in Figure 4.2. While presenting lower lysis efficiencies, the same residence time dependence can be noted in the lyzosyme

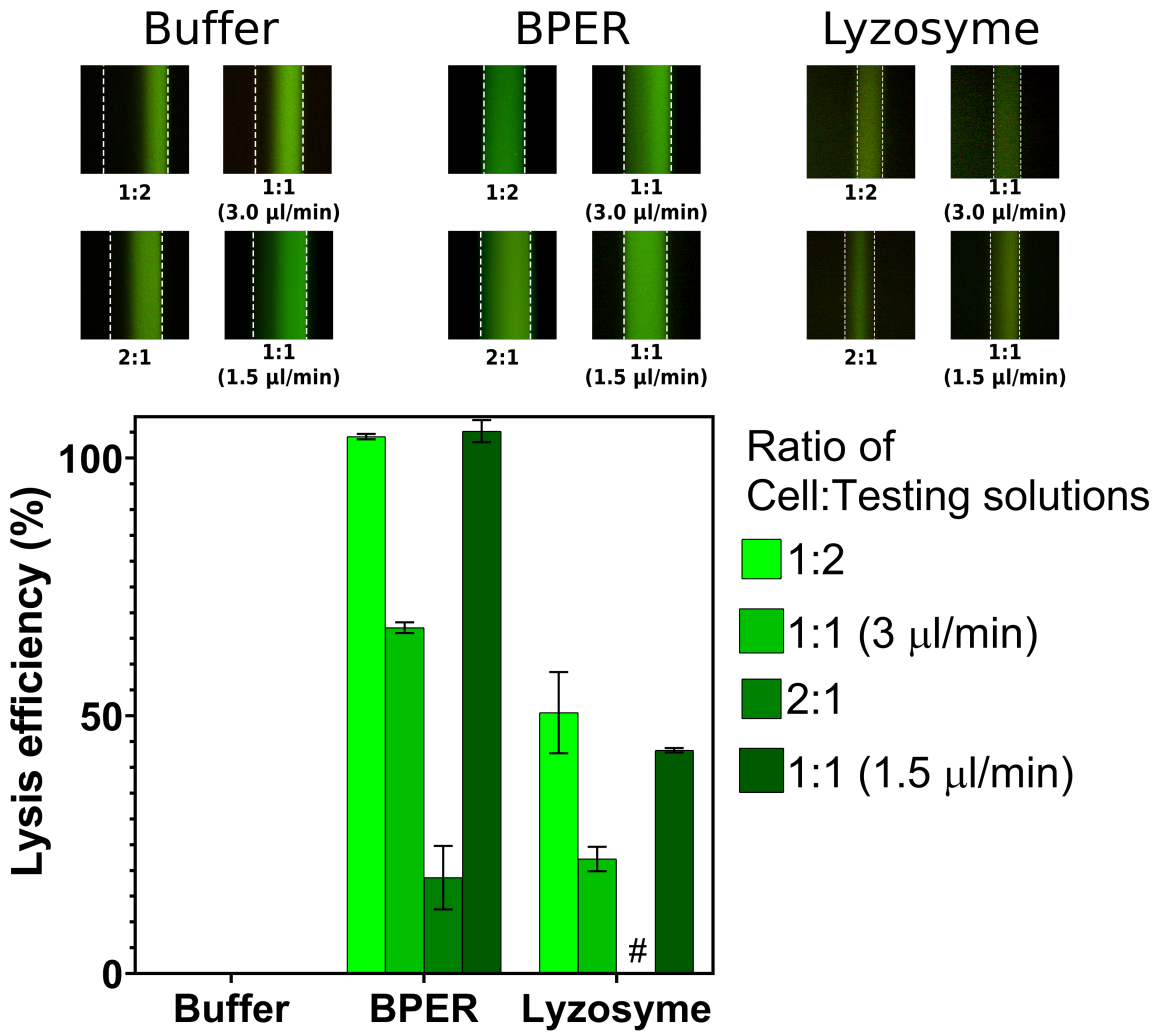

Figure 4.2: Cell lysis efficiencies obtained using Tris-HCl buffer, B-PER® or lysozyme, derived from the cell lysis/fluorescence ratio relation for a square, 50 µm × 50 µm, 30 cm long channel, as previously described in Fradique et al. [185]. Different residence times were tested, using a 1:1 ratio (v/v) of cell suspension:lysis solutions, as well as different flow rate ratios, corresponding to different lysis solutions dilutions. The top micrographs are representative of the fluorescence profiles obtained for each condition. Each point was measured in triplicate. # - refers to non measurable conditions

assays, with increasing lysis efficiency for longer residence times.

Comparing the different cell suspension:lysis solution volume ratios, the chemical lysis solution efficiency decreased with increasing cell suspension fraction, with a sharp decrease above a 1:1 ratio, showing a dependence on the concentration of lysis solution in the system, while for the enzyme solution, increasing the fraction of cells in the system decreased the lysis efficiency when up to a 1:1 ratio. Further increasing the cell suspension fraction to a 2:1 ratio led to the appearance of a viscous phase in the middle of the channel, resulting from the excess release of genomic material by the increased amount of cells, impeding an accurate measurement of cell lysis efficiency using this method.

These results are consistent with previous measurements on an isolated lysis module [185], presenting lysis efficiencies with the same profile for each condition, demonstrating that the fundamental

characteristics of the lysis device were preserved after upstream integration with the ATPS module, maintaining its function.

4.3.3 ATPS module

4.3.3.1 Binodal curve characterization

4.3 shows the different binodal curves obtained when either a cell suspension or a mixture of cell suspension and B-PER® were loaded with the system (representing 20% of the total volume), to test the effect of each of these solutions on the formation of the two phases. From the results of Figure 4.3, one can conclude that none of these solutions had any significant impact on the behavior of the PEG/Phosphate system. This demonstrates the ability of the system to characterize the formation of an ATPS at the microscale, showing a good correlation with the macroscale data, while using a fraction of the reagents and time compared with the traditional methods. Initial concerns that the surfactant-based lysis solution could impair the formation of the biphasic system by interfering with surface tension proved unfounded, likely due to the relatively low amount present in the final composition given the low loading fraction used. Also, in the case of the system involving cell samples, where the presence of various salts and cell debris could potentially affect the system separation, but no effect was noted.

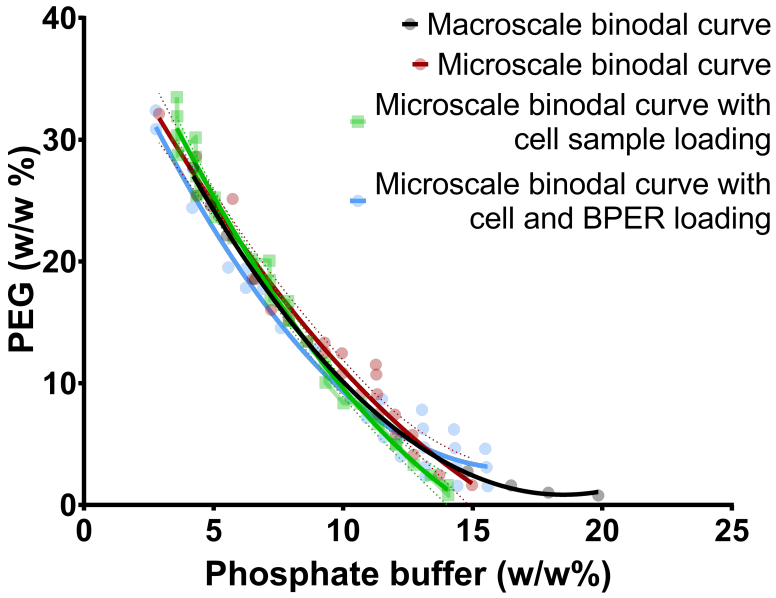

Figure 4.3: Plot of the PEG 3350/Phosphate buffer system binodal curve. Each axis represents the percentage of polymer and salt to the total system by weight. The remaining percentage is water, or water and the loading solutions when indicated. The translucent points represent the measured data points used to fit the curves. The macroscale binodal curve, in black, was reported from Zaslavsky [66] relative to PEG 3400.

4.3.3.2 Aqueous two phase extraction

Following cell lysis, it is important to isolate the maximum amount of product with the minimum number of operations possible. ATPS have already been demonstrated as a potential method for

the purification of proteins from complex biological samples [158]. This effect can be intensified by genetically tagging the recombinant protein of interest with short affinity tags that increase their partition into one of the phases [165], as is the case with the GFP used in this study. This effect was exploited in this study to improve the separation of the protein of interest from the lysate. A second aspect is the removal of whole cells remaining after an incomplete lysis. Although an incomplete lysis results in a lower release of the target product, the reduction in cell debris, and thus reduction in purification and increased productivity, could prove advantageous for certain applications.

While the mechanism governing protein partition in an ATPS is complex, it can be described as the combined effect of the hydrophobicity of both proteins and phases, the electrochemical potential between phases and proteins, the size of the molecule being separated, the biospecific affinity of the protein to any of the phases, and the protein conformation [186]. However, when used to separate larger particles such as cells, other forces can also influence the partition, namely inertial and viscous drag forces [187]. These are a consequence of the different viscosities of the phases, the dimensions of both the microchannel and the phase flow section, and the flow velocity in each of the phases [188].

GFP-LYTAG has been previously described to have an increased partition to the polymer rich phase (PRP), due to salting out effects that decrease the solubility of the protein in the salt rich phase (SRP), combined with the increased affinity for PEG molecules given by LYTAG ligand [165]. The partition of *E. coli* in an ATPS has been described as dependent on the surface hydrophobicity and net charge of the cell, and the ionic strength of the system [165, 189], with its behavior also being influenced by flow rate and medium viscosity in microchannels [187, 190]. To observe the partition behavior of *E. coli* cells and free protein, isolated cell and GFP samples were loaded into the system, as shown in Figure 4.1 (d). It is possible to observe the clear partition of GFP into the PRP (left), while the cells tend to partition to the SRP (right). This preference of the cells has been observed before [191, 192], and is dependent on the type of cell, on the proteins the cells present at the surface, and on the cell interactions with both phases of the ATPS [192]. It should be noted that while cells showed a preference for the SRP, it was still possible to detect a fluorescent signal from the PRP. Given the relatively large size of a bacterial cell, as well as the smaller volume fraction of the SRP, it is possible to create a condition with reduced available free volume, effectively saturating the SRP [191]. In contrast, when a clarified cell lysate sample was loaded, containing no cells, the fluorescence profile focused on the PRP, showing the increased affinity of the target protein, an effect that was also previously described in greater detail [165]. This differential partition can thus be exploited as a method to separate the protein from the remaining cells under incomplete lysis conditions. Also, of note are the previous reports that both genomic material and cell debris tend to accumulate either at the interface or in the SRP, making ATPS an ideal method to remove these contaminants [158].

4.3.3.3 Combining modules for screening overall process conditions

Having demonstrated the partition behavior of both whole cells and free protein when injected into the system, these were replaced with the various lysates resultant from the output of the lysis module for the various conditions tested, and the partition coefficient was calculated from the fluorescent

intensity in each phase. Considering the results from section 4.3.3.2, it should be taken into account that the fluorescence in each phase will be mainly a function of the remaining whole cells, in the case of the SRP, and the released free protein for the PRP, as well as the particular affinity and partition of the system, and any effect that cell debris have on the partition.

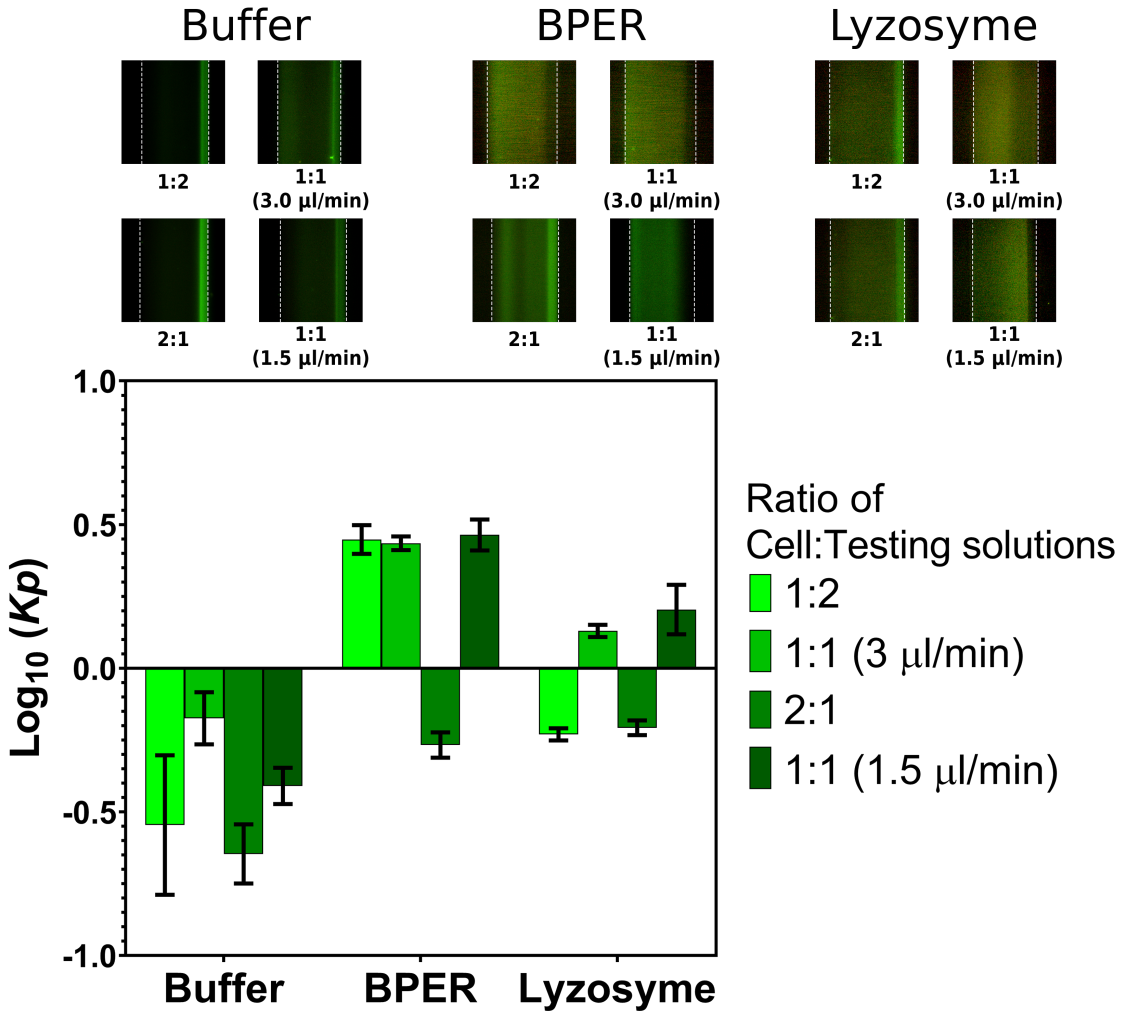

Figure 4.4: Level of extraction of GFP-LYTAG in PEG/Phosphate ATPS from different lysates. Each lysate is composed by 1:2, 1:1, or 2:1 ratio of cell suspension to test solution (v/v), for different total flow rates (as detailed in table 4.1)

As mentioned above, when no lysis occurs the cells tend to partition to the SRP, as demonstrated in all the experiments using buffer.

Overall, comparing the assays using B-PER® and lyzosyme, it is also possible to note that the partition coefficient is decreased when the enzyme is used. Given the lower lysis efficiencies obtained with the enzyme solution, the higher number of remaining cells that partition to the SRP can account for this decrease. In addition, considering that lyzosyme can also be partitioned into the PRP [193], this can decrease the amount of free-space available for the GFP to diffuse into, further decreasing the partition coefficient. While this can be a possible limitation of this ATPS, it is also possible to use an additional back extraction step using choline, exploiting the natural affinity of the LYTAG to isolate

the tagged protein and extract it to a different phase [165].

Focusing on the different conditions tested for each solution, it is possible to note that the partition coefficient tends to follow the lysis results for the surfactant-based solution, that is, conditions presenting higher lysis efficiencies, and thus higher amounts of free protein and lower number of remaining whole cells, also present higher partition coefficients. This is a good indicator that the partition is dependent solely on the amount of free protein and whole cells remaining, without being affected by the lysis solution.

On the other hand, the lyzosyme results present different profiles. While the 1:2 (cell:lysis solution) condition presented a lysis efficiency of about 50%, its partition coefficient shows that most of the fluorescence remains in SRP. A possible explanation for this is the higher amount of lyzosyme in suspension, due to the higher volume fraction of lysis solution being injected. This increased protein content can contribute to the saturation of the PRP, decreasing the partition coefficient of the target fluorescent protein, also combined with the lower amount of GFP, resulting from the lower volume fraction of cell suspension used in this condition. In fact, while increasing the volume fraction of cell suspension and decreasing the volume fraction of lyzosyme solution resulted in a lower lysis efficiency, it also allowed for an increased partition of the target protein, with increased fluorescence in the PRP. The lower amount of lyzosyme in suspension avoids the saturation of the PRP, highlighting the need for a holistic approach to process development, since in this case the most efficient conditions on one step caused severe limitations on the next.

While decreasing the relative amount of lyzosyme in solution appears to improve the separation process, the condition using 2:1 cell:lyzosyme solution presented issues in the lysis stage. While not measurable in the experimental setup, some lysis had to have to occurred given the increased viscosity presented inside the microchannel, presenting some amount of released product that could be separated in the ATPS. Nevertheless, only the SRP presented a fluorescent signal. This can be the result of multiple effects. One possibility is that the lower lyzosyme concentration results in a slower and less effective lysis, which is further hindered by the increased viscosity due to the release of genomic material from a higher number of cells in suspension. This results in lower amounts of free GFP in suspension to be separated. In addition, before the partition of a molecule can be affected by its properties and affinities for a given phase, it has to have contact with that phase [192]. The highly viscous environment that surrounds the cells in this condition can also hinder the diffusion and contact between the released protein and any of the system phases, further decreasing its partition coefficient.

Finally, given the limitations presented by the different ratios of cell:lysozyme solution with the 1:1 ratio presenting the best partitioning, increasing the residence time by decreasing the flow rate could improve the system performance by increasing the lysis efficiency while maintaining the partition behavior. In fact, this was observed with a slight increase in the partition coefficient due to the relatively lower number of whole cells remaining that partition to the SRP, combined with an increase in product release from the first stage.

4.4 Conclusions

This chapter describes the application of a multimodular microfluidic device for the screening of continuous lysis and separation conditions. By combining multiple unit operations on a single device, it was possible to screen not only for the optimal conditions for each operation, but to account for the combined effect of each on the overall process.

The lysis module was tested using different dilutions of the lysis solutions, as well as different residence times. It was possible to determine that the efficiencies of both the chemical and enzymatic lysis solutions mainly depend on residence time, and thus on contact time. Lysis efficiencies increased from about 65% to 100% for the chemical lysis solution, and from about 20% to 40% in the case of the enzymatic solution, by halving the flow rate, and thus doubling the residence time. It was also possible to note a sharp loss of efficiency with dilution when using the chemical lysis solution, rapidly decaying for ratios above 1:1. On the other hand, when using a 2:1 cell:enzymatic lysis solution ratio, it was possible to once again identify the formation of a highly viscous phase forming within the channel, result of the rapid release of genomic material. The fact that these results closely follow the results from Chapter 3 are a good indicator that the integration with a subsequent downstream module, with the required structural adjustements, did not fundamentally change the behaviour of the lysis module, and that indeed microfluidic modules can be combined for more complex applications.

The microfluidic device also allowed for the characterization of the ATPS itself, so that the possible effect of any component of the solution to be combined in an ATPS can be rapidly observed and accounted for. In this way, the microfluidic device delivered a rapid process screening and optimization, with very low reagent consumption, and using a simple fluorescence microscope for data collection. Multiple ATPS were tested in rapid succession, with different loadings, and showing that none of the tested conditions would impact the formation of the system in itself. The overlap of the obtained binodal curves with the previously described curve for the same system is also a further evidence for the applicability of this microfluidic for the characterization and optimization of scalable ATPE systems.

Evaluating the performance of the combined system, it was first possible to note that the partition coefficients in the conditions using the chemical lysis solution mostly follow the results from the lysis module, with higher lysis efficiencies also presenting higher partitions. However, it was interesting no note that the same is not true for the enzymatic lysis. Increasing the enzyme solution fraction resulted in higher lysis efficiencies, however, the increased protein content of this condition hinders the extraction process, presenting a lower partition coefficient. This result is a demonstration that the optimal conditions of each individual process are not necessarily the optimal conditions for the combined process, and how this type of approaches can accelerate the development of new processes by integrating multiple operations in a single device.

Once more, the continuous nature of the device makes it possible to be combined with modules, such as other downstream processing operations for further testing or product purification, or the microbioreactor described in chapter 2 as an upstream cell sample source. It would be useful to also integrate fluorescence sensors along the channel, to measure both the lysis efficiencies and

partition coefficients in line in an automated fashion. This would possible require changes to the microfluidic channel to separate the streams into isolated measurement chambers, to avoid light cross-contamination, but could rapidly accelerate the data collection and analysis of this type of system that for now relies on scripted analysis of micrographs.

5

Conclusions and Future Work

5.1 Outlook and conclusions

Microfluidics hold a great promise as tools for the faster and cheaper development of biomanufacturing processes. The scope of this thesis work focused on the development of microfluidic platforms that could be capable of guiding process development, rapidly screening for multiple conditions, while taking into account any cascading effects that could arise.

In Chapter 2 a microfluidic bioreactor was developed with the goal of emulating the upstream stage of a biomanufacturing process. The integrated peristaltic pump reached a flow rate of $55\,\mu l\,min^{-1}$, while the integrated heater managed to keep the system within the $36\,°C$ to $39\,°C$ range. A laser and photodiode combination used the microfluidic channel as an optical guide to increase the optical path of the measurement which, combined with the use of opaque PDMS structures, resulted in a compact system capable of measuring the optical density of a fermentation in real time. When operated in batch mode using *E. coli* cells, this combination resulted in a duplication time of about $30\,min$, slightly lower than the typical $20\,min$ described for this organism. Overall, this demonstrates that this small integrated microfluidic device can function as a cell supply source, with the ability to grow bacterial fermentations in very low volumes.

Nevertheless, it would be useful to understand the root causes of the decreased growth of the bacteria in the device, to better guide further improvements. In addition, modifying the device for continuous operation, and improving the laser stage and handling, would be key changes required in a future work. This would then open the possibility of using the device as a method to test different cell cultures against multiple disturbances, like the presence of antibiotics or contaminants, in continuum.

With a method capable of supplying cell samples, chapter 3 focused on one of the first stages of downstream processing, product release. This chapter describes the development of a microfluidic

device for cell lysis screening and optimization, capable of continuous operation. By combining chemical and enzymatic lysis solutions with a fluorescent product, the microfluidic device is able to rapidly test a variety of conditions for product release, capable of testing different contact times, cell:lysis solution volume ratios, and dilutions with near real time results.

Starting with the chemical lysis solution, it was possible to note a high dependence of the lysis efficiency with the residence time, with the lysis efficiency increasing from aproximately 50% for the highest flow rate, to 100% for the lowest, for buffer resuspended cells. The same behavior was observed for the raw fermentation samples, with the efficiency increasing from about 75% to 100%, showing that at a 1:1 dilution, the surrounding medium has no effect on the lysis. The same could not be said for the tests using different ratios of cell:lysis solution. Where the buffer resuspended samples presented no particular difference between the different ratios, the raw fermentation samples showed a hard limit for dilution, with the lysis efficiency sharply decreasing with the increased cell fraction. Of particular note are the results of the enzymatic lysis solution. While also presenting a dependence on residence time, this solution demonstrated the ability of the microfluidic device to detect potential downstream problems for a particular condition. The rapid release of genomic material in some of the combinations resulted in the formation of a viscous phase in the channel, which was decreased for conditions that included a higher enzyme solution fraction. The lower enzyme concentration, coupled with the increased concentration of inhibitory lipopolysaccharide (LPS) contributed to a milder cell lysis, which allowed for improved results.

This work would greatly benefit by the integration of other methods of detection and quantification, such as optical or impedimetric sensors. This would allow for the integration of data analysis methods, that coupled with the use microfluidic valves to control the input of multiple solutions, and design of experiment approaches, could lead to a fully automated platform capable of completely characterizing a space of lysis conditions in a very short time.

Finally, in chapter 4 the method described in chapter 3 is coupled to a microfluidic separation method, ATPE. Starting with an initial characterization of each of the two modules, the integrated lysis module confirmed the results obtained from the previous work, showing that it is possible to integrate multiple microfluidic modules with minimal design changes, without fundamentally affecting its function. As for the ATPS module, an initial characterization demonstrated that the device could correctly determine the binodal curves of several systems, with multiple different loadings, and with comparable results to larger scale systems. It also showed that none of the components used in the lysis module would affect the formation of the system in the ATPS module.

Testing the combined modules, it became clear that the GFP partition in the chemical lysis conditions was mostly dependent on the lysis efficiency, with higher partitions for increased efficiencies. However, much more interesting were the results for the enzymatic lysis conditions, where the condition with higher lysis efficiency presenting one of the lowest protein partitions. The increased protein content induced by the higher enzyme solution fraction hinders the extraction process, demonstrating a case where the optimal conditions for a particular operation do not correlate with the optimal conditions for the full process. In this way the device becomes a useful tool in the screening and

optimization of bioprocesses, allowing for the early detection of potential issues that would only be encoutered at a later stage.

By combining these two methods, this device made possible the evaluation of the effect that different lysis conditions can have on the extraction process. With this knowledge, the same device can also be used to further refine and optimize the ATPE process, creating a screening platform for the cascading effects of these downstream processes.

In future applications it should be possible to further improve this device in multiple ways. First, given the reliance of the device in the flow rates of the inputs, integrating a form of electronic control to these inputs should accelerate the process of screening for multiple conditions, as well as the initial system characterization. In addition, the integration of optical or impedimetric sensors at the output of each module would open the possibility for a fully automated platform, that could detect the extent of cell lysis for a determined condition, characterize the binodal curve for an ATPS, and combine this information to rapidly screen a variety of condition permutations, in effect creating an automated optimization platform.

Taking all the previous work in consideration, a final future perspective is the integration of the microreactor developed in chapter 2 with the screening device from 4, which would become one of the first described microfluidic platforms integrating both upstream and downstream operations into a single device.

5.2 Future work

5.2.1 Microchemostat operation and integration

One of the first steps in bioprocess development is to choose the type and strain of organism to use, and what type of modifications are required. The current methodologies for strain screening and optimization can be limited in the number of variations that can be tested due to time and resource constraints. Not only this, but the decoupling between the development of the organism and that of the extraction and purification processes can also create issues later on. As such, it is important that the microfluidic integration of these processes can account for all stages. The integration of a microchemostat device with other downstream processing modules would become a very interesting solution, allowing for the rapid, and possibly automated, testing of multiple growth and product manufacturing conditions.

A microchemostat could provide a continuous supply of cells for other downstream modules, where the extraction and purification conditions can be rapidly altered and optimized. By then varying the growth conditions, it would be possible to observe how these changes could affect the downstream processing, for example in organisms were higher productivities also result in higher amounts of contaminants being produced. It could also be used by itself as a method to screen for optimal growth conditions, noting the effects of different medium compositions, cell densities, and sheer stress.

A second useful approach for this type of device would be the combination with other microfluidic modules for upstream operations, for example by coupling to a microfluidic cell factory, a device where

microorganism cell libraries can be created and tested. The resulting device could not only create multiple variations of an organism, but also rapidly select the most promissing ones for a certain goal, isolate them, and grow them under a variety of conditions. This could greatly accelerate the selection process for new strains and for the manufacturing of new products.

5.2.2 Automated screening of downstream processing conditions

Microfluidic devices are currently being increasingly used as tools in the development of new bioprocesses for their parallel and automated process operation. However, most described applications are still single process devices, and usually include little more than basic function automation. In order to fully explore the potential of microfluidic applications it is important to not only integrate the various modules into a functioning device, but also to include data acquisition and control systems capable of operating the device in an automated fashion. This type of integrated systems would greatly benefit from a combination with data science tools, where the extracted data from each sensor or device could be included into a larger data set from multiple runs or devices, which could then be used to guide the next set of experimental conditions.

This type of approach obviously depends on the integration of multiple sensors and actuation mechanisms capable of enacting the conditions inputed. While several works have already started to include these types of components in their designs, there is still room for improvement in their applicability for screening and optimization. For example, it should be possible to combine fluid control mechanisms, such as syringe pumps and pneumatic valves, with optical sensors, to automatically characterize an ATPS in a microchannel. This information could then be combined with the use of optical sensors for the quantification of the partition coefficient of a protein in the system, to derive a set of optimal conditions for its purification, without the need for other inputs.

5.3 Microfluidics, the tools of the future for bioprocess development

After their impact on medical diagnostics with the development of LoC systems, microfluidic technologies now have the potential to rapidly accelerate the development of new bioprocesses. Starting with the creation and selection of new strains, many of the DNA processing techniques firstly developed for sample treatment are now being adapted for process development, and being combined with new technologies such as CRISPR. This is allowing for the development of microfluidic chips that can create, sort and evaluate entire libraries of cells in a fraction of the time. The use of droplet microfluidics is also starting to rival the performance of the first generation of FACS systems, paving the way for a new wave of devices for strain selection.

In addition, microfluidic technologies are also being employed in the study of the metabolic pathways used in various organisms, enabling the development of new systems capable of high troughput with single cell resolution, where individual cells can be followed and isolated from a large population growing in a microbioreactor chamber. This type of devices is also being used to evaluate the use of

new substrates and applications, for example in studying the treatment of waste waters using microbial cultures by testing multiple organisms with different types of contaminated water, where a single device can replace multiple laboratory scale experiments.

Regarding the production of biopharmaceuticals, the combination of cell factory devices with the use of microbioreactors can radically greatly accelerate development times for new drugs. The creation of a large variety of modified organisms, combined with the capability to test orders of magnitude more strains in the same time frame using parallel devices, can become a powerful tool in the optimization of new production models.

When it comes to product separation and purification, the current microfluidic applications are either adapting previous techniques used for sample treatment in LoC applications, or creating miniaturized versions of large scale methods that can be optimized in smaller scale. Either way, this type of devices is already demonstrating their worth in the optimization of bioprocesses. Several devices are now capable of testing the susceptibility of an organism to a variety of lysis methods, so that product release can be optimized. The down-scale of multiple unit operations has also been successful so far, with good correlations between large-scale results and small-scale data. For example, microfluidic chromatography devices have been able to identify a range of optimal conditions for different resins, avoiding the need to test the whole range of conditions at larger scale.

As it stands, the future development of microfluidics will likely progress in two directions. One, with further integration and automatization, this type of devices will likely be combined with the current development frameworks used by large companies, where large amounts of data are collated from different sources to guide the development stage. The ability to generate large amounts of data from parallel experiments will make microfluidic devices a key source of inputs for this type of system.

On the other hand, with sufficient advances in personalized medicine and LoC devices, as well as further developments in microfluidic bioprocesses, it would not be impossible to imagine a future were entire biomanufacturing processes can be integrated into a single device, and made available for health care applications. This combined application could be the key for true personalized medicine. Where now the cost of fully personalized pharmaceuticals is prohibitively expensive for general use, this type of futuristic devices could use a sample from a patient to determine the optimal treatment, and locally produce and purify it at a fraction of the cost. While still in the realm of science fiction, microfluidic technologies have the potential to make it a reality, with the various components needed for this type of application in development at various laboratories around the world.

Bibliography

[1] J. Conner, D. Wuchterl, M. Lopez, B. Minshall, R. Prusti, D. Boclair, J. Peterson, and C. Allen. Chapter 26 - The Biomanufacturing of Biotechnology Products . In C. Shimasaki, editor, *Biotechnology Entrepreneurship*, pages 351–385. Academic Press, Boston, 2014. ISBN 978-0-12-404730-3. doi: https://doi.org/10.1016/B978-0-12-404730-3.00026-9. URL https://www.sciencedirect.com/science/article/pii/B9780124047303000269.

[2] M. R. Aires-Barros and A. M. Azevedo. 7 - Fundamentals of Biological Separation Processes . In A. Pandey and J. A. C. Teixeira, editors, *Current Developments in Biotechnology and Bioengineering*, pages 187–237. Elsevier, 2017. ISBN 978-0-444-63668-3. doi: https://doi.org/10.1016/B978-0-444-63668-3.00007-X. URL https://www.sciencedirect.com/science/article/pii/B9780444636683000068.

[3] F. Kadir, P. Ives, A. Luitjens, and E. van Corven. *Production and Purification of Recombinant Proteins: Fundamentals and Applications*, pages 47–67. Springer New York, New York, NY, 2013. ISBN 978-1-4614-6486-0. doi: 10.1007/978-1-4614-6486-0_3.

[4] D. Kuhn, L. M. Blank, A. Schmid, and B. Bühler. Systems biotechnology - Rational whole-cell biocatalyst and bioprocess design. *Engineering in Life Sciences*, 10(5):384, 2010. doi: 10.1002/elsc.201000009.

[5] A. Moser. *General Methodology in Bioprocess Engineering*, pages 349–364. Springer Netherlands, Dordrecht, 1996. ISBN 978-94-009-0177-3. doi: 10.1007/978-94-009-0177-3_29. URL https://doi.org/10.1007/978-94-009-0177-3_29.

[6] T. M. Squires and S. R. Quake. Microfluidics: Fluid physics at the nanoliter scale. *Rev. Mod. Phys.*, 77(3):977–1026, Oct 2005. doi: 10.1103/RevModPhys.77.977. URL https://link.aps.org/doi/10.1103/RevModPhys.77.977.

[7] O. M. de Bruin and H. C. Birnboim. A method for assessing efficiency of bacterial cell disruption and DNA release. *BMC Microbiol.*, 16(1):197, 2016. doi: 10.1186/s12866-016-0815-3.

[8] Y. Wen and S.-T. Yang. The future of microfluidic assays in drug development. *Expert Opin Drug Discov*, 3(10):1237–53, 2008. doi: 10.1517/17460441.3.10.1237.

[9] D. J. Beebe, G. A. Mensing, and G. M. Walker. Physics and applications of microfluidics in biology. *Annu Rev Biomed Eng*, 4:261–86, 2002. doi: 10.1146/annurev.bioeng.4.112601.125916.

[10] R. Ghosh. *Overview of bioseparations engineering*, pages 1–12. WORLD SCIENTIFIC, 2012. doi: 10.1142/9789812773012_0001. URL http://www.worldscientific.com/doi/abs/10.1142/9789812773012_0001.

[11] K. L. P. M. G. Gunter Jagschies, Eva Lindskog. *Biopharmaceutical Processing: Development, Design, and Implementation of Manufacturing Processes*. Elsevier, 1 edition, 2018. ISBN 0081006233,9780081006238. URL http://gen.lib.rus.ec/book/index.php?md5=a3e67f355b03fc10f20440ada97c1dda.

[12] C. L. Cramer, J. G. Boothe, and K. K. Oishi. *Transgenic Plants for Therapeutic Proteins: Linking Upstream and Downstream Strategies*, pages 95–118. Springer Berlin Heidelberg, Berlin, Heidelberg, 2000. ISBN 978-3-642-60234-4. doi: 10.1007/978-3-642-60234-4_5. URL https://doi.org/10.1007/978-3-642-60234-4_5.

[13] J. Geciova, D. Bury, and P. Jelen. Methods for disruption of microbial cells for potential use in the dairy industry—a review. *International Dairy Journal*, 12(6):541, 2002. doi: 10.1016/S0958-6946(02)00038-9.

[14] Y. Chisti and M. Moo-Young. Disruption of microbial cells for intracellular products. *Enzyme and Microbial Technology*, 8(4):194, 1986. doi: 10.1016/0141-0229(86)90087-6.

[15] A. P. Middelberg. Process-scale disruption of microorganisms. *Biotechnology Advances*, 13(3):491, 1995. doi: 10.1016/0734-9750(95)02007-P.

[16] Š. Peternel. Bacterial cell disruption: a crucial step in protein production. *N Biotechnol*, 30(2):250–4, 2013. doi: 10.1016/j.nbt.2011.09.005.

[17] M. B. Lopes, T. Scholtz, D. Silva, I. Santos, T. Silva, P. Sampaio, A. Couto, V. V. Lopes, and C. R. C. Calado. Modelling, monitoring and control of plasmid bioproduction in Escherichia coli cultures. In *2012 IEEE 2nd Portuguese Meeting in Bioengineering (ENBENG)*, page 1, 2012. doi: 10.1109/ENBENG.2012.6331370.

[18] Y. K. Leong, P. L. Show, C. W. Ooi, T. C. Ling, and J. C.-W. Lan. Current trends in polyhydroxyalkanoates (PHAs) biosynthesis: insights from the recombinant Escherichia coli. *J. Biotechnol.*, 180:52–65, 2014. doi: 10.1016/j.jbiotec.2014.03.020.

[19] J. B. Kaper, J. P. Nataro, and H. L. Mobley. Pathogenic Escherichia coli. *Nat. Rev. Microbiol.*, 2(2):123–40, 2004. doi: 10.1038/nrmicro818.

[20] T. Matsumoto, T. Tanaka, and A. Kondo. Engineering metabolic pathways in Escherichia coli for constructing a "microbial chassis" for biochemical production. *Bioresour. Technol.*, 245(Pt B):1362–1368, 2017. doi: 10.1016/j.biortech.2017.05.008.

[21] F. G. Prendergast and K. G. Mann. Chemical and physical properties of aequorin and the green fluorescent protein isolated from aequorea forskålea. *Biochemistry*, 17(17):3448–53, 1978. doi: 10.1021/bi00610a004.

[22] R. Y. Tsien. The green fluorescent protein. *Annu. Rev. Biochem.*, 67:509–44, 1998. doi: 10.1146/annurev.biochem.67.1.509.

[23] J. W. Hastings and J. G. Morin. Comparative biochemistry of calcium-activated photoproteins from ctenophore, mnemiopsis and coelenterates aequorea, obelia, pelagia and renilla. In *Biological Bulletin*, volume 137, page 402, 1969.

[24] M. Zimmer. Green fluorescent protein (gfp): applications, structure, and related photophysical behavior. *Chem. Rev.*, 102(3):759–81, 2002. doi: 10.1021/cr010142r.

[25] R. H. Valdivia, B. P. Cormack, and S. Falkow. *The Uses of Green Fluorescent Protein in Prokaryotes*, chapter 8, pages 163–178. John Wiley & Sons, Ltd, 2005. ISBN 9780471739494. doi: 10.1002/0471739499.ch8. URL https://onlinelibrary.wiley.com/doi/abs/10.1002/0471739499.ch8.

[26] W. W. Ward. *Biochemical and Physical Properties of Green Fluorescent Protein*, chapter 3, pages 39–65. John Wiley & Sons, Ltd, 2005. ISBN 9780471739494. doi: 10.1002/0471739499.ch3. URL https://onlinelibrary.wiley.com/doi/abs/10.1002/0471739499.ch3.

[27] F. Yang, L. G. Moss, and G. N. Phillips. The molecular structure of green fluorescent protein. *Nat. Biotechnol.*, 14(10):1246–51, 1996. doi: 10.1038/nbt1096-1246.

[28] A. S. Rose, A. R. Bradley, Y. Valasatava, J. M. Duarte, A. Prlic, and P. W. Rose. Ngl viewer: web-based molecular graphics for large complexes. *Bioinformatics*, 34(21):3755–3758, 2018. doi: 10.1093/bioinformatics/bty419.

[29] T. J. Lambert. Fpbase: a community-editable fluorescent protein database. *Nat. Methods*, 16 (4):277–278, 2019. doi: 10.1038/s41592-019-0352-8.

[30] C.-F. Mandenius. *Challenges for Bioreactor Design and Operation*, pages 1–34. Wiley-VCH Verlag GmbH & Co. KGaA, 2016. ISBN 9783527683369. doi: 10.1002/9783527683369.ch1.

[31] G. D. Najafpour. CHAPTER 6 - Bioreactor Design . In G. D. Najafpour, editor, *Biochemical Engineering and Biotechnology*, pages 142–169. Elsevier, Amsterdam, 2007. ISBN 978-0-444-52845-2. doi: 10.1016/B978-044452845-2/50006-9.

[32] R. Sindhu, A. Pandey, and P. Binod. 2 - Design and Types of Bioprocesses . In C. Larroche, M. Á. Sanromán, G. Du, and A. Pandey, editors, *Current Developments in Biotechnology and Bioengineering*, pages 29–43. Elsevier, 2017. ISBN 978-0-444-63663-8. doi: 10.1016/B978-0-444-63663-8.00002-1.

[33] R. E.-M. M. M. D. M. . N. J. Allman, Tony; Carlson. *Fermentation microbiology and biotechnology*. CRC Press, fourth edition edition, 2019. ISBN 9781138581029,113858102X,9780429506987,9780429015960,9780429015953,9780429015946. doi: 10.1201/9780429506987. URL http://gen.lib.rus.ec/book/index.php?md5=5b12f638ec5ec8b298ced2429e931215.

[34] F. R. Schmidt. Optimization and scale up of industrial fermentation processes. *Appl. Microbiol. Biotechnol.*, 68(4):425–35, 2005. doi: 10.1007/s00253-005-0003-0.

[35] E. Kadic and T. J. Heindel. *Stirred-Tank Bioreactors*, volume 10.1002/9781118869703, pages 69–123. John Wiley & Sons, Inc., 2014. ISBN 9781118869703,9781118104019. doi: 10.1002/9781118869703.ch6.

[36] G. D. A. P. Christian Larroche, M. Angeles Sanroman. *Current Developments in Biotechnology and Bioengineering. Bioprocesses, Bioreactors and Controls*. Elsevier, 1 edition, 2016. ISBN 0444636633,978-0-444-63663-8,9780444636744,0444636749. URL http://gen.lib.rus.ec/book/index.php?md5=149fb9fbcf2eeab36b4eec9e9733b07d.

[37] A. Lübbert. *Bubble Column Bioreactors: Modeling and Control*, pages 247–273. Springer Berlin Heidelberg, Berlin, Heidelberg, 2000. ISBN 978-3-642-59735-0. doi: 10.1007/978-3-642-59735-0_9. URL https://doi.org/10.1007/978-3-642-59735-0_9.

[38] N. Kantarci, F. Borak, and K. O. Ulgen. Bubble column reactors. *Process Biochemistry*, 40(7): 2263, 2005. doi: 10.1016/j.procbio.2004.10.004.

[39] D. A. Mitchell, M. Berovič, and N. Krieger. *Solid-State Fermentation Bioreactor Fundamentals: Introduction and Overview*, pages 1–12. Springer Berlin Heidelberg, Berlin, Heidelberg, 2006. ISBN 978-3-540-31286-4. doi: 10.1007/3-540-31286-2_1.

[40] L. Thomas, C. Larroche, and A. Pandey. Current developments in solid-state fermentation. *Biochemical Engineering Journal*, 81(Supplement C):146–161, 2013. ISSN 1369-703X. doi: 10.1016/j.bej.2013.10.013. URL http://www.sciencedirect.com/science/article/pii/S1369703X13002830.

[41] A. Pandey. Solid-state fermentation. *Biochemical Engineering Journal*, 13(2-3):81, 2003. doi: 10.1016/S1369-703X(02)00121-3.

[42] R. R. Singhania, A. K. Patel, C. R. Soccol, and A. Pandey. Recent advances in solid-state fermentation. *Biochemical Engineering Journal*, 44(1):13, 2009. doi: 10.1016/j.bej.2008.10.019.

[43] U. Hölker and J. Lenz. Solid-state fermentation–are there any biotechnological advantages? *Curr. Opin. Microbiol.*, 8(3):301–6, 2005. doi: 10.1016/j.mib.2005.04.006.

[44] P. M. Doran. Chapter 14 - Reactor Engineering . In P. M. Doran, editor, *Bioprocess Engineering Principles*, pages 761–852. Academic Press, London, Second Edition edition, 2013. ISBN 978-0-12-220851-5. doi: 10.1016/B978-0-12-220851-5.00014-9.

[45] O. Bernard and I. Quelinnec. *Dynamic Models of Biochemical Processes: Properties of Models*, volume 10.1002/9780470611128, pages 17–45. ISTE, 2010. ISBN 9780470611128,9781848210257. doi: 10.1002/9780470611128.ch2.

[46] G. D. Najafpour. CHAPTER 1 - Industrial Microbiology . In G. D. Najafpour, editor, *Biochemical Engineering and Biotechnology*, pages 1–13. Elsevier, Amsterdam, 2007. ISBN 978-0-444-52845-2. doi: 10.1016/B978-044452845-2/50001-X.

[47] C. W. Ho, T. K. Chew, T. C. Ling, S. Kamaruddin, W. S. Tan, and B. T. Tey. Efficient mechanical cell disruption of Escherichia coli by an ultrasonicator and recovery of intracellular hepatitis B core antigen. *Process Biochemistry*, 41(8):1829, 2006. doi: 10.1016/j.procbio.2006.03.043.

[48] N. Bao and C. Lu. *Microfluidics-Based Lysis of Bacteria and Spores for Detection and Analysis: Biosensors, Recognition Receptors and Microsystems*, pages 817–831. Springer New York, New York, NY, 2008. ISBN 978-0-387-75113-9. doi: 10.1007/978-0-387-75113-9_30.

[49] X. Ren, D. Yu, L. Yu, G. Gao, S. Han, and Y. Feng. A new study of cell disruption to release recombinant thermostable enzyme from Escherichia coli by thermolysis. *J. Biotechnol.*, 129(4): 668–73, 2007. doi: 10.1016/j.jbiotec.2007.01.038.

[50] H. Anand, B. Balasundaram, A. Pandit, and S. Harrison. The effect of chemical pretreatment combined with mechanical disruption on the extent of disruption and release of intracellular protein from E. coli. *Biochemical Engineering Journal*, 35(2):166, 2007. doi: 10.1016/j.bej.2007.01.011.

[51] I. Agerkvist and S. O. Enfors. Characterization of E. coli cell disintegrates from a bead mill and high pressure homogenizers. *Biotechnol. Bioeng.*, 36(11):1083–9, 1990. doi: 10.1002/bit.260361102.

[52] L. Benov and J. Al-Ibraheem. Disrupting Escherichia coli: A Comparison of Methods. *BMB Reports* , 35(4):428, 2002. doi: 10.5483/BMBRep.2002.35.4.428.

[53] A. C. Grabski. Chapter 18 Advances in Preparation of Biological Extracts for Protein Purification. In R. R. Burgess and M. P. Deutscher, editors, *Guide to Protein Purification, 2nd Edition*, volume 463, chapter Chapter 18 Advances in Preparation of Biological Extracts for Protein Purification, pages 285–303. Academic Press, 2009. doi: 10.1016/S0076-6879(09)63018-4.

[54] S. T. Harrison. Bacterial cell disruption: A key unit operation in the recovery of intracellular products. *Biotechnology Advances*, 9(2):217, 1991. doi: 10.1016/0734-9750(91)90005-G.

[55] P. R. Gogate and A. M. Kabadi. A review of applications of cavitation in biochemical engineering/biotechnology. *Biochemical Engineering Journal*, 44(1):60, 2009. doi: 10.1016/j.bej.2008.10.006.

[56] Z. Wang, G. Le, Y. Shi, and G. Wegrzyn. Studies on recovery plasmid DNA from Echerichia coli by heat treatment. *Process Biochemistry*, 38(2):199, 2002. doi: 10.1016/S0032-9592(02)00072-9.

[57] M. A. Kohanski, D. J. Dwyer, B. Hayete, C. A. Lawrence, and J. J. Collins. A common mechanism of cellular death induced by bactericidal antibiotics. *Cell*, 130(5):797–810, 2007. doi: 10.1016/j.cell.2007.06.049.

[58] T. M. Arnold, G. N. Forrest, and K. J. Messmer. Polymyxin antibiotics for gram-negative infections. *Am J Health Syst Pharm*, 64(8):819–26, 2007. doi: 10.2146/ajhp060473.

[59] C. L. Ventola. The antibiotic resistance crisis: part 1: causes and threats. *P T*, 40(4):277–83, 2015.

[60] J. Urthaler, C. Ascher, H. Wöhrer, and R. Necina. Automated alkaline lysis for industrial scale cGMP production of pharmaceutical grade plasmid-DNA. *J. Biotechnol.*, 128(1):132–49, 2007. doi: 10.1016/j.jbiotec.2006.08.018.

[61] L. O. Ingram. Mechanism of lysis of Escherichia coli by ethanol and other chaotropic agents. *J. Bacteriol.*, 146(1):331–6, 1981.

[62] O. Salazar and J. A. Asenjo. Enzymatic lysis of microbial cells. *Biotechnol. Lett.*, 29(7):985–94, 2007. doi: 10.1007/s10529-007-9345-2.

[63] G. D. Shockman, L. Daneo-Moore, R. Kariyama, and O. Massidda. Bacterial walls, peptidoglycan hydrolases, autolysins, and autolysis. *Microb. Drug Resist.*, 2(1):95–8, 1996. doi: 10.1089/mdr.1996.2.95.

[64] R. Young. Phage Lysis. In *Phages*, pages 92–128. American Society of Microbiology, 2005. doi: 10.1128/9781555816506.ch6.

[65] R. R. G. Soares, A. M. Azevedo, J. M. Van Alstine, and M. R. Aires-Barros. Partitioning in aqueous two-phase systems: Analysis of strengths, weaknesses, opportunities and threats. *Biotechnol J*, 10(8):1158–69, 2015. doi: 10.1002/biot.201400532.

[66] B. Y. Zaslavsky. *Aqueous two-phase partitioning : physical chemistry and bioanalytical applications*. M. Dekker, 1995. ISBN 0824794613,9780824794613. URL `http://gen.lib.rus.ec/book/index.php?md5=89fab385fd58022543bf99b4a62bcbc4`.

[67] D. F. Faria, T. P. Silva, M. R. Aires-Barros, and A. M. Azevedo. A chronology of the development of aqueous two-phase systems as a viable liquid-liquid extraction for biological products*. In *Reference Module in Chemistry, Molecular Sciences and Chemical Engineering*. Elsevier, 2019. ISBN 978-0-12-409547-2. doi: https://doi.org/10.1016/B978-0-12-409547-2.14393-8. URL `http://www.sciencedirect.com/science/article/pii/B9780124095472143938`.

[68] R. R. G. Soares, D. F. C. Silva, P. Fernandes, A. M. Azevedo, V. Chu, J. P. Conde, and M. R. Aires-Barros. Miniaturization of aqueous two-phase extraction for biological applications: From micro-tubes to microchannels. *Biotechnol J*, 11(12):1498–1512, 2016. doi: 10.1002/biot.201600356.

[69] K. Köhler, A. Veide, and S.-O. Enfors. Partitioning of β-galactosidase fusion proteins in peg/potassium phosphate aqueous two-phase systems. *Enzyme and Microbial Technology*, 13(3):204, 1991. doi: 10.1016/0141-0229(91)90129-X.

[70] J. Asenjo, R. Turner, S. Mistry, and A. Kaul. Separation and purification of recombinant proteins from escherichia coli with aqueous two-phase systems. *Journal of Chromatography A*, 668(1): 129, 1994. doi: 10.1016/0021-9673(94)80101-0.

[71] M. J. Sarmento, M. J. Pires, J. M. Cabral, and M. R. Aires-Barros. Liquid-liquid extraction of a recombinant protein, cytochrome b5, with aqueous two-phase systems of polyethylene glycol and potassium phosphate salts. *Journal of Chromatography A*, 668(1):117, 1994. doi: 10.1016/0021-9673(94)80099-5.

[72] M. J. Sebastião, P. Martel, A. Baptista, S. B. Petersen, J. M. S. Cabral, and M. R. Aires-Barros. Predicting the partition coefficients of a recombinant cutinase in polyethylene glycol/phosphate aqueous two-phase systems. *Biotechnology and Bioengineering*, 56 (3):248–257, 1997. doi: 10.1002/(SICI)1097-0290(19971105)56:3<248::AID-BIT2>3.0.CO;2-J. URL https://onlinelibrary.wiley.com/doi/abs/10.1002/%28SICI%291097-0290%2819971105%2956%3A3%3C248%3A%3AAID-BIT2%3E3.0.CO%3B2-J.

[73] J. Marcos, L. Fonseca, M. Ramalho, and J. Cabral. Variation of penicillin acylase partition coefficient with phase volume ratio in poly(ethylene glycol)–sodium citrate aqueous two-phase systems. *Journal of Chromatography B: Biomedical Sciences and Applications*, 711(1-2):295, 1998. doi: 10.1016/S0378-4347(97)00633-6.

[74] G. M. Whitesides. The origins and the future of microfluidics. *Nature*, 442(7101):368–73, 2006. doi: 10.1038/nature05058.

[75] F. K. Balagadde. The new role of the microchemostat in the bioengineering revolution. *Conf Proc IEEE Eng Med Biol Soc*, 2009:1064–6, 2009. doi: 10.1109/IEMBS.2009.5335037.

[76] M. A. Day. The no-slip condition of fluid dynamics. *Erkenntnis*, 33(3):285, 1990. doi: 10.1007/BF00717588.

[77] M. S. Ferry, I. A. Razinkov, and J. Hasty. Microfluidics for synthetic biology: from design to execution. *Meth. Enzymol.*, 497:295–372, 2011. doi: 10.1016/B978-0-12-385075-1.00014-7.

[78] R. Soares, D. Ramadas, V. Chu, M. Aires-Barros, J. Conde, A. Viana, and A. Cascalheira. An ultrarapid and regenerable microfluidic immunoassay coupled with integrated photosensors for point-of-use detection of ochratoxin a. *Sensors and Actuators B: Chemical*, 235:554, 2016. doi: 10.1016/j.snb.2016.05.124.

[79] R. R. G. Soares, A. M. Azevedo, P. Fernandes, V. Chu, J. P. Conde, and M. R. Aires-Barros. A simple method for point-of-need extraction, concentration and rapid multi-mycotoxin immunodetection in feeds using aqueous two-phase systems. *J Chromatogr A*, 1511:15–24, 2017. doi: 10.1016/j.chroma.2017.07.004.

[80] R. R. G. Soares, D. R. Santos, V. Chu, A. M. Azevedo, M. R. Aires-Barros, and J. P. Conde. A point-of-use microfluidic device with integrated photodetector array for immunoassay multiplexing: Detection of a panel of mycotoxins in multiple samples. *Biosens Bioelectron*, 87:823–831, 2017. doi: 10.1016/j.bios.2016.09.041.

[81] R. Epifania, R. R. Soares, I. F. Pinto, V. Chu, and J. P. Conde. Capillary-driven microfluidic device with integrated nanoporous microbeads for ultrarapid biosensing assays. *Sensors and Actuators B: Chemical*, 265:452, 2018. doi: 10.1016/j.snb.2018.03.051.

[82] B. Ziaie, A. Baldi, M. Lei, Y. Gu, and R. A. Siegel. Hard and soft micromachining for biomems: review of techniques and examples of applications in microfluidics and drug delivery. *Adv. Drug Deliv. Rev.*, 56(2):145–72, 2004. doi: 10.1016/j.addr.2003.09.001.

[83] J. W. Judy. Microelectromechanical systems (mems): fabrication, design and applications. *Smart Materials and Structures, Volume 10, Issue 6, pp. 1115-1134 (2001).*, 10:1115–1134, dec 2001. doi: 10.1088/0964-1726/10/6/301.

[84] C. Iliescu, H. Taylor, M. Avram, J. Miao, and S. Franssila. A practical guide for the fabrication of microfluidic devices using glass and silicon. *Biomicrofluidics*, 6(1):16505–1650516, 2012. doi: 10.1063/1.3689939.

[85] B. Ziaie, A. Baldi, and M. Z. Atashbar. *Introduction to Micro-/Nanofabrication*, pages 231–269. Springer Berlin Heidelberg, Berlin, Heidelberg, 2010. ISBN 978-3-642-02525-9. doi: 10.1007/978-3-642-02525-9_8.

[86] M. AA. Microfluidics devices manufacturing and biomedical applications. *J Biosens Bioelectron*, 2019. doi: 10.4172/2155-6210.1000265.

[87] B. Gale, A. Jafek, C. Lambert, B. Goenner, H. Moghimifam, U. Nze, and S. Kamarapu. A review of current methods in microfluidic device fabrication and future commercialization prospects. *Inventions*, 3(3):60, 2018. doi: 10.3390/inventions3030060.

[88] N. Bao, Q. Zhang, J.-J. Xu, and H.-Y. Chen. Fabrication of poly(dimethylsiloxane) microfluidic system based on masters directly printed with an office laser printer. *Journal of Chromatography A*, 1089(1-2):270, 2005. doi: 10.1016/j.chroma.2005.07.001.

[89] H. Hwang, G. Kang, J. H. Yeon, Y. Nam, and J.-K. Park. Direct rapid prototyping of PDMS from a photomask film for micropatterning of biomolecules and cells. *Lab Chip*, 9(1):167–70, 2009. doi: 10.1039/b810341k.

[90] K. W. Oh and C. H. Ahn. TOPICAL REVIEW: A review of microvalves. *Journal of Micromechanics and Microengineering*, 16:R13–R39, may 2006. doi: 10.1088/0960-1317/16/5/R01.

[91] C. Zhang, D. Xing, and Y. Li. Micropumps, microvalves, and micromixers within PCR microfluidic chips: Advances and trends. *Biotechnol. Adv.*, 25(5):483–514, 2007. doi: 10.1016/j.biotechadv.2007.05.003.

[92] R. Pal, M. Yang, B. N. Johnson, D. T. Burke, and M. A. Burns. Phase change microvalve for integrated devices. *Anal. Chem.*, 76(13):3740–8, 2004. doi: 10.1021/ac0352934.

[93] A. K. Au, H. Lai, B. R. Utela, and A. Folch. Microvalves and Micropumps for BioMEMS. *Micromachines*, 2(4):179, 2011. doi: 10.3390/mi2020179.

[94] B. D. Iverson and S. V. Garimella. Recent advances in microscale pumping technologies: a review and evaluation. *Microfluidics and Nanofluidics*, 5(2):145, 2008. doi: 10.1007/s10404-008-0266-8.

[95] D. J. Laser and J. G. Santiago. TOPICAL REVIEW: A review of micropumps. *Journal of Micromechanics and Microengineering*, 14:R35–R64, jun 2004. doi: 10.1088/0960-1317/14/6/R01.

[96] X. Wang, C. Cheng, S. Wang, and S. Liu. Electroosmotic pumps and their applications in microfluidic systems. *Microfluid Nanofluidics*, 6(2):145, 2009. doi: 10.1007/s10404-008-0399-9.

[97] N.-T. Nguyen and Z. Wu. TOPICAL REVIEW: Micromixers—a review. *Journal of Micromechanics and Microengineering*, 15:R1–R16, feb 2005. doi: 10.1088/0960-1317/15/2/R01.

[98] K. S. Lee, P. Boccazzi, A. J. Sinskey, and R. J. Ram. Microfluidic chemostat and turbidostat with flow rate, oxygen, and temperature control for dynamic continuous culture. *Lab Chip*, 11 (10):1730–9, 2011. doi: 10.1039/c1lc20019d.

[99] C.-Y. Lee, W.-T. Wang, C.-C. Liu, and L.-M. Fu. Passive mixers in microfluidic systems: A review. *Chemical Engineering Journal*, 288:146, 2016. doi: 10.1016/j.cej.2015.10.122.

[100] W. P. Eaton and J. H. Smith. Micromachined pressure sensors: review and recent developments. *Smart Materials and Structures, Volume 6, Issue 5, pp. 530-539 (1997).*, 6:530–539, oct 1997. doi: 10.1088/0964-1726/6/5/004.

[101] A. Boisen, S. Dohn, S. Sylvest Keller, S. Schmid, and M. Tenje. Cantilever-like micromechanical sensors. *Reports on Progress in Physics, Volume 74, Issue 3, id. 036101 (2011).*, 74:036101, mar 2011. doi: 10.1088/0034-4885/74/3/036101.

[102] E. A. Wachter and T. Thundat. Micromechanical sensors for chemical and physical measurements. *Review of Scientific Instruments, Volume 66, Issue 6, June 1995, pp.3662-3667*, 66: 3662–3667, jun 1995. doi: 10.1063/1.1145484.

[103] V. P. Carey. Microsensors: Principles and applications. *Experimental Thermal and Fluid Science*, 13(1):81, 1996. doi: 10.1016/0894-1777(96)00002-7.

[104] N. L. Jeon, D. T. Chiu, C. J. Wargo, H. Wu, I. S. Choi, J. R. Anderson, and G. M. Whitesides. Microfluidics Section: Design and Fabrication of Integrated Passive Valves and Pumps for Flexible Polymer 3-Dimensional Microfluidic Systems. *Biomedical Microdevices*, 4(2):117, 2002. doi: 10.1023/A:1014683114796.

[105] Y. Feng, Z. Zhou, X. Ye, and J. Xiong. Passive valves based on hydrophobic microfluidics. *Sensors and Actuators A: Physical*, 108(1-3):138, 2003. doi: 10.1016/S0924-4247(03)00363-7.

[106] W. H. Grover, M. G. von Muhlen, and S. R. Manalis. Teflon films for chemically-inert microfluidic valves and pumps. *Lab Chip*, 8(6):913–8, 2008. doi: 10.1039/b800600h.

[107] M. A. Unger, H.-P. Chou, T. Thorsen, A. Scherer, and S. R. Quake. Monolithic microfabricated valves and pumps by multilayer soft lithography. *Science, Volume 288, Issue 5463, pp. 113-116 (2000).*, 288:113–116, apr 2000. doi: 10.1126/science.288.5463.113.

[108] N. S. Satarkar, W. Zhang, R. E. Eitel, and J. Z. Hilt. Magnetic hydrogel nanocomposites as remote controlled microfluidic valves. *Lab Chip*, 9(12):1773–9, 2009. doi: 10.1039/b822694f.

[109] H. van Lintel, F. van De Pol, and S. Bouwstra. A piezoelectric micropump based on micromachining of silicon. *Sensors and Actuators*, 15(2):153, 1988. doi: 10.1016/0250-6874(88)87005-7.

[110] J. F. Liu, S. Yadavali, A. Tsourkas, and D. Issadore. Microfluidic diafiltration-on-chip using an integrated magnetic peristaltic micropump. *Lab Chip*, 17(22):3796–3803, 2017. doi: 10.1039/c7lc00954b.

[111] Y. Takamura, H. Onoda, H. Inokuchi, S. Adachi, A. Oki, and Y. Horiike. Low-voltage electroosmosis pump for stand-alone microfluidics devices. *Electrophoresis*, 24(1-2):185–92, 2003. doi: 10.1002/elps.200390012.

[112] D. Juncker, H. Schmid, U. Drechsler, H. Wolf, M. Wolf, B. Michel, N. de Rooij, and E. Delamarche. Autonomous Microfluidic Capillary System. *Analytical Chemistry*, 74(24):6139, 2002. doi: 10.1021/ac0261449.

[113] V. Kumaran and P. Bandaru. Ultra-fast microfluidic mixing by soft-wall turbulence. *Chemical Engineering Science*, 149:156, 2016. doi: 10.1016/j.ces.2016.04.001.

[114] L.-L. Fan, X.-L. Zhu, H. Zhao, J. Zhe, and L. Zhao. Rapid microfluidic mixer utilizing sharp corner structures. *Microfluidics and Nanofluidics*, 21(3), 2017. doi: 10.1007/s10404-017-1874-y.

[115] C.-C. Hong, J.-W. Choi, and C. H. Ahn. A novel in-plane passive microfluidic mixer with modified Tesla structures. *Lab Chip*, 4(2):109–13, 2004. doi: 10.1039/b305892a.

[116] M. Ballard, D. Owen, Z. G. Mills, P. J. Hesketh, and A. Alexeev. Orbiting magnetic microbeads enable rapid microfluidic mixing. *Microfluidics and Nanofluidics*, 20(6), 2016. doi: 10.1007/s10404-016-1750-1.

[117] L. Cortelezzi, S. Ferrari, and G. Dubini. A scalable active micro-mixer for biomedical applications. *Microfluidics and Nanofluidics*, 21(3), 2017. doi: 10.1007/s10404-017-1868-9.

[118] W. Cui, H. Zhang, H. Zhang, Y. Yang, M. He, H. Qu, W. Pang, D. Zhang, and X. Duan. Localized ultrahigh frequency acoustic fields induced micro-vortices for submilliseconds microfluidic mixing. *Applied Physics Letters*, 109:253503, dec 2016. doi: 10.1063/1.4972484.

[119] N. M. M. Pires, T. Dong, U. Hanke, and N. Hoivik. Recent developments in optical detection technologies in lab-on-a-chip devices for biosensing applications. *Sensors (Basel)*, 14(8): 15458–79, 2014. doi: 10.3390/s140815458.

[120] W. Dungchai, O. Chailapakul, and C. S. Henry. Electrochemical detection for paper-based microfluidics. *Anal. Chem.*, 81(14):5821–6, 2009. doi: 10.1021/ac9007573.

[121] Micrux Technologies, Online Catalogue. http://en.calameo.com/read/003992140ba25ca529ea0. Accessed 01-01-2018.

[122] R. M. R. Pinto, P. Brito, V. Chu, and J. P. Conde. Thin-film silicon mems for dynamic mass sensing in vacuum and air: Phase noise, allan deviation, mass sensitivity and limits of detection. *Journal of Microelectromechanical Systems*, 28(3):390, 2019. doi: 10.1109/JMEMS.2019.2911666.

[123] J. L. Arlett, E. B. Myers, and M. L. Roukes. Comparative advantages of mechanical biosensors. *Nature Nanotechnology, Volume 6, Issue 4, pp. 203-215 (2011).*, 6:203–215, apr 2011. doi: 10.1038/NNANO.2011.44.

[124] K. Y. Gfeller, N. Nugaeva, and M. Hegner. Rapid biosensor for detection of antibiotic-selective growth of Escherichia coli. *Appl. Environ. Microbiol.*, 71(5):2626–31, 2005. doi: 10.1128/AEM.71.5.2626-2631.2005.

[125] S. Leahy and Y. Lai. A cantilever biosensor based on a gap method for detecting Escherichia coli in real time. *Sensors and Actuators B: Chemical*, 246:1011, 2017. doi: 10.1016/j.snb.2017.02.144.

[126] D. R. Santos, R. R. G. Soares, V. Chu, and J. P. Conde. Performance of hydrogenated amorphous silicon thin film photosensors at ultra-low light levels: towards attomole sensitivities in labon- chip biosensing applications. *IEEE Sensors Journal*, page 1, 2017. doi: 10.1109/JSEN.2017.2751253.

[127] M. Gan, J. Su, J. Wang, H. Wu, and L. Chen. A scalable microfluidic chip for bacterial suspension culture. *Lab Chip*, 11(23):4087–92, 2011. doi: 10.1039/c1lc20670b.

[128] Z. Zhang, N. Szita, P. Boccazzi, A. J. Sinskey, and K. F. Jensen. A well-mixed, polymer-based microbioreactor with integrated optical measurements. *Biotechnol. Bioeng.*, 93(2):286–96, 2006. doi: 10.1002/bit.20678.

[129] A. Novick and L. Szilard. Description of the Chemostat. *Science, Volume 112, Issue 2920, pp. 715-716*, 112:715–716, dec 1950. doi: 10.1126/science.112.2920.715.

[130] A. Zanzotto, N. Szita, P. Boccazzi, P. Lessard, A. J. Sinskey, and K. F. Jensen. Membrane-aerated microbioreactor for high-throughput bioprocessing. *Biotechnol. Bioeng.*, 87(2):243–54, 2004. doi: 10.1002/bit.20140.

[131] M. M. Maharbiz, W. J. Holtz, R. T. Howe, and J. D. Keasling. Microbioreactor arrays with parametric control for high-throughput experimentation. *Biotechnol. Bioeng.*, 85(4):376–81, 2004. doi: 10.1002/bit.10835.

[132] A. Buchenauer, M. Funke, J. Büchs, W. Mokwa, and U. Schnakenberg. Microbioreactors with microfluidic control and a user-friendly connection to the actuator hardware. *Journal of Micromechanics and Microengineering*, 19(7):074012, jun 2009. doi: 10.1088/0960-1317/19/7/074012. URL `https://doi.org/10.1088%2F0960-1317%2F19%2F7%2F074012`.

[133] X. Luo, K. Shen, C. Luo, H. Ji, Q. Ouyang, and Y. Chen. An automatic microturbidostat for bacterial culture at constant density. *Biomed Microdevices*, 12(3):499–503, 2010. doi: 10.1007/s10544-010-9406-5.

[134] A. Zanzotto, P. Boccazzi, N. Gorret, T. K. Van Dyk, A. J. Sinskey, and K. F. Jensen. In situ measurement of bioluminescence and fluorescence in an integrated microbioreactor. *Biotechnol. Bioeng.*, 93(1):40–7, 2006. doi: 10.1002/bit.20708.

[135] A. Buchenauer, M. C. Hofmann, M. Funke, J. Büchs, W. Mokwa, and U. Schnakenberg. Microbioreactors for fed-batch fermentations with integrated online monitoring and microfluidic devices. *Biosens Bioelectron*, 24(5):1411–6, 2009. doi: 10.1016/j.bios.2008.08.043.

[136] M. Funke, A. Buchenauer, W. Mokwa, S. Kluge, L. Hein, C. Müller, F. Kensy, and J. Büchs. Bioprocess control in microscale: scalable fermentations in disposable and user-friendly microfluidic systems. *Microb. Cell Fact.*, 9:86, 2010. doi: 10.1186/1475-2859-9-86.

[137] H. L. T. Lee, P. Boccazzi, R. J. Ram, and A. J. Sinskey. Microbioreactor arrays with integrated mixers and fluid injectors for high-throughput experimentation with ph and dissolved oxygen control. *Lab Chip*, 6(9):1229–35, 2006. doi: 10.1039/b608014f.

[138] N. Szita, P. Boccazzi, Z. Zhang, P. Boyle, A. J. Sinskey, and K. F. Jensen. Development of a multiplexed microbioreactor system for high-throughput bioprocessing. *Lab Chip*, 5(8):819–26, 2005. doi: 10.1039/b504243g.

[139] F. K. Balagaddé, L. You, C. L. Hansen, F. H. Arnold, and S. R. Quake. Long-Term Monitoring of Bacteria Undergoing Programmed Population Control in a Microchemostat. *Science, Volume 309, Issue 5731, pp. 137-140 (2005).*, 309:137–140, jul 2005. doi: 10.1126/science.1109173.

[140] M. Aly Saad Aly, M. Gauthier, and J. Yeow. On-chip cell lysis by antibacterial non-leaching reusable quaternary ammonium monolithic column. *Biomed Microdevices*, 18(1):2, 2016. doi: 10.1007/s10544-015-0025-z.

[141] J. R. Buser, A. Wollen, E. K. Heiniger, S. A. Byrnes, P. C. Kauffman, P. D. Ladd, and P. Yager. Electromechanical cell lysis using a portable audio device: enabling challenging sample preparation at the point-of-care. *Lab Chip*, 15(9):1994–7, 2015. doi: 10.1039/c5lc00080g.

[142] C. d. l. Rosa and K. V. I. S. Kaler. Electro-Disruption of Escherichia coli Bacterial Cells on a Microfabricated Chip. In *2006 International Conference of the IEEE Engineering in Medicine and Biology Society*, pages 4096–4099, Aug 2006. doi: 10.1109/IEMBS.2006.259517.

[143] K.-Y. Hwang, S. H. Kwon, S.-O. Jung, H.-K. Lim, W.-J. Jung, C.-S. Park, J.-H. Kim, K.-Y. Suh, and N. Huh. Miniaturized bead-beating device to automate full DNA sample preparation processes for gram-positive bacteria. *Lab Chip*, 11(21):3649–55, 2011. doi: 10.1039/c1lc20692c.

[144] X. Jiang, W. Jing, L. Zheng, S. Liu, W. Wu, and G. Sui. A continuous-flow high-throughput microfluidic device for airborne bacteria pcr detection. *Lab Chip*, 14(4):671–6, 2014. doi: 10.1039/c3lc50977j.

[145] J. Kim, S. Hee Jang, G. Jia, J. V. Zoval, N. A. Da Silva, and M. J. Madou. Cell lysis on a microfluidic CD (compact disc). *Lab Chip*, 4(5):516–22, 2004. doi: 10.1039/b401106f.

[146] M. D. Kulinski, M. Mahalanabis, S. Gillers, J. Y. Zhang, S. Singh, and C. M. Klapperich. Sample preparation module for bacterial lysis and isolation of DNA from human urine. *Biomed Microdevices*, 11(3):671–678, 2009. doi: 10.1007/s10544-008-9277-1.

[147] H. J. Lee, J.-H. Kim, H. K. Lim, E. C. Cho, N. Huh, C. Ko, J. C. Park, J.-W. Choi, and S. S. Lee. Electrochemical cell lysis device for dna extraction. *Lab Chip*, 10(5):626–33, 2010. doi: 10.1039/b916606h.

[148] M. Mahalanabis, H. Al-Muayad, M. D. Kulinski, D. Altman, and C. M. Klapperich. Cell lysis and DNA extraction of gram-positive and gram-negative bacteria from whole blood in a disposable microfluidic chip. *Lab Chip*, 9(19):2811–7, 2009. doi: 10.1039/b905065p.

[149] N. Privorotskaya, Y.-S. Liu, J. Lee, H. Zeng, J. A. Carlisle, A. Radadia, L. Millet, R. Bashir, and W. P. King. Rapid thermal lysis of cells using silicon-diamond microcantilever heaters. *Lab Chip*, 10(9):1135–41, 2010. doi: 10.1039/b923791g.

[150] T. Tandiono, D. S.-W. Ow, L. Driessen, C. S.-H. Chin, E. Klaseboer, A. B.-H. Choo, S.-W. Ohl, and C.-D. Ohl. Sonolysis of Escherichia coli and Pichia pastoris in microfluidics. *Lab Chip*, 12 (4):780–6, 2012. doi: 10.1039/c2lc20861j.

[151] K. Tsougeni, G. Papadakis, M. Gianneli, A. Grammoustianou, V. Constantoudis, B. Dupuy, P. S. Petrou, S. E. Kakabakos, A. Tserepi, E. Gizeli, and E. Gogolides. Plasma nanotextured polymeric lab-on-a-chip for highly efficient bacteria capture and lysis. *Lab Chip*, 16(1):120–31, 2016. doi: 10.1039/c5lc01217a.

[152] L. Van Heirstraeten, P. Spang, C. Schwind, K. S. Drese, M. Ritzi-Lehnert, B. Nieto, M. Camps, B. Landgraf, F. Guasch, A. H. Corbera, J. Samitier, H. Goossens, S. Malhotra-Kumar, and

T. Roeser. Integrated dna and rna extraction and purification on an automated microfluidic cassette from bacterial and viral pathogens causing community-acquired lower respiratory tract infections. *Lab Chip*, 14(9):1519–26, 2014. doi: 10.1039/c3lc51339d.

[153] W. Wan and J. T. W. Yeow. Study of a novel cell lysis method with titanium dioxide for lab-on-a-chip devices. *Biomed Microdevices*, 13(3):527–32, 2011. doi: 10.1007/s10544-011-9521-y.

[154] H.-Y. Wang, A. K. Bhunia, and C. Lu. A microfluidic flow-through device for high throughput electrical lysis of bacterial cells based on continuous dc voltage. *Biosens Bioelectron*, 22(5): 582–8, 2006. doi: 10.1016/j.bios.2006.01.032.

[155] E. A. Schilling, A. E. Kamholz, and P. Yager. Cell Lysis and Protein Extraction in a Microfluidic Device with Detection by a Fluorogenic Enzyme Assay. *Analytical Chemistry*, 74(8):1798, 2002. doi: 10.1021/ac015640e.

[156] N. Bao and C. Lu. A microfluidic device for physical trapping and electrical lysis of bacterial cells. *Applied Physics Letters, Volume 92, Issue 21, id. 214103 (3 pages) (2008).*, 92:214103, may 2008. doi: 10.1063/1.2937088.

[157] H. Kido, M. Micic, D. Smith, J. Zoval, J. Norton, and M. Madou. A novel, compact disk-like centrifugal microfluidics system for cell lysis and sample homogenization. *Colloids Surf B Biointerfaces*, 58(1):44–51, 2007. doi: 10.1016/j.colsurfb.2007.03.015.

[158] R. J. Meagher, Y. K. Light, and A. K. Singh. Rapid, continuous purification of proteins in a microfluidic device using genetically-engineered partition tags. *Lab Chip*, 8(4):527–32, 2008. doi: 10.1039/b716462a.

[159] I. F. Pinto, D. Santos, R. Soares, M. Aires-Barros, V. Chu, A. Azevedo, and J. Conde. Integration of Photosensors in a Nano-liter Scale Chromatography Column for the Online Monitoring of Adsorption/Desorption Kinetics of a Fluorophore-labeled Monoclonal Antibody. *Procedia Engineering*, 168:1426, 2016. doi: 10.1016/j.proeng.2016.11.405.

[160] I. F. Pinto, M. R. Aires-Barros, and A. M. Azevedo. Multimodal chromatography: debottlenecking the downstream processing of monoclonal antibodies. *Pharmaceutical Bioprocessing*, 3(3):263, 2015. doi: 10.4155/pbp.15.7.

[161] N. Malmstadt, P. Yager, A. S. Hoffman, and P. S. Stayton. A Smart Microfluidic Affinity Chromatography Matrix Composed of Poly(N-isopropylacrylamide)-Coated Beads. *Analytical Chemistry*, 75(13):2943, 2003. doi: 10.1021/ac034274r.

[162] I. Pinto, D. Santos, R. Soares, M. Aires-Barros, V. Chu, A. Azevedo, and J. Conde. A regenerable microfluidic device with integrated valves and thin-film photodiodes for rapid optimization of chromatography conditions. *Sensors and Actuators B: Chemical*, 2017. doi: 10.1016/j.snb.2017.09.167.

[163] A. L. Zydney. Continuous downstream processing for high value biological products: A review. *Biotechnol. Bioeng.*, 113(3):465–75, 2016. doi: 10.1002/bit.25695.

[164] D. F. C. Silva, A. M. Azevedo, P. Fernandes, V. Chu, J. P. Conde, and M. R. Aires-Barros. Determination of aqueous two phase system binodal curves using a microfluidic device. *J Chromatogr A*, 1370:115–20, 2014. doi: 10.1016/j.chroma.2014.10.035.

[165] E. J. S. Bras, R. R. G. Soares, A. M. Azevedo, P. Fernandes, M. Arévalo-Rodríguez, V. Chu, J. P. Conde, and M. R. Aires-Barros. A multiplexed microfluidic toolbox for the rapid optimization of affinity-driven partition in aqueous two phase systems. *J Chromatogr A*, 1515:252–259, 2017. doi: 10.1016/j.chroma.2017.07.094.

[166] M. R. Dhakad. Experimental analysis and optimization of cutting parameters for the surface roughness in the facing operation of pmma material. *IOSR Journal of Mechanical and Civil Engineering*, 17(01):52, 2017. doi: 10.9790/1684-17010015260.

[167] D. J. Guckenberger, T. E. de Groot, A. M. D. Wan, D. J. Beebe, and E. W. K. Young. Micromilling: a method for ultra-rapid prototyping of plastic microfluidic devices. *Lab Chip*, 15(11):2364–78, 2015. doi: 10.1039/c5lc00234f.

[168] V. Silverio, A. V. Silva, K. Przykaza, L. F. Santos, L. V. Melo, and S. Cardoso. Dark matters: black-pdms nanocomposite for opaque microfluidic systems. *Physical Chemistry Chemical Physics, vol. 21, issue 5, pp. 2719-2726*, 21:2719–2726, jan 2019. doi: 10.1039/c8cp06828c.

[169] D. Caputo, G. de Cesare, M. Nardini, A. Nascetti, and R. Scipinotti. Monitoring of temperature distribution in a thin film heater by an array of a-si:h temperature sensors. *IEEE Sensors Journal, vol. 12, issue 5, pp. 1209-1213*, 12:1209–1213, may 2012. doi: 10.1109/JSEN.2011.2167506.

[170] E. J. Brás, V. Chu, M. R. Aires-Barros, J. P. Conde, and P. Fernandes. A microfluidic platform for physical entrapment of yeast cells with continuous production of invertase. *Journal of Chemical Technology & Biotechnology*, 92(2):334, 2016. doi: 10.1002/jctb.5010.

[171] O. Salazar. Bacteria and yeast cell disruption using lytic enzymes. *Methods Mol. Biol.*, 424: 23–34, 2008. doi: 10.1007/978-1-60327-064-9_2.

[172] M. Derde, V. Lechevalier, C. Guérin-Dubiard, M.-F. Cochet, S. Jan, F. Baron, M. Gautier, V. Vié, and F. Nau. Hen egg white lysozyme permeabilizes Escherichia coli outer and inner membranes. *J. Agric. Food Chem.*, 61(41):9922–9, 2013. doi: 10.1021/jf4029199.

[173] A. Kamholz. Theoretical Analysis of Molecular Diffusion in Pressure-Driven Laminar Flow in Microfluidic Channels. *Biophysical Journal, vol. 80, issue 1, pp. 155-160*, 80:155–160, jan 2001. doi: 10.1016/S0006-3495(01)76003-1.

[174] A. Einstein. *Investigations on the Theory of the Brownian Movement*. Dover Books on Physics Series. Dover Publications, 1956. ISBN 9780486603049. URL https://books.google.pt/books?id=AOIVupH_hboC.

[175] M. Arriodupont. Translational Diffusion of Globular Proteins in the Cytoplasm of Cultured Muscle Cells. *Biophysical Journal, vol. 78, issue 2, pp. 901-907*, 78:901–907, feb 2000. doi: 10.1016/S0006-3495(00)76647-1.

[176] Y.-C. Kim and A. S. Myerson. Diffusivity of protein in aqueous solutions. *Korean Journal of Chemical Engineering*, 13(3):288, 1996. doi: 10.1007/BF02705952.

[177] R. Giordano, A. Salleo, S. Salleo, F. Mallamace, and F. Wanderlingh. Diffusion Coefficient of Lysozyme in Water. *Optica Acta, vol. 27, Issue 10, p.1465-1472*, 27:1465–1472, oct 1980. doi: 10.1080/713820150.

[178] R. M. Weinheimer, D. F. Evans, and E. L. Cussler. Diffusion in surfactant solutions. *Journal of Colloid and Interface Science, vol. 80, issue 2, pp. 357-368*, 80:357–368, apr 1981. doi: 10.1016/0021-9797(81)90194-6.

[179] M. H. Dehghani. Effectiveness of Ultrasound on the Destruction of E. coli. *American Journal of Environmental Sciences*, 1(3):187, 2005. doi: 10.3844/ajessp.2005.187.189.

[180] J. M. Newton, D. Schofield, J. Vlahopoulou, and Y. Zhou. Detecting cell lysis using viscosity monitoring in E. coli fermentation to prevent product loss. *Biotechnol. Prog.*, 32(4):1069–76, 2016. doi: 10.1002/btpr.2292.

[181] R. Repaske. Lysis of gram-negative bacteria by lysozyme. *Biochimica et Biophysica Acta*, 22 (1):189, 1956. doi: 10.1016/0006-3002(56)90240-2.

[182] N. Ohno and D. C. Morrison. Lipopolysaccharide interaction with lysozyme. Binding of lipopolysaccharide to lysozyme and inhibition of lysozyme enzymatic activity. *Journal of Biological Chemistry*, 264(8):4434–4441, 1989. URL http://www.jbc.org/content/264/8/4434.abstract.

[183] A. Rodríguez and M. Vaneechoutte. Comparison of the efficiency of different cell lysis methods and different commercial methods for RNA extraction from Candida albicans stored in RNAlater. *BMC Microbiol.*, 19(1):94, 2019. doi: 10.1186/s12866-019-1473-z.

[184] S. Yuan, D. B. Cohen, J. Ravel, Z. Abdo, and L. J. Forney. Evaluation of methods for the extraction and purification of DNA from the human microbiome. *PLoS ONE*, 7(3):e33865, 2012. doi: 10.1371/journal.pone.0033865.

[185] R. Fradique, A. M. Azevedo, V. Chu, J. P. Conde, and M. R. Aires-Barros. Microfluidic platform for rapid screening of bacterial cell lysis. *Journal of Chromatography A*, page 460539, 2019. doi: 10.1016/j.chroma.2019.460539.

[186] J. A. Asenjo and B. A. Andrews. Aqueous two-phase systems for protein separation: a perspective. *J Chromatogr A*, 1218(49):8826–35, 2011. doi: 10.1016/j.chroma.2011.06.051.

[187] M. A. Faridi, H. Ramachandraiah, I. Banerjee, S. Ardabili, S. Zelenin, and A. Russom. Elasto-inertial microfluidics for bacteria separation from whole blood for sepsis diagnostics. *J Nanobiotechnology*, 15(1):3, 2017. doi: 10.1186/s12951-016-0235-4.

[188] J. Zhang, W. Li, and G. Alici. *Inertial Microfluidics: Mechanisms and Applications*, pages 563–593. Springer International Publishing, Cham, 2017. ISBN 978-3-319-32180-6. doi: 10.1007/978-3-319-32180-6_25. URL https://doi.org/10.1007/978-3-319-32180-6_25.

[189] P. K. Periyannan Rajeswari, H. Ramachandraiah, J. Hansson, S. Ardabili, A. Veide, and A. Russom. Development of microfluidic aqueous two-phase system for continuous partitioning of e. coli strains. In *15th International Conference on Miniaturized Systems for Chemistry and Life Sciences 2011, MicroTAS 2011*, pages 1329–1331, 2011. ISBN 9781618395955. QC 20140915.

[190] M. Yamada, V. Kasim, M. Nakashima, J. Edahiro, and M. Seki. Continuous cell partitioning using an aqueous two-phase flow system in microfluidic devices. *Biotechnol. Bioeng.*, 88(4):489–94, 2004. doi: 10.1002/bit.20276.

[191] A. González-Mora, F. Ruiz-Ruiz, J. Benavides, R. C. Willson, and M. Rito-Palomares. Recovery and primary purification of bacteriophage m13 using aqueous two-phase systems. *Journal of Chemical Technology & Biotechnology*, 92(11):2808, 2017. doi: 10.1002/jctb.5359.

[192] P. Lutwyche, R. Norris-Jones, and D. E. Brooks. Aqueous two-phase polymer systems as tools for the study of a recombinant surface-expressed escherichia coli hemagglutinin. *Applied and Environmental Microbiology*, 61(9):3251–3255, 1995. ISSN 0099-2240. URL https://aem.asm.org/content/61/9/3251.

[193] C.-K. Su and B. H. Chiang. Partitioning and purification of lysozyme from chicken egg white using aqueous two-phase system. *Process Biochemistry*, 41(2):257, 2006. doi: 10.1016/j.procbio.2005.06.026.

A

Publications and other works

The work described in this thesis has led to some publications and scientific presentations. These are described in this section, followed by some relevant scientific activities.

During this time I was also involved in mentoring two students. The first was Niklas Floto, an exchange bachelor student from Hochschule Kaiserslautern (University of Applied Sciences, Germany), who studied the fabrication of microfluidic valves by the combination of hard plastic and PDMS structures. Part of this work served as basis for the integrated valves used on chapter 2. Followed by Andreia Jardim, a master student from Instituto Superior Técnico who worked on the development of microfluidic electrical lysis devices, with limited success. Her work was first focused on the use of 3D electrodes created by simple soft-lithography methods and liquid metal, that could not reach the required electrical field densities. Several attempts to solve this issue by modifying the composition of the PDMS mixture were met with problems with sealing the structures. A final attempt of using planar electrodes combined with switched high voltage AC fields resulted in electrode corrosion and degradation, likely caused by issues in the passivation film.

A.0.1 Published work

The work described in section 3 has already been published.

"Microfluidic platform for rapid screening of bacterial cell lysis"

Ricardo Fradique, Ana M. Azevedo, Virginia Chu, João P. Conde, M. Raquel Aires-Barros

Journal of Chromatography A, 2019, in press

DOI:10.1016/j.chroma.2019.460539

Abstract: Over the past decade significant progress has been found in the upstream production processes, shifting the main bottlenecks in current manufacturing platforms for biopharmaceuticals

towards the downstream processing. Challenges in the purification process include reducing the production costs, developing robust and efficient purification processes as well as integrating both upstream and downstream processes. Microfluidic technologies have recently emerged as effective tools for expediting bioprocess design in a cost-effective manner, since a large number of variables can be evaluated in a small time frame, using reduced volumes and manpower. Their modularity also allows to integrate different unit operations into a single chip, and consequently to evaluate the effect of each stage on the overall process efficiency. This paper describes the development of a diffusion-based microfluidic device for the rapid screening of continuous chemical lysis conditions. The release of a recombinant green fluorescent protein (GFP) expressed in Escherichia coli (E. coli) was used as model system due to the simple evaluation of cell growth and product concentration by fluorescence. The concept can be further applied to any biopharmaceutical production platform. The microfluidic device was successfully used to test the lytic effect of both enzymatic and chemical lysis solutions, with lysis efficiency of about 60% and close to 100%, respectively, achieved. The microfluidic technology also demonstrated the ability to detect potential process issues, such as the increased viscosity related with the rapid release of genomic material, that can arise for specific lysis conditions and hinder the performance of a bioprocess. Finally, given the continuous operation of the lysis chip, the microfluidic technology has the potential to be integrated with other microfluidic modules in order to model a fully continuous biomanufacturing process on a chip.

A.0.2 Prepared for submission

The work from chapter 4 has already been converted into paper form, and is undergoing the final preparations for submission.

"Integrated microfluidic device for the simultaneous screening of cell lysis and protein separation conditions in bacteria cells"

Ricardo Fradique, Andreia Jardim, Ana M. Azevedo, Virginia Chu, João P. Conde, M. Raquel Aires-Barros

Abstract: Microfluidic devices have been increasingly used as tools to accelerate the development of new biomanufacturing methods, given their ability to test a large set of variables in a short amount of time, with minimal reagent consumption. However, while being able to expedite a bioprocess design, the modular aspect of these devices has not been systematically explored, with most applications focusing on single unitary operations. This paper describes the development of a microfluidic chip that integrates two separate unitary operations into a single device in continuous operation: product release by chemical cell lysis; and product concentration by aqueous two phase system. In this way, it is possible to screen multiple conditions for each operation and evaluate their combined effect on the final product. A recombinant Escherichia coli (E. coli) strain producing green fluorescent protein (GFP) was used as model system, which allows for lysis efficiency and partition coefficient to be evaluated by fluorescence microscopy. Enzymatic and chemical lysis solutions were used in the lysis step, presenting lysis efficiencies of about 60% and 100%, respectively, while a polyethileneglycol (PEG)/Phosphate system was screened for the separation stage, presenting partition coefficients of

about 4. The device allowed for the continuous screening of multiple combinations of operation conditions, highlighting for example conditions where improvements on the lysis efficiency subsequently impaired the separation, decreasing the partition of the target product, thus demonstrating the need for the evaluation of a process in its entirety. In addition, the continuous operation of the device maintains the potential for further integration with other microfluidic modules, such a microbioreactor for cell production or the integration of further purification processes, potentially allowing for the modeling of a full biomanufacturing process on a chip.

A.0.3 Presentations in conferences

Oral Presentations

- *January 2018* "Microfluidic platform for bacterial cell lysis and protein concentration", in 12th European Symposium on Biochemical Engineering Sciences, at Lisbon, Portugal
- *November 2017* "Microfluidic platform for bacterial cell lysis and protein concentration", in Anything But Conventional Chromatography Workshop organized by ESBES, at Lisbon, Portugal

Posters

- *June 2019* "Integrated microfluidic platform for the rapids creening of bacterial cell lysis and protein concentration conditions", in Affinity 2019, Stockholm, Sweden
- *May 2018* "Microfluidic platform for bacterial cell lysis", in PhD Open Days, at Lisbon, Portugal
- *December 2017* "Continuous cell concentration and lysis using inertial microfluidics", in Congress of Microbiology and Biotechnology, at Porto, Portugal

B

Circuit schematic and bill of materials

Quantities	Component
1	LMC6482 OpAmp
2	330nF Capacitor
1	100pF Capacitor
1	EG&G FFD 100 photodiode
2	6 pin male connector
9	BC337 transistor
1	5000M Resistor
17	2.2k Resistor
1	Teensy3.6

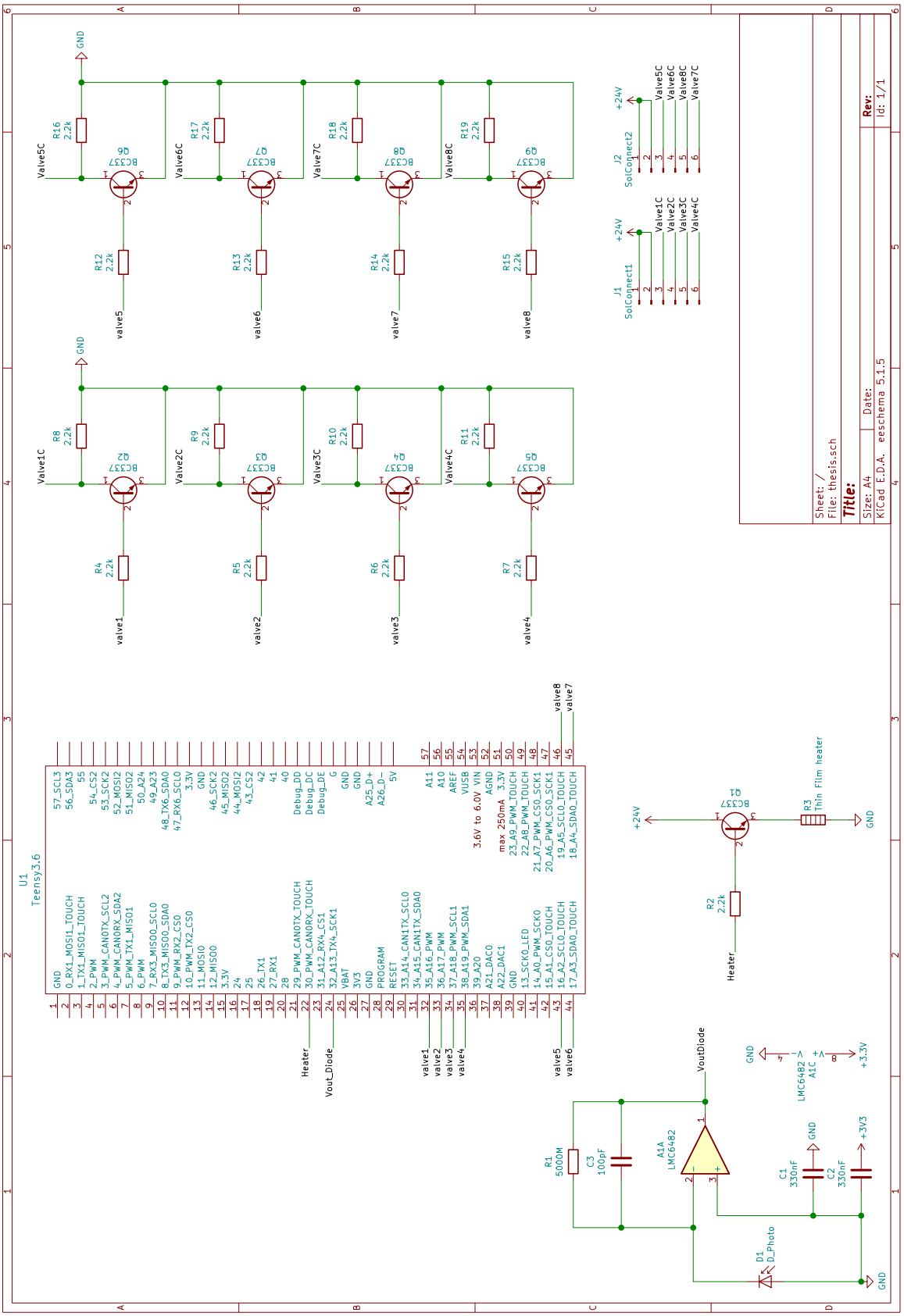
Sheet: /
File: thesis.sch
Title:
Size: A4
Date:
Rev:
KiCad E.D.A. eeschema 5.1.5
Id: 1/1
U1
Teensy3.6
J1
SolConnect1
J2
SolConnect2
Valve1C
Valve2C
Valve3C
Valve4C
Valve5C
Valve6C
Valve7C
Valve8C
+24V
GND
+3.3V
+3V3
Heater
Vout_Diode
VoutDiode
valve1
valve2
valve3
valve4
valve5
valve6
valve7
valve8
Thin Film heater
LMC6482 A1C
A1A LMC6482
D_Photo